A study of epithelial cell delamination in Drosophila

Eliana Marinari

A thesis submitted to University College London for the degree of Doctor of Philosophy

MRC Laboratory for Molecular Cell Biology
UCL

August, 2011

Declaration

I, Eliana Marinari, confirm that the work presented in this thesis is my own. Where information has been derived from other sources, I confirm that this has been indicated in the thesis.

Acknowledgments

First, I would like to thank my supervisor Buzz Baum, who has been extremely supportive during my PhD, for his advices and enthusiasm for Science.

Then, I would like to thank all members of the Baum's lab for being such amazing colleagues. Thanks to Marina, Helen, Jenny, Oscar, Remi, Julien, Pato; the students who collaborated with me, Jorge and Scott and former members of the lab who helped me at the beginning of my project, Marios and Tao. Finally, a special thank to Andre' and Nelio, for making the fly room such a lovely environment to work in and to Steffi and Cosetta, for the nice atmosphere in the office.

I would also like to acknowledge the LMCB and Cancer Research UK for the financial support.

Finally, I would like to thank my parents, for their support over so many years, and Simone, for sharing this experience with me.

Abstract

The developmental refinement of an epithelium requires finely balanced rates of growth and cell loss. However, the molecular mechanisms that regulate the achievement of homeostasis, which are likely to be deregulated in tumorigenesis, remain poorly understood.

In this work using the fly notum as a model system and laser cutting experiments to test in vivo tissue mechanics, I describe a novel process of live cell delamination that counter-balances tissue growth to ensure the achievement of mechanical equilibrium in the final phases of development. The fly notum is an ideal system to study this type of mechanical buffering since it remains approximately constant in size during the final phases of tissue refinement in development, whilst requiring cell growth, division and cell loss.

Individual cells leaving overcrowded regions of the notum by live cell delamination follow a path of progressive junctional and apical area loss, in a 2-step mechanism that is independent of cell death. Cells first undergo serial junctional loss, leading to a cell with a small apex and few sides, followed by Myosin-II driven apical extrusion. This process of live cell delamination can be recapitulated by a simple vertex model of epithelial mechanics, where pressure is relieved as cells leave the tissue via a series of stochastic neighbor exchange events.

These findings suggest that crowding-induced live cell delamination is a generic mechanism that buffers epithelia against variations in growth. This has important implications for our understanding of homeostasis and its deregulation in cancer, as well as for cancer cell invasion and metastasis.

Table of contents

1. INTRODUCTION

Here I introduce the background related to my research work. This introduction is divided in three sections.

The first part is focused on the mechanisms that control morphogenesis to reach the final size and shape of organs and tissues. In particular, pathways that regulate growth in development and homeostatic mechanisms that control the balance between cell growth and cell loss will be introduced. In the final paragraph, I will discuss mechanisms that result in the deregulation of tissue homeostasis.

The second part is focused on the problem of maintaining tissue integrity during morphogenesis and the role of force transmission across epithelial tissues in coordinating growth, cell loss and cell rearrangements, using examples from *Drosophila* embryogenesis.

The third part introduces the notum as a model system to study tissue refinement and the interplay between tissue mechanics and morphogenesis.

1.1 Tissue Biology: growth, cell division and apoptosis in the regulation of epithelial tissue shape and size

Animal shape and size is controlled with extreme precision during development. Thus organs and tissues grow until they reach a characteristic size and shape and then stop. This is achieved by coordinating three major processes: cell division, cellular growth (mass accumulation), and cell survival. Although external factors such as nutrient availability can alter overall animal size, local homeostatic interactions dominate in achieving the right shape and patterning of epithelial tissues. As a result, if cell size is altered locally, there is a corresponding change in cell number (and vice versa), to ensure that tissue size is conserved (Johnston and Gallant, 2002). Similarly, several experiments show that growth is regulated by an organ intrinsic-program. In the Salamander, when eyes or limbs are exchanged between different species with different organ size, they reach a size characteristic of the donor (Twitty and Schwind, 1931). A similar experiment in *Drosophila* showed that immature imaginal discs, when transplanted in a growth-permissive environment such as the abdomen of an adult female, grow at their normal rate until they reach their final size (Bryant and Simpson, 1984).

Imaginal discs of *Drosophila* represent one of the most extensively studied models in which to study growth. Each consists of a large number of similar epithelial cells. Once the hatched larva begins to feed, growth occurs rapidly; in particular, the wing disc expands from 50 to 50,000 cells in four days. From the beginning of its development, each imaginal disc is organized into different compartments specified by different selector genes, which can grow relatively independently of one another. Thus, each compartment can be considered as a unit of growth (Blair, 1995), which relies on intrinsic mechanisms to regulate its size and form, via cell-to-cell communication (Bryant and Simpson, 1984; de la Cova et al., 2004; Johnston and Gallant, 2002). A homeostatic mechanism proposed to support this hypothesis is cell competition, which balances growth regulation by PI3K signaling and the Hippo pathway.

1.1.1 Growth pathways in development

The control of growth and organ size has long been studied in different organisms. Classical embryological studies suggested that organs possess intrinsic information to regulate their size. This property of tissues and organs is achieved through the coordination of cell loss and growth, so that cells do not divide a fixed number of times but proliferation is regulated and stops when organs reach their characteristic size. An evidence of this is the process of compensatory proliferation in epithelial tissues in *Drosophila*. Following laser ablation of 60% of cells in imaginal discs, these tissues produce normal sized adult structures (Bryant and Simpson, 1984). Thus, global organ size information is transmitted to single cells, which regulate their growth and proliferation appropriately.

The Hippo pathway has recently emerged as a conserved signaling cascade that control tissue and organ growth in *Drosophila* and vertebrates (Fig. 1.1). This pathway restricts proliferation and promotes the apoptosis of excess cells, primarily affecting cell number in the tissue (Halder and Johnson, 2011). The core of the pathway is constituted by four components, the NDR family kinase Warts (Wts) (Justice et al., 1995; Xu et al., 1995), the WW domain-containing protein Salvador (Sav) (Kango-Singh et al., 2002; Tapon et al., 2002), the Ste20-like protein kinase Hippo (Hpo) (Harvey et al., 2003; Jia et al., 2003; Pantalacci et al., 2003; Udan et al., 2003; Wu et al., 2003) and the adaptor protein Mob-as-tumor suppressor (Mats) (Lai et al., 2005). These four tumor suppressors form a kinase cascade in which the Hpo-Sav complex phosphorylates and activates the Wts-Mats complex (Cubadda et al., 1997). The pathway is in an activated state and can be de-activated by dephosphorylation by the protein phosphatase 2A (PP2A) complex Striatin-interacting phosphatase and kinase (STRIPAK) (Ribeiro et al., 2010). The target of this kinase cascade is the transcriptional co-activator Yorkie (Yki), which is inhibited by Wts/Mts mediated phosphorylation at three separate sites (S111, S168 and S250) (Dong et al., 2007; Huang et al., 2005; Oh and Irvine, 2008; Oh et al., 2009; Zhao et al., 2007). When Yki is phosphorylated at the S168 site, it binds to 14-3-3 proteins, resulting in the retention of Yki in the cytoplasm and the inhibition of its transcriptional activity (Dong et al., 2007; Oh and Irvine, 2008; Oh and Irvine, 2009; Ren et al., 2010).

Moreover, direct interactions between Hpo, Yki, Wts and the upstream regulator Expanded (Ex) can suppress its activity (Oh et al., 2009; Ren et al., 2010). When active, Yki localizes to the nucleus, where it forms a complex with Scalloped (Sd), a TEAD family transcription factor, which binds to DNA (Goulev et al., 2008; Wu et al., 2008; Zhang et al., 2008; Zhao et al., 2008). This complex promotes growth by inducing the expression of target genes, such as the cell-cycle regulator *cyclinE*, the apoptotic inhibitor *diap1*, the growth promoter *Myc* and *bantam*, which drive cell proliferation and cell survival (Dong et al., 2007; Goulev et al., 2008; Harvey et al., 2003; Huang et al., 2005; Jia et al., 2003; Kango-Singh et al., 2002; Neto-Silva et al., 2009; Nolo et al., 2006; Pantalacci et al., 2003; Peng et al., 2009; Ren et al., 2010; Tapon et al., 2002; Thompson and Cohen, 2006; Udan et al., 2003; Wu et al., 2003; Zhang et al., 2008; Ziosi et al., 2010).

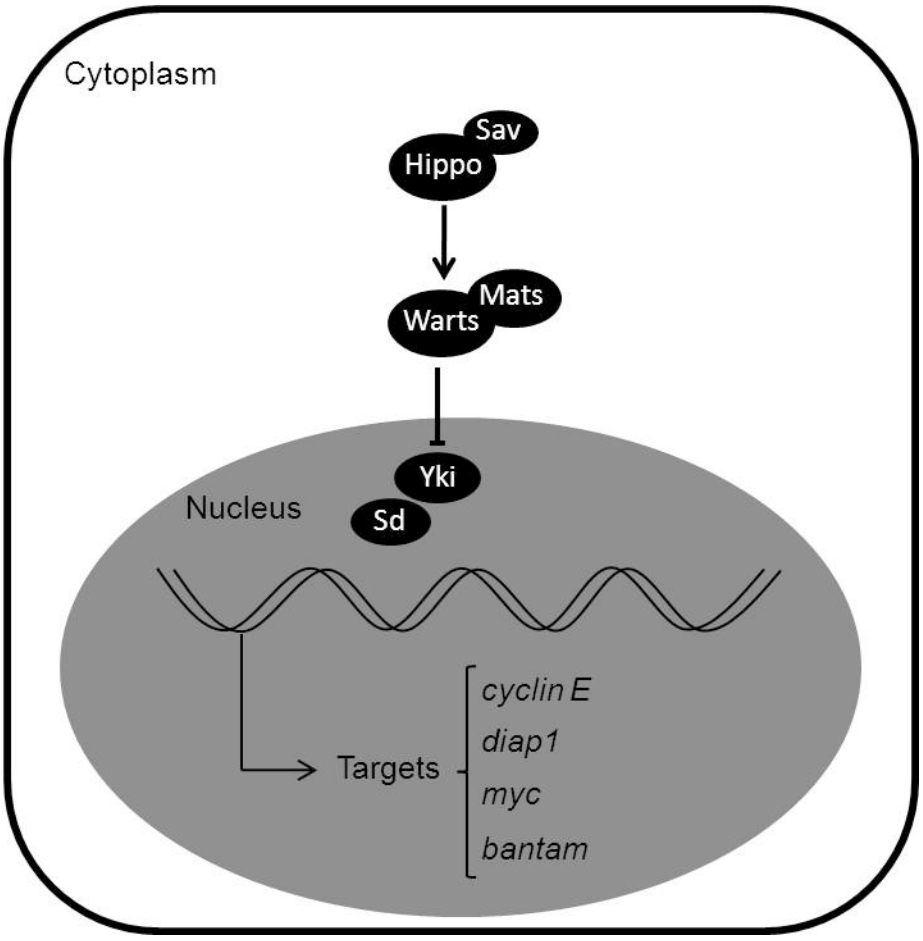

Figure 1.1 Hippo signaling pathway in *Drosophila*

Schematics of the Hippo pathway. Pointed and blunt arrowheads indicate activating and inhibitory interactions, respectively. Abbreviations: Mats, Mob as a tumor suppressor; Sav, Salvador; Sd, Scalloped; Yki, Yorkie.

In addition to the Hippo pathway, nutrition sensing and growth control are coordinated by the Insulin-IGF signaling pathway through the phosphatidylinositol 3-kinase (PI3K)/AKT cascade in *Drosophila* (Fig. 1.2). In response to insulin and other growth factors, PI3K is activated and phosphorylates the membrane lipid 4,5-biphosphate (PIP2) to form 3,4,5-triphosphate (PIP3) (Stocker and Hafen, 2000). PIP3 acts as a second messenger and induces the translocation of PDK1 and PKB/Akt to the plasma membrane via a Plekstrin-homology domain, which determines their activation (Alessi et al., 1997; Stephens et al., 1998). PDK1 activates PKB (Alessi et al., 1997; Stephens et al., 1998) and S6K (Alessi et al., 1998; Pullen et al., 1998). Then, activated PKB phosphorylates and inactivates GSK3 (Cross et al., 1995) and by an unknown mechanism activates mTOR (Cross et al., 1995), a large protein containing carboxy-terminal kinase domains. In turn, mTOR activates S6K (Burnett et al., 1998) and inhibits 4E-BP1 (Brunn et al., 1997), the initiation factor 4E binding protein, through phosphorylation, although the exact mechanism by which this occurs is not totally clear. S6K promotes the translation of components of the ribosome together with the phosphorylation of 4E-BP1, which releases the eukaryotic initiation factor 4E (eIF4E), to initiate transcription (Burnett et al., 1998). Other negative regulators of this pathway include PTEN (Myers et al., 1997), a phospholipid phosphatase that antagonizes the effect of PI3K, and the tuberous sclerosis complex proteins 1 and 2 (TSC1 and TSC2) (Gao and Pan, 2001; Potter et al., 2001; Tapon et al., 2001).

In *Drosophila,* all the effectors of this pathway have a striking effect on both cell size and number (Stocker and Hafen, 2000), with the exception of d4E-BP and S6K (Miron et al., 2001; Montagne et al., 1999). Loss of function mutants of d4E-BP have no effect on cell growth, but overexpression has a pronounced phenotype (Miron et al., 2001). In the case of dS6K, mutants have an effect on cell size but not on cell number (Montagne et al., 1999).

During normal organ development, cell growth and division appear tightly coordinated, in order to maintain a characteristic size of cells (Neufeld et al., 1998). Moreover, the analysis of PI3K signaling pathway in *Drosophila* shows that cell growth and division

are co-regulated. When cell division is inhibited, cells continue to accumulate mass and increase in size. Conversely, cell-cycle regulators such as Cdc25 promote cell division without a concomitant increase in growth and cells have smaller size (Neufeld et al., 1998). Thus, alterations in cell division rates do not affect growth, even if growth signaling is sufficient to drive cell division.

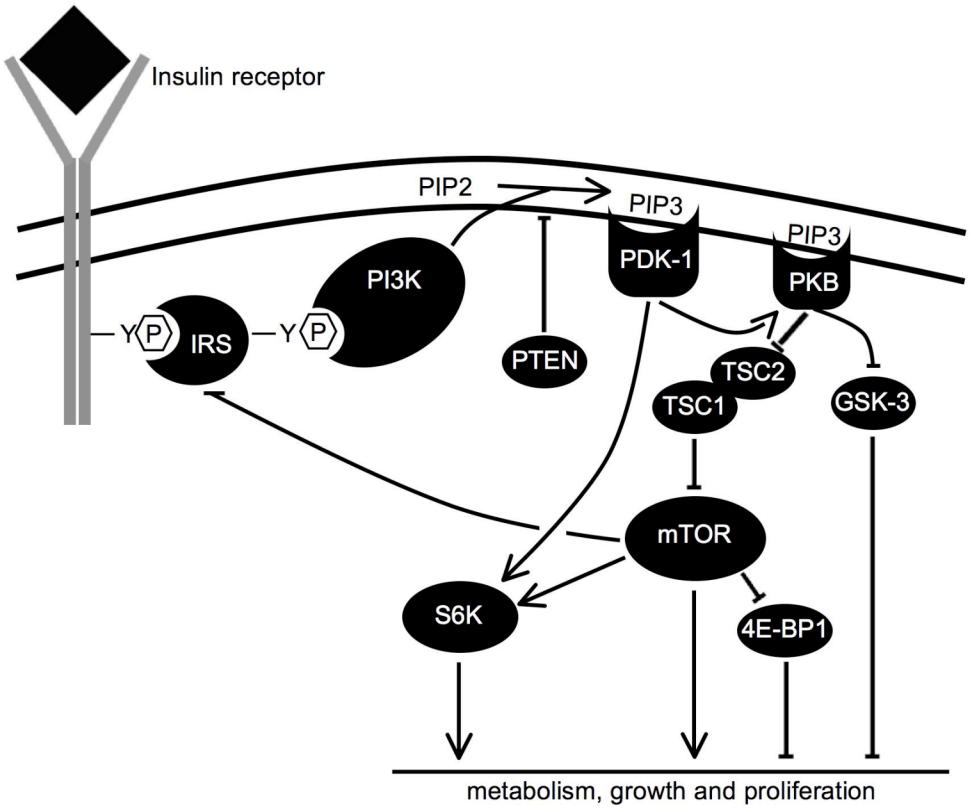

Figure 1.2 PI3K signaling pathway

Simplified schematic of the PI3K signalling pathway. Pointed and blunt arrowheads indicate activating and inhibitory interactions, respectively. Abbreviations: PI3K, phosphatydilinositol 3-kinase; IRS, insulin receptor substrate; PTEN, phosphatase and tensin homolog; PKB, protein kinase B; PDK-1, pyruvate dehydrogenase kinase; TSC1 and TSC2, tuberous sclerosis complex 1 and 2; GSK-3, glycogen synthase kinase 3; TOR, target of rapamycin; S6K, S6 kinase; 4E-BP1, 4E binding protein 1.

1.1.2 Disc size problem: role of cell competition in tissue homeostasis

Cell competition has long been known as a homeostatic mechanism by which cells compete with each other for space and morphogens to counterbalance growth in epithelial tissues. In this process, slowly dividing cells are eliminated from a population of more rapidly dividing cells (Morata and Ripoll, 1975), as the result of interaction between neighbouring cells. Importantly, the effect never crosses the boundaries of developmental compartments (de la Cova et al., 2004). So if weaker cells are protected in a distinct compartment, they are not eliminated from the tissue from wildtype cells in the adjacent compartment (Simpson, 1976). When death of outcompeted cells is prevented by inhibition of apoptosis, there is no longer a significant alteration in the size of the clones of super-competitor cells, indicating that growth rate is independent of cell competition and cell death, and the size of the compartment remains constant (Martin et al., 2009b). This constitutes an additional evidence that the final structure of the *Drosophila* wing is regulated as if predetermined and that organs have a maximum size, that determines growth arrests once it has reached its final volume (Day and Lawrence, 2000).

The process of cell competition was first identified in *Drosophila* when heterozygous *Minute* clones (*Minute*/+), a mutation that results in decreased ribosomal activity, were generated in a wildtype background (Morata and Ripoll, 1975). Cells in *Minute*/+ tissues proliferate slower than wildtype cells, but are viable. However, in a wildtype background, clones of *Minute*/+ cells are removed from the epithelium through apoptosis (Moreno et al., 2002). The same process was described for *tkv* and *dpp* mutant clones (Gibson and Perrimon, 2005; Shen and Dahmann, 2005). Thickvein (Tkv) is the receptor of Decapentaplegic (Dpp), a member of the TGF-β superfamily, critical for pattern formation, cell survival and growth of imaginal discs (Raftery and Sutherland, 1999). *tkv* hypomorph cells are removed from the wildtype wing disc by apoptosis. This process is blocked when JNK activity is reduced, so that cells are still extruded from the wing disc epithelium but survive underneath (Adachi-Yamada et al., 1999). Inappropriate Dpp signalling is thought to alter the cytoskeletal organization resulting in cell shape changes and loss of the apical cell-cell contacts in the epithelium.

Another gene inducing cell competition is the proto-oncogene Myc, suggesting a possible role for this process in tumor progression. Clones of cells that express a *myc* hypomorphic allele ($dmyc^{PO}$), die when surrounded by wildtype cells (de la Cova et al., 2004; Moreno and Basler, 2004). Conversely, clones of cells over-expressing dMyc out-compete wildtype cells, inducing them to die (Moreno and Basler, 2004). Although Myc overexpressing cells over-proliferate, overgrowth itself does not seem sufficient to trigger cell competition, because neighbouring differences in PI3K activity or Cyclin D/Cdk4 do not lead to the same phenomenon (de la Cova et al., 2004).

Another group of genes inducing cell competition are polarity proteins, particularly genes of the scribble complex: *lgl* mutants, Mahjong/VprBP, an Lgl binding protein, and Scribble (Brumby and Richardson, 2003; Froldi et al., 2010; Igaki et al., 2009; Leong et al., 2009; Menendez et al., 2010; Tamori et al., 2010). In a wildtype background, clones of cells mutant for these genes are out-competed by wildtype neighbours and eliminated from the wing disc epithelium.
More recently, the Hippo signaling pathway has been linked with cell competition in *Drosophila.* In *lgl* mutant clones, the transcriptional co-activator Yorkie, which negatively regulates the Hippo pathway, is localized to the nucleus and represses the Hippo pathway (Menendez et al., 2010). Moreover, mutation of *warts* and *salvador*, repressors of this pathway, increase the survival of M/+ clones (Tyler et al., 2007).

The molecular mechanisms of cell competition are not well understood. Two alternative hypotheses have been proposed to explain this process: i) cell competition arises from extracellular ligands or soluble factors; ii) cell competition results from direct cell-cell interaction between neighbouring cells.

The first hypothesis arises from the idea that cells in tissues may compete for a limited pool of extracellular morphogens, such as Dpp. Dpp is a secreted protein critical for pattern formation, growth and survival. This was suggested by the fact that M/+ cells in a wildtype background upregulate Brk, the repressor of Dpp activity, and have lower pMad signaling, indicating poor reception of Dpp ligand (Moreno et al., 2002). This

leads to JNK activation and cell death. The same sequence of events occurs in *tkv* mutant cells. Moreover, over-expression of a dominant negative form of its receptor Thickvein (Tkv^{QD}) in wildtype clones generated in a Myc over-expression background, increases the survival of outcompeted cells (Moreno and Basler, 2004). The extracellular ligand theory is also supported by the fact that 'loser' cells are protected from dying by Rab-5 over-expression, a small guanosine triphosphatase GTPase involved in endocytosis. In cell culture, co-culturing of wildtype and Myc over-expressing S2 cells resulted in cell competition independently of cell-cell contacts (Senoo-Matsuda and Johnston, 2007). These data suggested that cell competition could be mediated by soluble factors and extracellular ligands.

The second hypothesis is supported by the fact that cells at the borders of the clone in direct contact with the 'winner' neighbours undergo cell death (de la Cova et al., 2004; Tamori et al., 2010). During cell competition, dying M/+ loser cells are engulfed by nearby wild-type cells. When winner cells lack factors that regulate cell engulfment, like Draper, a trans-membrane receptor, Wiscott-Aldrich Syndrome protein (WASp), Phosphatidylserine receptor (PSR), the small GTPase RAC or MBC, death is repressed in M/+ cells at the border of the clone (Li and Baker, 2007). However, not all cells are engulfed by the 'winners', as many delaminate from the epithelium and phagocytosed by hemocytes (de la Cova et al., 2004; Moreno et al., 2002).

A key mechanism in cell competition is the induction of cell death in 'loser' cells. JNK is thought to play a role in apoptosis of out-competed cells in the case of *scribble*, *lgl* and *minute* clones (Brumby and Richardson, 2003; Moreno and Basler, 2004; Moreno et al., 2002; Tamori et al., 2010). In the case of cells with different levels of dMyc, the role of JNK in regulating apoptosis is less clear, since inhibition of JNK only rescued a small fraction of 'loser' cells from dying (de la Cova et al., 2004). In these cells, hid, a *Drosophila* pro-death protein, was shown to be the effector of apoptosis (de la Cova et al., 2004; Senoo-Matsuda and Johnston, 2007). Recently, Rhiner et al. screened for genes activated in cells with low levels of dMyc expression and identified as a candidate gene, a highly conserved trans-membrane protein called Flower (Fwe) (Rhiner et al.,

2010). Two splice isoforms are expressed in all 'loser' cells, Fwe^{LOSE-A} and Fwe^{LOSE-B}, while Fwe^{ubi} is expressed in all the cells in the imaginal disc. The overexpression of $Fwe^{LOSE-A/B}$ in all cells of the imaginal disc is not sufficient to induce cell death, which only occurs when these cells contact wildtype cells expressing Fwe^{ubi}. Finally, in experiments that rescue outcompeted clones, such as over-expression of Dpp and Rab-5, the induction of Fwe^{LOSE-A} is less pronounced (Rhiner et al., 2010). Importantly, caspase inhibition does not inhibit Fwe^{LOSE-A} expression, suggesting that this protein acts upstream of caspase activation.

An additional homeostatic mechanism related to cell competition is the process of morphogenetic apoptosis. This phenomenon results in non-autonomous cell death triggered by a discontinuity in a morphogen gradient, and occurs particularly across compartment boundaries. In *Drosophila*, discontinuities in Dpp or Wg gradient, lead to JNK dependent apoptosis on both sides of a compartment boundary (Adachi-Yamada et al., 1999; Adachi-Yamada and O'Connor, 2002). The death of cells at the discontinuity together with the proliferation of the remaining cells restores a continuous morphogen gradient. Similarly, cells over-expressing an activated form of the Dpp receptor Tkv (Tkv^{CA}), kill nearby cells expressing a wildtype form of the receptor via non-autonomous apoptosis (Adachi-Yamada and O'Connor, 2002).

1.1.3 Deregulation of tissue homeostasis

Mutations in several tumour suppressors genes cause perturbation of the fine balance between cell proliferation and cell loss in epithelial tissues, resulting in the deregulation of homeostasis and tissue overgrowth. These mutations can be divided into two categories, according to their overgrowth characteristics and effect on tissue architecture: i) 'neoplastic', when gene loss leads to defects in apical-basal polarity and epithelial organisation; ii) 'hyperplastic', when gene loss induces dramatic tissue overgrowth, without changes in epithelial architecture.

In *Drosophila*, forward genetic screens have identified three tumour suppressor genes that act together to regulate epithelial polarity and determine neoplastic transformation of the tissue when deregulated. The disruption of cell-cell junctions and cell-matrix contacts in large clones, results in aberrant proliferation, survival and migration of these mutant cells, leading to extensive overproliferation (Bilder, 2004). In small clones, however, these mutant cells are outcompeted by neighbouring wildtype cells and are extruded from the tissue and eliminated by apoptosis. This suggests that the tissue has a system to eliminate potentially tumorigenic cells (Brumby and Richardson, 2003; Igaki et al., 2009; Pagliarini et al., 2003; Pagliarini and Xu, 2003; Woods and Bryant, 1991). In the case of *scrib*-/- and *dlg*-/- clones, mutant cells are eliminated through cell competition between different cell types in the tissue by JNK-dependent apoptosis through endocytic activation of Eiger/TNF signalling. Eiger is a member of the tumor necrosis factor (TNF) superfamily that has been suggested to be a ligand during activation of the Drosophila JNK pathway, since its overexpression induces JNK cell death in imaginal epithelia (Igaki et al., 2002; Moreno et al., 2002). *Scrib* and *dlg* mutant cells are no longer eliminated in a *eiger* mutant background, as a result grow aggressively and cause lethality at pupal stage in all cases (Igaki et al., 2009). These data suggest that eiger/JNK pathway behaves as an intrinsic tumor suppressor system and the disruption of this pathway could promote tumor invasion in cancer.

In addition, genes that are involved in the breakdown of anoikis contribute to neoplastic transformation of epithelial cells (Juliano and Varner, 1993). Anoikis is the process of apoptosis induced by disruption of cell-matrix contacts. When this phenomenon is inhibited by mutations in genes encoding integrins, transformed cells survive in the absence of matrix (Juliano and Varner, 1993). The three primary integrin signalling molecules that are important for adhesion-dependent cell survival are Focal adhesion kinase (FAK), Shc and Integrin-linked kinase (ILK) (Aplin et al., 1999; Dedhar, 2000; Giancotti and Ruoslahti, 1999). For example, overexpression of ILK suppresses anoikis in certain epithelial cell lines (Attwell et al., 2000). These proteins promote cell survival by up-regulating the PI3K/Akt pathway (Aplin et al., 1999; Dedhar, 2000; Giancotti and

Ruoslahti, 1999). Activated FAK can therefore transform MDCK cells by inducing resistance to anoikis (Frisch et al., 1996).

The group of genes that when mutated induce hyperplasia includes several proteins involved in regulating cell-cell adhesion. Among them, Merlin/NF2 and Expanded are adaptor proteins that localize to the sub-apical region of epithelial cells and link transmembrane proteins to the cytoskeleton (Baumgartner et al., 2010; Boedigheimer et al., 1997; Cho et al., 2006; Genevet et al., 2010; Hamaratoglu et al., 2006; Pellock et al., 2007; Tyler and Baker, 2007; Yu et al., 2010). Mutations in Mer and Ex also cause tissue overgrowth by inactivation of Hpo and Sav (Hamaratoglu et al., 2006), which alters Yki signaling. Similarly, two genes, which encode for large atypical cadherin-related proteins, have been implicated in growth control in *Drosophila.* The *fat* and *fat-like* mutants cause massively overgrown discs, which show dramatic tissue folding (Bennett and Harvey, 2006; Cho et al., 2006; Silva et al., 2006; Tyler and Baker, 2007; Willecke et al., 2006) by activation of the transcription of Yki-target genes (Bennett and Harvey, 2006; Cho et al., 2006; Silva et al., 2006; Tyler and Baker, 2007; Willecke et al., 2006).

In mice and humans, mutations in E-cadherin are often associated with invasive tumours, and the binding partners α- and β-catenin cause hyperproliferation of epidermal cells when mutated in the mice skin (Polakis, 2000; Vasioukhin et al., 2001). When β-catenin is not associated with E-cadherin, it is degraded by the Axin-APC-complex. Wnt/Wingless blocks this process of degradation and allows β-catenin translocation to the nucleus, where it regulates transcription of growth genes (Polakis, 2000). Thus, activating mutations in Wnt/β-catenin signalling pathway are highly oncogenic. However, it is not clear whether β-catenin controls growth based on changes in epithelial mechanics and integrity, as it has been proposed (Polakis, 2000).

In summary, the molecular mechanisms that induce hyperplastic growth and determine deregulation of tissue homeostasis are highly conserved between mice, humans and flies. In addition, cell biological processes that eliminate damaged or oncogenic cells from the

tissue are likely to be evolutionary conserved. Since the mechanisms of cell delamination are similar in both physiological and pathological situations, like tumor progression, studying this process during development in *Drosophila* is likely to be a good way to better understand the link between tissue growth and cell delamination.

1.2 Molecular cell biology: maintaining epithelial integrity

Tissue morphogenesis is the result of three major events: i) cell proliferation, which includes growth and cell division; ii) apoptosis; iii) cell shape changes and rearrangements. These processes must be precisely coordinated and require dynamic remodelling of junctions and cytoskeleton proteins in order to maintain tissue integrity and stability during development. These morphogenetic events are regulated by the interplay between the acto-myosin network and adhesion molecules that localize at the zonula adherens, which together ensure the maintenance of cell-cell contacts and force transmission across developing tissues. The same networks coordinate deformations in the epithelial sheets. These processes include tissue bending, to generate invaginations and furrows, and elongation of epithelial sheets (Fristrom, 1988). The two most studied examples of tissue bending and elongation in *Drosophila* are represented respectively by ventral furrow formation and germ band elongation of the embryo.

The transmission of tension across the epithelial surface is thought to be important for tissue integrity. This is related to the idea proposed by Ingber, known as tensegrity (tensional integrity) (Ingber, 2008). Tensegrity was first used in architectural designs for describing "a structural network, composed of opposing tension and compression elements that self-stabilizes its shape through establishment of a mechanical force balance". In epithelia, mechanical tension generated or applied at the macroscopic scale level is likely to be felt by cell adhesion sites and by junctional acto-myosin structures at the cellular scale (Ingber, 2008). This may be necessary to maintain the mechanical integrity of the tissue.

In addition, epithelia have to deal with individual cell dynamics, such as apoptosis and cell division. Apoptotic cells need to be removed from the epithelium without leaving any gap behind, in order to maintain an intact functional barrier. Similarly, this requires the interplay of the contractile acto-myosin ring and remodeling of adherens junctions (Rosenblatt et al., 2001).

1.2.1 The machinery: adherens junctions and acto-myosin network

The physical link between AJs and the actin cytoskeleton allows the transmission of cortical forces exerted by the acto-myosin network to the AJs (Cavey et al., 2008; Martin et al., 2009a; Rauzi et al., 2010). Conversely, AJs can modulate the cytoskeletal organisation inside the cell and around the cortex (Drees et al., 2005; Nakagawa et al., 2001; Noren et al., 2001). Below, I discuss: i) E-cadherin, ii) the acto-myosin network, iii) the interplay between AJs and the acto-myosin network.

1.2.1.1 E-cadherin and adherens junctions

Adherens junctions (AJs) form the zonula adherens (ZA) at the apical side of epithelial cells and are constituted by the cadherin-catenin complex (Farquhar and Palade, 1963). E-cadherins are transmembrane molecules that associate in trans-homophilic dimers between neighbouring epithelial cells in a Ca^{2+}-dependent manner (Gumbiner, 2005). At cell junctions, E-cadherins interact with binding partners that modulate their adhesion, such as β-catenin, p120-catenin and α-catenin (Oda et al., 1993; Peifer, 1993; Reynolds et al., 1994). β-catenin acts as a linker between α-catenin and E-cadherin and is required for E-cadherin export from the ER to the plasma membrane. α-catenin is important for tissue integrity, since it cross-links cadherins with the actin cytoskeleton. It can bind F-actin directly or through actin-binding proteins such as vinculin, α-actinin and ZO1 (Kobielak and Fuchs, 2004; Rimm et al., 1995). Recently it has been shown that β-catenin and α-catenin interact to modulate the F-actin cytoskeleton in a mutually exclusive manner (Drees et al., 2005; Yamada et al., 2005). Although it is not clear how

this works, the dynamic interaction between E-cadherin, β-catenin, α-catenin and F-actin plays an important role in the transmission of tensile forces across the surface of the epithelium and in the dynamic regulation of cell-cell adhesion.

Adhesion regulates acto-myosin assembly and contractility by modulating the concentration of two types of actin nucleators: the ARP 2/3 complex, which promotes actin branching, and formins, which promote linear growth of actin filaments (Drees et al., 2005). α-catenin and ARP2/3 may compete for binding to F-actin filaments. By contrast, Formin-1 binds directly α-catenin (Drees et al., 2005).

1.2.1.2 Acto-myosin

The acto-myosin network is constituted by actin and non-muscle Myosin-II. It exerts forces on AJs to reshape and remodel cells in fundamental biological processes such as cell migration, cell adhesion and division (Paluch et al., 2006).

Actin is a globular protein and cycles between two states, a monomeric (G-actin) and filamentous (F-actin) form (Pollard et al., 2000). Actin filaments grow in a polarized way as actin-ATP-monomers are added to uncapped barbed ends (plus ends) and monomers are released from the pointed ends (minus ends). Indirectly, the binding of capping proteins at the plus end leads to the actin filament shortening by minus end depolymerisation. This is driven by the hydrolysis of ATP in aged filaments (Pollard and Borisy, 2003). ADP-actin regions of filaments are then disassembled by the action of severing proteins to release ADP-monomers, which can be recycled following the conversion of ADP in ATP (Pollard et al., 2000). The formation of actin filaments is mediated by three distinct mechanisms (Pollard and Borisy, 2003): i) *de novo* nucleation of actin filaments; ii) severing of existing filaments to create uncapped barbed ends, which can elongate; iii) uncapping of existing barbed ends.

Two distinct types of actin nucleators mediate new actin filament formation: Formins and the Arp 2/3 complex (Pollard and Borisy, 2003). The Arp2/3 complex is composed

by the Actin related proteins 2 and 3 (Arp 2/3) that forms a complex with other proteins (Pollard and Beltzner, 2002). This complex nucleates filaments which grow by barbed end elongation and induces actin branching by binding to existing actin filaments and nucleating new filament formation at 70° angles to the mother filament (Mullins et al., 1998). SCAR/Wave and Wiskott-Aldrich Syndrome protein family (WASp) promote the activity of Arp 2/3, which is inactive in their absence (Machesky et al., 1999; Rohatgi et al., 1999; Yarar et al., 1999).

The nucleation activity of formins is constitutively inhibited, by the interaction of their N-terminal GTPase binding domain (GBD) with their C-terminal DAD domain. They are activated by GTP-bound-Rho-GTPase, which releases formins from auto-inhibition and promotes linear actin filament nucleation (Castrillon and Wasserman, 1994; Kovar et al., 2006). Formins drive the elongation of actin filaments by competing with capping proteins for binding to barbed ends, where they catalyze the addition of Profilin-bound ATP actin (Castrillon and Wasserman, 1994; Kovar et al., 2006). In *Drosophila*, Diaphanous (Dia) is the only formin so far identified to play a role in cellularisation of the embryo, cytokinesis and junctional organisation (Castrillon and Wasserman, 1994; Grosshans et al., 2005).

Mechanical force is driven by the motor protein nonmuscle Myosin-II, which generates mechanical movement by sliding along actin filaments, through hydrolysis of ATP. Nonmuscle Myosin-II is a hexamer composed of two heavy chains, two light chains and myosin regulatory light chains (MRLCs) (Sellers, 2000). Vertebrates have 40 isoforms of Myosin genes (Krendel and Mooseker, 2005), while *Drosophila* has 13, including one isoform of nonmuscle Myosin-II (Tzolovsky et al., 2002). In *Drosophila* each gene encodes a subunit. Zipper (zip) encodes the heavy chain MHC (Kiehart et al., 1989), which is composed of an N-terminal globular head, a neck region that binds the light chains and a long alpha helical tail that mediates coiled-coil dimerisation to form a homodimer (Sellers, 2000). The globular head binds actin and ATP to generate the motor activity. The gene *mlc-c* encodes the Myosin light chain (Edwards et al., 1995) and *spaghetti squash (sqh)* the Myosin regulatory light chain (Karess et al., 1991). All

Myosin subunits participate in the generation of contractile force. The hydrolysis of ATP induces conformational changes in the MHC head domain causing a rotation of this module. The rigid neck acts as a lever arm to mediate this movement, known as 'power stroke' (De La Cruz and Ostap, 2004; Sellers, 2000). In this way, Myosin-II drives the sliding of actin filaments past one another.

Myosin-II regulation is essential to control fundamental biological processes including cell division (Matsumura, 2005) and migration (Leung et al., 1998). Myosin is regulated by three mechanisms: i) an activating phosphorylation of MRLC on two highly conserved residues (in *Drosophila* Serine 22 and a nearby Threonine), which is mediated by several kinases, including the myosin light chain kinase (MLCK), Rho kinase (Drok), (activated by the GTPase RhoA) (Winter et al., 2001) and other kinases in vertebrates (Leung et al., 1998; Matsumura, 2005); ii) phosphorylation of MHC, which prevents *de novo* assembly and destabilizes existing filaments (Egelhoff et al., 1993; Yumura et al., 2005); iii) F-actin, which promotes minifilament assembly in vitro, probably by concentrating Myosin-II (Mahajan and Pardee, 1996). Conversely, Myosin-II minifilament assembly increases its affinity for F-actin, resulting in a positive feedback loop, which generates contractile acto-myosin fibers.

1.2.1.3 The interplay between adherens junctions and the acto-myosin network

E-cadherin, F-actin and Myosin-II must be tightly coupled during morphogenesis. This physical association however, is extremely dynamic as a result of cell-cell contacts remodeling and the reversible association with the acto-myosin network (Lecuit, 2010).

F-actin participates in the generation of tissue-level forces in cells in several ways. F-actin was shown to control junctional E-cadherin stability and mobility (Cavey et al., 2008). An F-actin α-catenin-independent pool, which concentrates in patches at the site of E-cadherin enriched domains, controls AJs stability (Cavey et al., 2008). In addition, a second pool of junctional actin pulls on AJs in a mechanism dependent on α-catenin

and forms a contractile network together with Moesin and Bitesize to tether AJs, regulating their mobility (Cavey et al., 2008).

Myosin-II exerts the contractile force that drives topological junction rearrangement during tissue remodeling and stabilizes AJs by inhibiting membrane protrusions (Gloushankova et al., 1997). Myosin-II is not only responsible for inducing cell contractility but is also thought to be recruited in response to ectopic forces in a positive feedback loop (Fernandez-Gonzalez et al., 2009). In addition, Myosin-II, activated downstream of RhoGEF2, controls the initiation of E-cadherin endocytosis through the accumulation of clathrin and AP2 (Levayer et al., 2011).

A recent model proposes a feedback mechanism between AJs and the contractile network, through α-catenin, as a tension transducer of acto-myosin force generation (Lecuit, 2010) (Fig. 1.3). In the model, vinculin recruitment to the AJs through α-catenin, requires acto-myosin tension (le Duc et al., 2010; Lecuit, 2010; Yonemura et al., 2010). Treatment with a Myosin-II ATPase inhibitor prevents vinculin localization at the membrane. Several pieces of evidence show that α-catenin is essential to recruit vinculin at AJs, since deletion in a domain C-terminal to the vinculin binding site determines a failure to recruit vinculin at the AJs. This indicates that the C-terminal region of α-catenin contains a domain that competes with vinculin for binding to the N-terminal. However, when F-actin binds to α-catenin, this inhibition is relieved (Yonemura et al., 2010). This results in a positive feedback loop in which vinculin is recruited at the AJs in a force dependent manner by the acto-myosin network and in turns stabilizes α-catenin at the AJs (le Duc et al., 2010), as showed by FRAP experiments with the fluorescent protein (Yonemura et al., 2010). Thus, tissue tension determines junction stabilization through vinculin recruitment.

The integration of the contractile force generated by the acto-myosin network with E-cadherin at the AJs has an important role in several morphogenetic processes. In the following paragraphs, I describe the most studied examples in which single cell shape

changes driven by the interplay between acto-myosin contractility and E-cadherin, determine tissue remodeling during development.

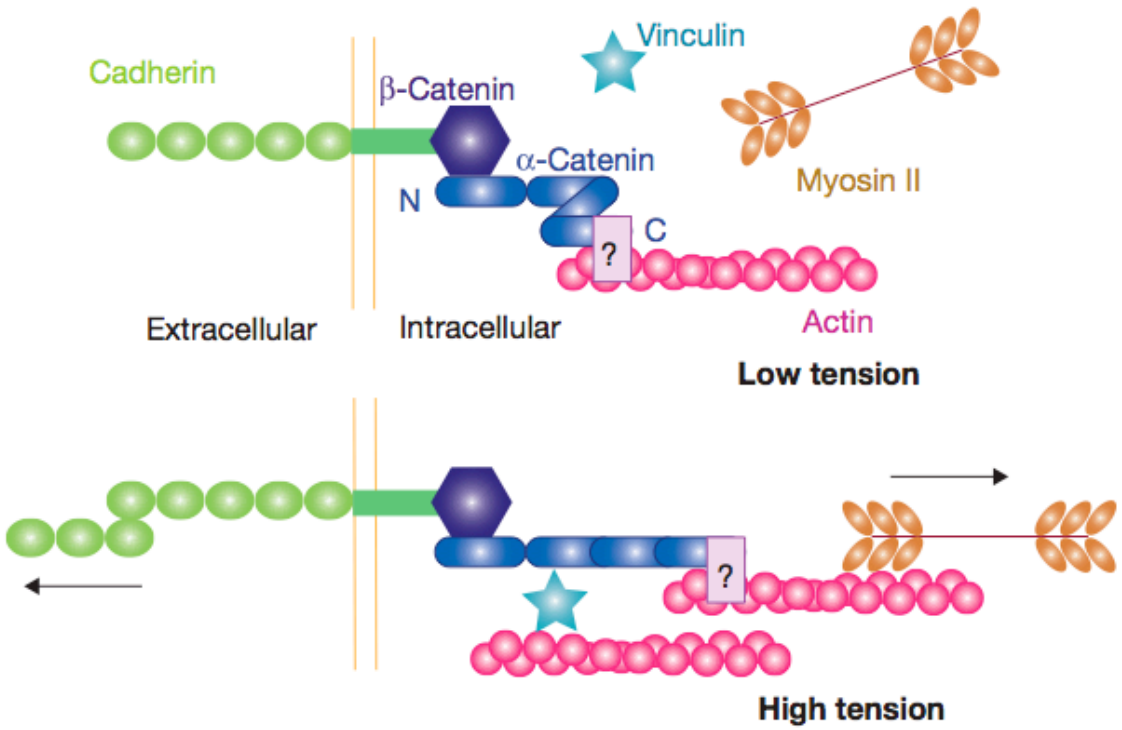

Figure 1.3 Model for α-catenin, as a tension transducer of acto-myosin force generation

The model represents acto-myosin binding to α-catenin. Tension induces a conformational change in α-catenin, unmasking the vinculin-binding domain. N and C indicate the termini of α-catenin. Question mark indicates a possible unknown linker. Based upon Yonemura et al. (Yonemura et al., 2010).

1.2.2 Force generation and transmission during morphogenesis: cell intercalation, apical constriction and apoptosis

Tissue morphogenesis results from the precise regulation and of local forces generated at the level of single cells acting together in a coordinated fashion. Many of these forces are produced by the acto-myosin network and are transmitted along the cell cortex through adherens junctions. In the following section, I discuss first three well-studied morphogenetic processes during embryogenesis of *Drosophila*, in which changes in tissue form result from single cell shape changes generated from the polarized regulation of cell tension and contractility: i) germband extension (GBE), ii) ventral furrow invagination, iii) dorsal closure. Then, I discuss in detail the process of apoptotic cell extrusion, which is not only important in morphogenesis, but also for maintaining epithelial homeostasis in adult tissues.

1.2.2.1 Examples from *Drosophila* embryogenesis: germband extension, ventral furrow invagination and dorsal closure

In *Drosophila*, germband extension occurs 2 h after the onset of gastrulation and is complete within 45 minutes. During this process, the tissue elongates two and half fold along the anterior-posterior axis of the embryo, while it undergoes a corresponding decrease in width along the dorsal-ventral axis (Irvine and Wieschaus, 1994) (Fig. 1.4A). This process occurs in the absence of cell division or cell shape changes and is the result of cell intercalation, which determines an increase in cell number along the anterior-posterior axis (Irvine and Wieschaus, 1994). Cell intercalation is driven by local junction remodeling and modulation of interfacial tension (Bertet et al., 2009; Bertet et al., 2004; Blankenship et al., 2006; Rauzi and Lecuit, 2009; Rauzi et al., 2010; Rauzi et al., 2008; Zallen and Wieschaus, 2004). First, cell junctions oriented along the dorso-ventral (vertical) axis shrink to a vertex, then a new junction forms and elongates along the anterior-posterior axis (Fig. 1.4A'). This polarized remodeling of cell-cell contacts, known as a T1 transition, is a two-step process and is driven by polarized Myosin-II distribution (Bertet et al., 2004; Zallen and Wieschaus, 2004). The accumulation of

Myosin-II at vertical AJs generates anisotropic cortical tension, as measured using laser ablation of AJs (Rauzi et al., 2008). E-cadherin, β-catenin and PAR-3 show a complementary localization to myosin-II, enriched at the anterior-posterior junctions (Blankenship et al., 2006), and the planar polarized distribution of E-cadherin/α-catenin/β-catenin complexes was shown to determine a direct flow of medial acto-myosin towards junctions with lower amounts of these adhesion molecules. It was also suggested that the localisation of Myosin-II to AJs to drive GBE is controlled by the activation of JAK/STAT signaling acting upstream of Wasp. Inactivation of this pathway causes germband defects, due to apical constriction mediated by medial Myosin-II accumulation (Bertet et al., 2009). In this way, anisotropic forces induced by polarisation of the acto-myosin cytoskeleton drive a dramatic rearrangement of the epithelial sheet.

Ventral furrow invagination, during which the ectoderm layer bends inwards prior to its internalisation, constitutes another example of tissue remodelling by force generated at intra-cellular level. At the beginning of gastrulation, the mesoderm cells at the ventral side of the embryo change in shape. They undergo apical flattening and their nuclei begin to migrate from the apical cortex basally (Leptin and Grunewald, 1990; Sweeton et al., 1991). These cells progressively constrict their apices to adopt a wedge shape. Initially, these morphological changes lead to the formation of a ventral furrow. Then, cell shortening along the apical-basal axis drives the complete internalization of the mesoderm. Once internalized, these cells lose their epithelial structure and migrate as mesenchymal cells laterally and dorsally along the overlying ectoderm (Leptin and Grunewald, 1990; Sweeton et al., 1991). The process of apical constriction of ventral furrow cells is essential for the invagination of the monolayer and has been recently characterized in detail using live cell imaging (Martin et al., 2009a). During the first two minutes of this process, cells undergo periodic and asynchronous apical constriction, followed by stretching of the cells. Afterwards, repeated constrictions are interrupted by pauses during which the constricted cell apex is stabilized (Fig. 1.4B), generating a ratchet-like movement. The force necessary to pull the junctions inwards is generated by maternal cytoplasmic myosin. This forms a contractile network together with F-actin at

the medial-apical side of invaginating cells, as they begin to constrict. The transcription factor Twist controls the stabilization of the apically constricted cell shape. Twist induces the expression of folded gastrulation (fog) and T48 (Costa et al., 1994; Kolsch et al., 2007; Seher et al., 2007; Sweeton et al., 1991; Zusman and Wieschaus, 1985), which via recruitment of RhoGEF2 activate the Rho1 GTPase, known to induce Myosin-II contractility (Barrett et al., 1997; Perrimon et al., 1996). As a result, *twist* mutant embryos form a narrow and shallow furrow because, although Myosin-II coalesces and pulsed constrictions still occur in its absence, the furrow doesn't fully invaginate, since the constricted apex of the cells is not stabilized and cells do not shorten. Another transcription factor, Snail is necessary to induce the pulses of apical constriction through the contraction of the actin-myosin of the mesoderm cells (Martin et al., 2009a). E-cadherin mediated cell-cell adhesion also plays a role in the epithelial sheet bending, as the absence of AJs during gastrulation results in widespread cell dissociation (Harris and Peifer, 2004). E-cadherins undergo several changes during ventral furrow formation. Initially, they are concentrated apically at the AJs during the transition to the wedge cell shape. During tissue internalization, AJs are destabilized as E-cadherin expression is downregulated by Snail-mediated repression (Ip et al., 1992), while N-cadherin is upregulated by Twist (Kosman et al., 1991; Leptin, 1991). As cells delaminate, the residual membrane associated E-cadherin then becomes distributed over the entire cell surface, before being degraded (Oda et al., 1998). This loss of E-cadherin is thought to be sufficient to induce many of the dramatic changes in polarity and morphology that characterize the transition from epithelial to mesenchymal cells. Thus, ventral furrow invagination is another example in which contractile acto-myosin meshworks act together with AJs to generate the force to drive single cell shape changes to induce tissue morphogenesis.

Dorsal closure constitutes a third example of integration of forces generated at the level of single cells to drive tissue morphogenesis in *Drosophila*. It takes place at the end of gastrulation and functions to close an elliptically shaped discontinuity on the dorsal surface of the embryo, which is covered by an extra-embryonic tissue, called amnioserosa (AS) (Jacinto et al., 2002). Closure proceeds from the anterior and posterior

ends (or canthi) of the opening towards the middle (Fig. 1.4C). This process requires the simultaneous efforts of the leading edge (LE) cells, which are migratory cells at the borders of the two epithelial sheets, and the amnioserosa, as contraction of the AS (Solon et al., 2009) is coupled to elongation and movement of the lateral epidermis towards the dorsal midline (Fernandez et al., 2007; Franke et al., 2005; Homem and Peifer, 2008; Kiehart et al., 2000). AS cells have an apical actomyosin network that forms a contractile meshwork, since laser incisions in the middle of the apical cortex relieve tension (Solon et al., 2009). Kierhart et al. (Kiehart et al., 2000) observed that amnioserosa cells constrict their apices and leave the epithelium into the interior of the embryo, where they start blebbing and fragment as they go to apoptosis. This was suggested to contribute to generate the force required to trigger dorsal closure, since the expression of anti-apoptotic and pro-apoptotic proteins respectively reduce and increase the rate of closure (Toyama et al., 2008).

Other forces act together with the AS cell contraction to drive this process. An acto-myosin cable beneath the cell membrane at the dorsalmost domain of LE cells act as a supra-cellular purse string (Kaltschmidt et al., 2002; Kiehart et al., 2000; Stronach and Perrimon, 2001; Young et al., 1991). Moreover, protrusions, filopodia and lamellipodia drive the elongation and adhesion of cells at the dorsal midline (Jacinto et al., 2000; Liu et al., 2008; Millard and Martin, 2008). Thus, several forces contribute to dorsal closure: i) contraction of the supra-cellular acto-myosin purse; ii) pulsatile contractions of AS cells; iii) AS cell apoptosis; and requires coordinated acto-myosin contraction acting together with AJs.

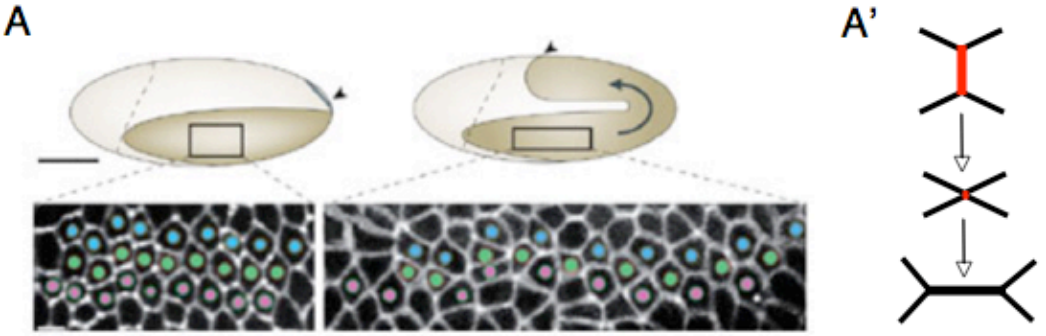

Lecuit and Lenne, 2007

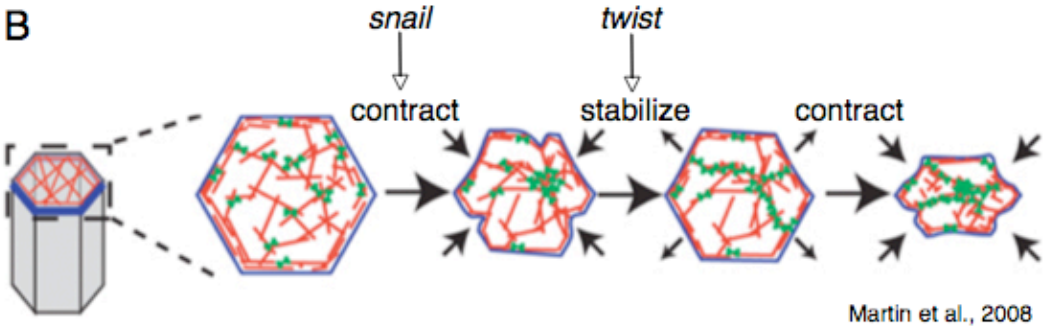

Martin et al., 2008

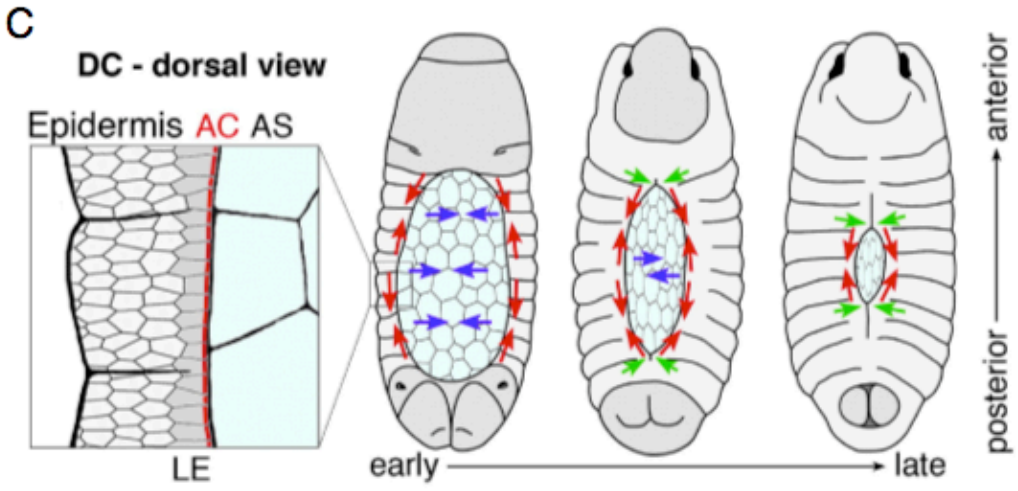

Solon et al., 2009

Figure 1.4 Force generation and transmission in morphogenesis: germband elongation, ventral furrow formation, dorsal closure

(A) germband extension of the embryo (above) and cell intercalation (below). (A') T1 transition. Myosin-II accumulation is indicated in red. (B) Apical constriction of cells from the ventral furrow is followed by stabilization of the constricted apex. Myosin is in green, actin in red. (C) dorsal closure (DC) of the embryo. Colored arrows indicate forces produced by AS cells (blue), actin cable (red), and zippering of the leading edge (LE) (green).

1.2.2.2 Apoptotic cell extrusion

The interplay between AJs and the acto-myosin network is essential to maintain an intact epithelial barrier, during development and in the regulation of epithelial homeostasis in adult tissues, as cells change shape, divide and die. AJs and the acto-myosin network act together at the interface between dying cells and their neighbours, to ensure that the epithelial integrity is maintained. Thus, apoptotic cells are extruded from the epithelium through the formation of an acto-myosin ring. The contraction of this multicellular cable triggers cell extrusion and prevents the formation of gaps in the epithelium, since the neighbouring cells contract inward in the direction of the extruding cell, taking its space (Rosenblatt et al., 2001).

This process was shown in vivo and in vitro after UV irradiation (Rosenblatt et al., 2001), when apoptotic cells could be detected in a monolayer by condensed nuclei and the progressive accumulation of an acto-myosin ring. Inhibitors of either actin, Myosin-II and Rho, when injected in the neighbouring cells, inhibited this process, indicating that the contraction of this ring in the neighbours is Rho-mediated and essential for extrusion (Rosenblatt et al., 2001). The signal for extrusion is an early event in the apoptotic process, which precedes caspase activation and requires sphingosine-1-phosphatase receptor 2 activation in neighbouring cells (Gu et al., 2011). The bioactive lipid S1P produced by the apoptotic cell binds and activates S1P2 receptor, which triggers the contraction of an intercellular acto-myosin ring (Gu et al., 2011). However, during dorsal closure of *Drosophila*, apoptotic cell extrusion appears to be triggered by mithocondrial fragmentation, which precedes the activation of the apoptotic cascade and it is necessary and sufficient to induce delamination in AS cells (Muliyil et al., 2011).

Importantly, cells can be extruded either apically into the lumen of organs or basally from the tissue. The direction of extrusion is determined by the site of acto-myosin contraction. During apical extrusion, the actin ring is thicker and forms around the base of the cell, while during basal extrusion the ring forms at the plane of AJs. This decision is thought to be determined by the orientation of microtubules (Slattum et al., 2009). Apical extrusion requires reorientation of microtubule plus ends towards the basolateral

surface between the dying cell and the neighbouring cells. Destabilisation of microtubules with different drugs reduces the percentage of apically extruded cells in favor of basal extrusion (Slattum et al., 2009). Thus, microtubules appear to regulate basolateral contraction of the acto-myosin ring by localising p115 RhoGEF to activate Rho (Slattum et al., 2009).

The process of extrusion is evolutionary conserved in epithelial tissues and plays a key role in maintaining the integrity of the monolayer. In situations in which cell death is blocked such as in cancer, extruded cells may invade surrounding tissues to initiate metastasis. Thus, this mechanism has important implications not only in development but also in the molecular biology of cancer progression. Thus, single cell delamination has been described in several systems in *Drosophila* during development and in zebrafish embryogenesis.

In *Drosophila*, apoptotic cell extrusion appears to play a major role in shaping the tracheal system, generating dorsal branches of five cells at the end of development (Baer et al., 2011). Single cells delaminate from the tracheal system in the embryo and appear to be engulfed by macrophages. The detachment of single cells is preceded by apoptotic activation, as observed by activation of the apoptotic probe Apoliner (Bardet et al., 2008). Like in *Drosophila*, during zebrafish embryogenesis, cell extrusion contributes in shaping organs and tissues during development. This process consists on the removal of apoptotic cells following tissue remodeling, like the clearance of apoptotic cells in the tail bud of embryos or the retina cells in the developing eye (Cole and Ross, 2001). Interestingly, the peak of retinal cell death coincides with the initial outgrowth of the retinal ganglion cell axons, suggesting the hypothesis that the elimination of retinal cells creates space for axonal growth (Cole and Ross, 2001).

Cell extrusion, however, is not always associated with apoptosis, as in the case of zebrafish gastrulation, during mesoendodermal progenitor internalization (Montero et al., 2005). The mesoendoderm internalise by delamination of single cells, which change their adhesiveness up-regulating E-cadherin. This allows their internalization and

separation from the pool of ectodermal progenitor. Once delaminated, these cells do not die but undergo epithelial to mesenchymal transition (Montero et al., 2005).

1.3 The notum as a model system to study tissue refinement

The system chosen for this study is the *Drosophila* notum. The notum forms the dorsal thorax in the adult fly, a very well organized and patterned epithelium, in which mechanosensory bristles are evenly spaced (Simpson, 2007). This tissue arises during pupal development from two distinct epithelial sheets that approach and fuse at the midline to generate a continuous monolayer epithelium (Zeitlinger and Bohmann, 1999). Afterwards, a series of morphogenetic events contribute to reach the final shape and size of the tissue prior to hatching. Thus, the notum represents a good model system in which to study the process of tissue refinement at the end of development.

1.3.1 Thorax closure

The pupal notum is formed via a process called thorax closure, as two epithelial sheets of the two wing imaginal discs displace the polyploid cells of the larval tissue, which are extruded and die by apoptosis (Fig. 1.5A). The wing discs fuse at the midline between 6 and 8 hours after pupariation (AP) to form the dorsal thorax, or notum (Fig. 1.5B, C) (Zeitlinger and Bohmann, 1999). At 9 hours AP, the wing imaginal disc is attached to all its neighbouring discs: anteriorly, to the eye-antennal disc and the dorsal prothoracic disc and, posteriorly, to the abdomen and haltere disc (Fig.1.5D).

JNK signaling plays a central role in this process of thorax closure. JNK is a stress-induced kinase, which is activated when phosphorylated by Hemipterous (Hep), a JNKK JNK-kinase. Other components of the pathway include the transcription factors AP-1, dJun and Kayak (D-Fos) (Riesgo-Escovar and Hafen, 1997; Zeitlinger and Bohmann, 1999). All components of the pathway are required for the expression of Dpp and Puckered (Puc), a phosphatase that inactivates Bsk in a negative feedback loop. As a result, hypomorphic alleles of Hep and D-Fos or Puc overexpression all result in a

thorax cleft phenotype, due to failed thorax closure. JNK is activated in the cells of the leading edge by Fos, while Puc negatively regulates this process (Martin-Blanco et al., 2000; Zeitlinger and Bohmann, 1999). Thus, Puc is specifically expressed in the peripodial stalk and its expression broadens during the eversion of the disc, while Fos is expressed throughout the disc at different levels, with higher expression at the imaginal discs borders, where Puc is expressed (Agnes et al., 1999).

The movements of the imaginal discs towards the midline involves actin-myosin cables contraction, elongation of leading edge cells and the formation of extensive thick filopodia that contact the cells of the other wing disc (Martin-Blanco et al., 2000). Interestingly, this process is thought to be regulated by the small GTPase Cdc42, acting upstream of JNK signaling (Agnes et al., 1999), and Dpp signalling. Both Rac1 and Cdc42 drive upregulation of Puc and are activated by PVR, the *Drosophila* homolog of the PDGF/VEGF receptor (Ishimaru et al., 2004). In JNKK (*hep*) mutants, filopodia are rare and cell adhesiveness is compromised (Martin-Blanco et al., 2000), larval cells detach from each other and the wing imaginal discs cannot spread over the larval epidermis. Although Dpp signaling is activated downstream of JNK, Dpp is thought to specifically affect filopodia formation and cell polarity, but not the integrity of the larval epidermis. Dpp is initially expressed in a stripe along the A-P boundary, perpendicular to the future dorsal midline and in third instar larva, Dpp expression anteriorly overlaps Puc expression in the midline. As a result of the tightly regulated circuits that control thorax closure, mutations in genes affecting PVR, JNK and Dpp signaling pathways all lead to flies with a thorax cleft phenotype (Agnes et al., 1999; Martin-Blanco et al., 2000).

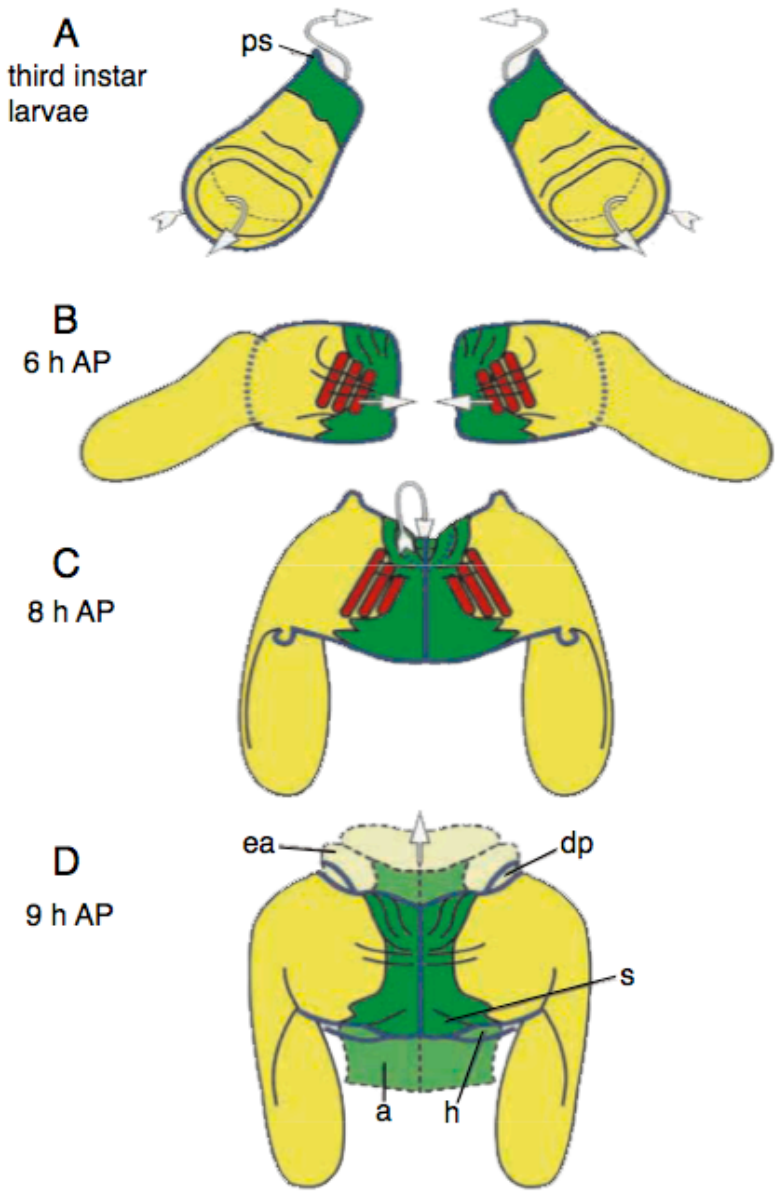

Zeitlinger and Bohmann, 1999

Figure 1.5 Thorax closure

(A) Wing imaginal disc eversion in third instar larvae. Abbreviation: ps, peripodial stalk. (B) The two epithelial sheets spread inside the pupal case. (C) Fusion of the wing discs at the midline. (D) The wing discs are attached to the other discs. Abbreviations: ea, eye-antennal disc; dp, dorsal prothoracic disc; a, abdomen; h, haltere disc; s, scutellum. The *pnr* expression domain is indicated in green; in red, oblique flight muscles. Arrows indicate imaginal discs eversion.

1.3.2 Patterning and pattern refinement of the notum

The notum is patterned by the activity of Apterous and Dpp, which activates Pannier (Pnr), a transcription factor of the GATA family, in the medial half of the tissue. Pnr restricts the expression of the selector gene Iro to the lateral half of the notum (Calleja et al., 2000; Cavodeassi et al., 2001; Cavodeassi et al., 2002; Sato and Saigo, 2000). The Iro complex encodes for homeodomain containing proteins and, together with Pnr, is responsible for patterning most of the notum (Gomez-Skarmeta et al., 1996; Ramain et al., 1993). A further subdivision of the tissue is made by Eyegone (Eye), a Pax-homeobox-containing gene, whose expression is restricted to the anterior part of the tissue (Aldaz et al., 2003). Pnr, Iro and Eye subdivide the notum into four distinct domains. Pnr activates Wingless, which activates the Achaete-Scute members of the basic helix–loop–helix family that, together with *daughterless,* determine bristle pre-patterning in *Drosophila* (Simpson, 2007).

In addition, Pannier and Apterous activate Stripe (Sr), while Wingless represses it. Stripe encodes for a transcription factor with zinc finger motifs, which represses bristle formation and is important for tendon development. Tendons, specified in the third instar larva, attach the indirect flight muscles (IFMs) that lie just below the surface of the notum to the cuticle, and are therefore important for the movement of the wings (Ghazi et al., 2000; Ghazi et al., 2003). Sr specifies tendon differentiation and is crucial for the establishment of the early espression pattern of muscle funders, starting during pupariation. This is suggested by the observation that flight muscles develop juxtaposed to Sr-attachment sites (Ghazi et al., 2003). The indirect flight muscles include 6 dorsal longitudinal muscles (DLMs) and 3 dorsoventral muscles (DVMs), which are attached to each hemi-notum by tendons.

The dorsal thorax of the adult fly exhibits a very precise and even pattern of mechanosensory bristles. Thus, it has been previously studied as a model of pattern formation in tissue morphogenesis (Cohen et al., 2011; Simpson et al., 1999). Bristles are distinguished in macrochaetes and microchaetes. Macrochaetes are large mechanosensory bristles, which are placed relatively precisely on the thorax during earlier stages of development and are conserved between different species (Usui and

Kimura, 1993). Microchaetes spacing instead varies between different species and between different animals within the same species, indicating that it is not precisely pre-patterned but is likely to be self-organising (Cohen et al., 2011; Simpson et al., 1999; Usui and Kimura, 1993). Microchaetes patterning is mediated by Delta-Notch lateral inhibition (Artavanis-Tsakonas et al., 1999; Hartenstein and Posakony, 1990; Heitzler and Simpson, 1991; Kooh et al., 1993; Parks and Muskavitch, 1993) and the gradual refinement of this pattern is dependent upon dynamic, basal actin-based filopodia (Cohen et al., 2011). This makes the notum an ideal system in which to study tissue refinement, since genetic variations could result in uneven bristle spacing and perturb tissue organization.

1.4 Aims of the thesis

Tissue morphogenesis is the result of a fine balance between different biological processes. Together cell growth and division, cell loss and cell shape changes generate the force that define the final size and shape of tissues in the adult. The development of the notum of *Drosophila* constitutes a good model system in which to study the interplay between these different processes. These all contribute to the gradual refinement of the tissue between 9 h AP and 26 h AP to give rise to a well-ordered adult epithelium. Thus, in this study I use this system to characterize the events that regulate tissue refinement in order to achieve a well-ordered epithelium. In particular, I analyse the balance between cell growth and cell loss and the contribution of these processes to tissue mechanics and cell organisation.

2. MATERIALS AND METHODS

2.1 Genetic techniques

Gene over-expression and dsRNA expression were driven using the GAL4/UAS system (Brand et al., 1994). The GAL4/UAS system derives from yeast and has been adapted for genetic manipulation in *Drosophila*. GAL4 is a DNA-binding protein that specifically recognizes target UAS motifs and binds to UAS sites in the genome. Thus, GAL4 expression regulates the expression of target genes downstream of UAS sites. Expression of GAL4 can be driven under the control of an inducible promoter or that of another gene to control gene expression in space and time. The generic GAL4/UAS system was used to drive the expression of a hairpin RNA. These double-stranded RNAs are processed within each cell by endogenous Dicer into siRNAs which direct sequence-specific degradation of the target mRNA.

Mitotic clones were generated by flp-FRT mediated mitotic recombination (Xu and Rubin, 1993), which generates mosaic patches of mutant tissue in a wildtype background. This technique takes the advantage of mitotic recombination between chromosomes within a single dividing cell. Recombination is promoted by flp recombinase activity under the control of a specific promoter. Flp induces recombination between specific target FRT sites. Mutant cells can be distinguished from the wildtype background by the differential expression of a reporter (GFP, RFP, lacZ).

The model system used in this thesis was notum development. For this reason, most perturbations relied on expression driven by the *pannier* promoter, which is active in the medial notum (Simpson, 2007). An additional driver used in this thesis is the ND638-GAL4, which is expressed in the lateral domain of the notum (Gerlitz et al., 2002).

2.2 Conditions

Stocks of *Drosophila Melanogaster* were maintained at 18ºC, 22ºC or 25ºC. Fly food was made as follows: 39 l dH2O, 675 g yeats, 390 g soy flour, 2.85 kg yellow cornmeal, 224 g agar, 3 l light corn syrup, 188 ml propionic acid. For starvation experiments, the concentration of dead yeast in the medium was decreased to 8 g in 1L of solution (De Moed et al., 1999).

Crosses were kept at 25ºC and dissected at pupal stages at 14h-16hAP. For RNAi experiments, males from each UAS-IR fly line were crossed with Ecad::GFP *pnr*-GAL4 virgin females. Crosses between UAS-hairpin RNAi males and Ecad::GFP *pnr*-GAL4 females were raised at 22 °C and shifted to 29 °C during larval stages. In the case of toxic dsRNA, crosses were raised at 25 °C or 18 °C.

All RNAi lines came from the Vienna *Drosophila* RNAi Center (VDRC) library and their details are published (Dietzl et al., 2007).

2.3 Fly stocks

The following stocks used are described in the indicated references:
pnr-GAL4 (3039; Bloomington *Drosophila* Stock Center (BDSC)), E-cadherin-GFP (Niimura et al.) (*ubi-DE-cad-GFP*) (Oda and Tsukita, 2001), E-cadherin-GFP (Niimura et al.) His-RFP (III) (*ubi-DE-cad-GFP/*CyO*;His-RFP/*TM6B) (gift from Franck Pichaud), *Act-5c*-GAL4 (25374; Bloomington *Drosophila* Stock Center (BDSC)), p110 over-expression (Niimura et al.) (*w;*UAS-*myc-Dp110*) (Leevers et al., 1996), DIAP1 over-expression (III) (if/CyO;UAS-*DIAP1*) (gift from Barry J. Thompson), TSC1 and TSC2 over-expression (III) (hsFLP;;UAS-*Tsc1,Tsc2*) (gift from Nic Tapon), *Resille::GFP* (Niimura et al.) (Morin et al., 2001).

E-cadherin::GFP was crossed with *pnr*-GAL4 line (*ubi-DE-cad-GFP;pnr*-GAL4/TM6B) to drive the expression of the dsRNA or ectopic genes previously mentioned. All RNAi lines used came from the Vienna *Drosophila* RNAi Center (VDRC) library (Dietzl et al., 2007), excluding the Cdc42 RNAi line (NIG-Fly library, stock ID 12530R-3). The list of RNAi lines used is shown in the table below (Table 3.1).

Gene name	**VDRC ID number**
Cdc25	17760
Fwe	1049932
Bsk (JNK)	34138
PI3K	38985
PTEN	35731
r5s	27792
Warts	9928

Table 3.1 List of RNAi lines used from the VDRC Drosophila stock center.

2.4 Live imaging and dissections

Live imaging (Georgiou et al., 2008) was performed by cutting a window in the pupal case attached to a slide with double-sided tape, and placing a coverslip carrying a drop of injection oil over the notum, supported by coverslips at either end. Nota were imaged from 14 hr AP for 12 hr during development. For stained tissues, nota from pupae 16 hr after pupariation (AP) were dissected in PBS for direct fixation in 4% formaldehyde for 20 min before being permeabilized by PBS containing 0.1% Triton X-100 (PBT). The nota were then stained 2 hr at RT with DAPI (Sigma) for nuclei and Alexa-568 Phalloidin (invitrogen) for actin. The acquisition was performed using a Leica SP2 laser scanning SP2 confocal microscope with 40X/1.3 oil objective for both fixed and live-imaging experiments, three or more animals were used for each experiment and, when data were quantified, significance was established with an unpaired t-test in Excel.

2.5 UV irradiation

Pupae were dissected at 15 hr AP and the exposed notum was irradiated with Stratalinker, 1800 at 10 mJ/cm^2. Pupae were imaged between 1h and 2h after irradiation.

2.6 Laser ablation

Single junctions in pupae at 14 hr-16 hr (early pupae) and 24 hr-26 hr (late pupae) were ablated using 730 nm multiphoton excitation from a Chameleon-XR Ti-Sapphire laser, under software control (AIM, Zeiss). A 3x3 pixel (pixel size, 0.17 μm) region of the junction was irradiated at slow scan speed (pixel dwell time, 2.56 μs) at 25% laser power, under software control. The amount of power required to ablate the junctions was determined empirically but the same amount was used in each experiment. (AIM, Zeiss). Ablations were triggered during time-lapse imaging (every 2s) using 488 nm light from an Ar-Kr laser coupled to a Zeiss 510NLO upright confocal microscope and 40X/1.3 oil objective. The Sapphire laser used for nano-ablation emits light in the NIR (near infrared) spectrum range, in ultrashort pulses with a pulsed energy of up to 170 kW and a repetition rate of 76 to 90 MHz. This high pulse repetition rate deposits lower pulse energies and have higher spatial resolution giving higher precision in the ablation mechanism, but causing higher generation of heat during the ablation. The laser beam excites fluorescence if at least two photons are absorbed within less than a femtosecond (10^{-15} s). This effect varies exponentially with the intensity of the excitation light. Thus, the probability of excitation is maximum at the objective focus, outside of which drops radically. Since the energy of a photon is inversely proportional to its wavelength, the two absorbed photons must have a wavelength about twice that required for one-photon excitation. For laser nano-dissection we needed a high energy light, the ultraviolet light (approximately 350 nanometers wavelength), which can be excited by two photons of near-infrared light (approximately 700 nanometers wavelength) if both reach the spot at the same time. This methodology of nano-ablation has been previously used in developing *Drosophila* embryos (Cavey et al., 2008).

Laser ablation of single junctions was monitored by ablation of E-cadherin::GFP at the AJs. However, other molecules associated with AJs are ablated, in particular the acto-myosin cytoskeleton.

2.7 Dextran assay

Nota were dissected in Serum-free M3 medium. After dissection, serum-free M3 medium containing 0.3 mM TRITC-labeled low-molecular-weight Dextran (Molecular Probes) was added for 20 minutes at RT. The tissue was then washed in serum-free M3, fixed and stained for immunocytochemistry (Georgiou et al., 2008).

2.8 Cell tracking and quantification

The percentage of cell delamination was quantified by manually tracking all the cells (n=900 cells) in a field of view of a confocal microscope (275 μm x 275 μm) for each notum. An average percentage of delaminating cells was calculated on 3 different pupae for each genotype. A Student t-test in Excel was used to calculate the *P* value in comparison with the control. The midline was defined by the elongated shape of the cells and included 150 cells on 4-5 rows. Cells with elongated shape were positive for Puc-LacZ staining.

2.9 Image processing and analysis

The images presented were processed using ImageJ (http://rsb.info.nih.gov/ij/) and Adobe Photoshop CS (Adobe Systems, Inc., San Jose, CA). Unless otherwise noted, images of the tissue represent maximum intensity z-projections, with z-slice of 0.9 μm. In the case of laser ablation the vertex displacement after cut was measured after visualizing the junction displacements over time with the ImageJ plugin Kymograph.

For each case, statistics were calculated with Student t-test on 15 junctions, in 5 different pupae.

Myosin-II:Cherry intensity was quantified on a single z apical slice in the red channel with Image J. A region was drawn around the apex of delaminating cell to measure Myosin-II pixel intensity (Analyze>Measure>mean pixel intensity) at each time point. A region of equal area was selected in the background and the mean obtained was subtracted to the one measured for Myosin-II. The subtracted value of Myosin-II intensity for each time point was plotted in a curve.

3. THE MORPHOGENESIS OF THE NOTUM

3.1 Introduction

The *Drosophila* notum is formed through a process called thorax closure (Zeitlinger and Bohmann, 1999) and act as a mechanical platform for flight muscles, which are attached to the cuticles through tendons (Fernandes et al., 1996; Lee et al., 1995). The two wing imaginal discs evert and approach each other at the midline to form a continuous epithelium, giving the dorsal thorax by 6-8h AP. Actin fibers are enriched at the midline where the two epithelial sheets fused (Martin-Blanco et al., 2000). The margin cells that undergo the most substantial rearrangements are characterized by increased JNK signaling and Puc expression (Zeitlinger and Bohmann, 1999). JNK and Dpp are required for thorax closure. The spreading of the wing imaginal disc epithelia is driven by accumulation of filopodia-based actin bridges that enable them to replace the larval tissue (Martin-Blanco et al., 2000). Moreover, Dpp contributes to activate selector factors such as Pannier and Iro, which together contribute to the patterning of the whole notum (Simpson, 2007).

The final stages of notum development, between 12h and 26h after pupariation (AP), represent an ideal setting in which to examine the mechanisms involved in achieving the completion of development. First, the midline of the notum is the result of the fusion of two distinct tissues to give rise to a continuous epithelium, which needs to rearrange in order to reach mechanical equilibrium. Second, the topological rearrangements accompanying tissue refinement involve substantial changes in cell shape and packing, without concomitant changes in overall tissue form or size (Cohen et al., 2011). Cells in the midline have a very anisotropic shape at the beginning of this process, but by 26h AP they are isotropic in shape and cannot be distinguished from the other epithelial cells in the tissue. This represents a simple model in which to understand the generic mechanisms that establish and maintain a well-ordered tissue in multicellular organisms. During this period of development three major events contribute to the final refinement of the tissue. First, cells change position through topological rearrangements common to epithelial tissues, called T1 transitions (Fristrom, 1988). Second, cells complete one wave of cell division. This begins at 16h AP and is mostly complete by 24h AP. Third,

we observe a significant level of regionalized epithelial cell delamination in this tissue, which predominates in the midline region of the notum.

The aim of this chapter is to investigate the role of delamination in the morphogenesis of the notum. Since this process is prevalent in the midline, we analysed the morphology of midline cells and the forces acting on this region of the tissue. We tested the forces by measuring the recoil after laser-induced ablation of single junctions (Bertet et al., 2004).

3.2 Characterisation of the topology of the system

To study morphogenesis of the pupal notum, we analysed the form and topology of the tissue during this final step of development from 14h AP to 26h AP by imaging the tissue marked with E-cadherin::GFP for 12h AP every 5 min. The notum of the pupa has a curved shape and a subtle furrowing at the midline (Fig. 3.1). To analyse the order and topology of the system we used a software able to track cells in tissues, called Packing Analyzer © (2007-2010 Benoit Aigouy), which detects the geometry of epithelial tissues, segments epithelial cells and tracks cells over time. We first compared the geometry of midline cells versus outside the midline, since they appeared to have distinct morphologies. Cells within the midline of the tissue were on average 2.7 fold longer than they were wide when measured along the anterior-posterior axis of the animal, despite their having similar apical areas (48.5 ± 14.2 μm^2 in the midline and 51.3 ± 12.7 μm^2 outside the midline, n=30). By 26h AP, however, midline cells were isotropic in form and could no longer be distinguished from those outside the midline (Fig.3.2). A similar result was observed by looking at the nuclei morphology, visualized with His::RFP (Fig. 3.3). Nuclei in the midline region were found to be deformed, having a long/short axis ratio of 1.9 ± 0.4 (n=20), and were found at variable heights along the z-axis. By contrast, nuclei outside the midline appeared round, with a long/short axis ratio of 1.1 ± 0.1 (n=20), and were all found at the same apical-basal height. This suggests that midline cells are compressed. By 26h AP, however, nuclei in

the midline and outside the midline were indistinguishable, round in form and were all found in the same plane. This suggests an equilibration of tissue forces over time.

To analyse the order of the system, we plotted the polygonal distribution of the cells over time in the midline and outside, to understand change in topology of the cells in regions with different cell geometry (Fig. 3.4). The analysis of the experimental data suggests that cell proliferation, which starts around 16h AP, dominates tissue topology in the short term. Subsequently however, cell rearrangements bring the tissue into a well-ordered equilibrium state, resulting in hexagonal packing. As a starting condition, at 14h AP, less than 40% cells in the midline have a hexagonal configuration and 4-sided cells are common, (representing ~ 10% of the total). However, outside the midline, more than 50% of cells have a hexagonal shape as a starting condition, with no 4-sided cells at 14h AP. At 16h AP, when division starts, disorder is introduced into the tissue, and the number of cells with 6 neighbours drops throughout the tissue in favour of cells with fewer or higher number of sides. After relaxation post-division, number of hexagonal cells increases in the midline to 40 % and outside the midline to more than 50%, as it returns to a less disordered “equilibrium” state.

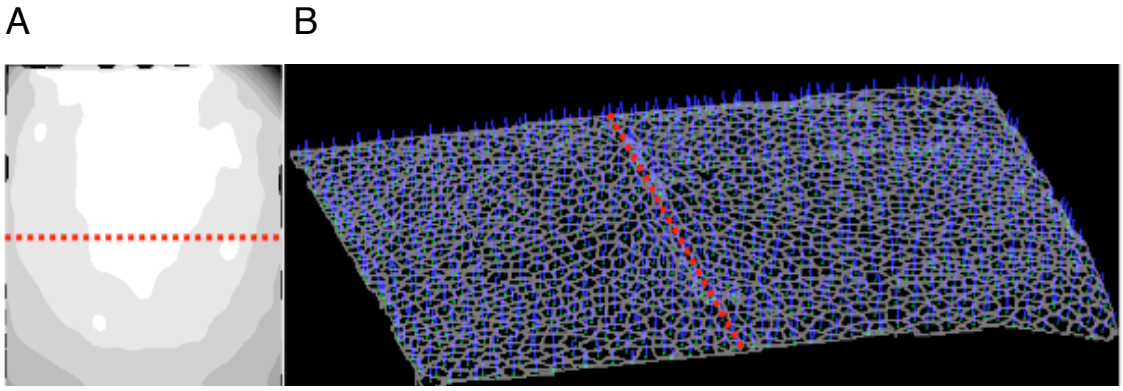

Figure 3.1 Shape and curvature of the developing notum

(A) Shape of the tissue surface, colour-coded by depth (the darker the deeper). The red dashed line indicates the midline. (B) Surface showing apical cell outlines in grey with normals to the surface for each cell in blue (midline is indicated by the red dashed line). There is negligible furrowing along the midline but a little curvature in the bottom right-hand corner.

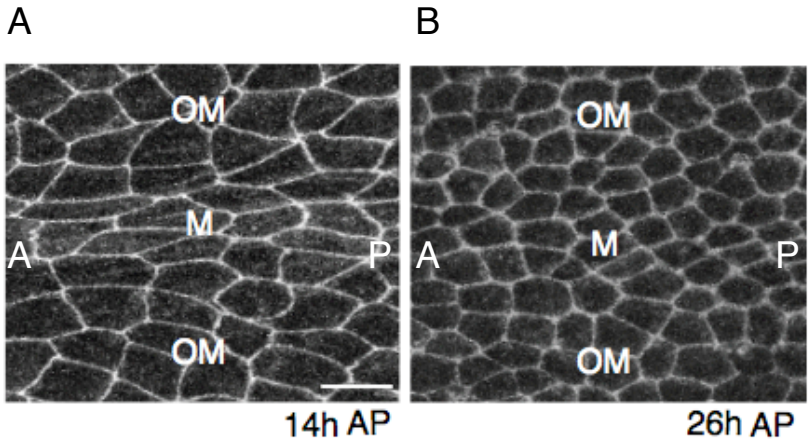

Figure 3.2 Midline cells have anisotropic shape at 14hAP but after 12 h of development assume an isotropic form

E-cadherin::GFP notum at 14h (A) and 26h AP (B). The midline is indicated with M in the tissue and OM for outside the midline. A=anterior; P=posterior of the notum.

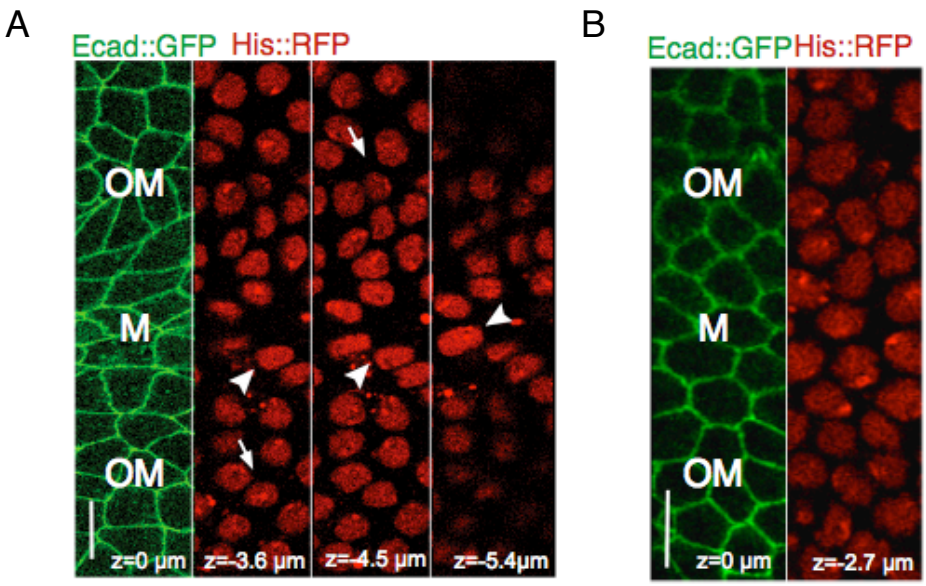

Figure 3.3 Midline cells nuclei have an elongated shape at 14hAP

E-cadherin::GFP His::RFP notum at 14h (A) and 26h AP (B) along different z-slices. Midline is indicated with M in the tissue and OM for outside the midline. In (A) midline nuclei are indicated by arrowheads and those outside the midline by arrows. Scale bar, 10 µm.

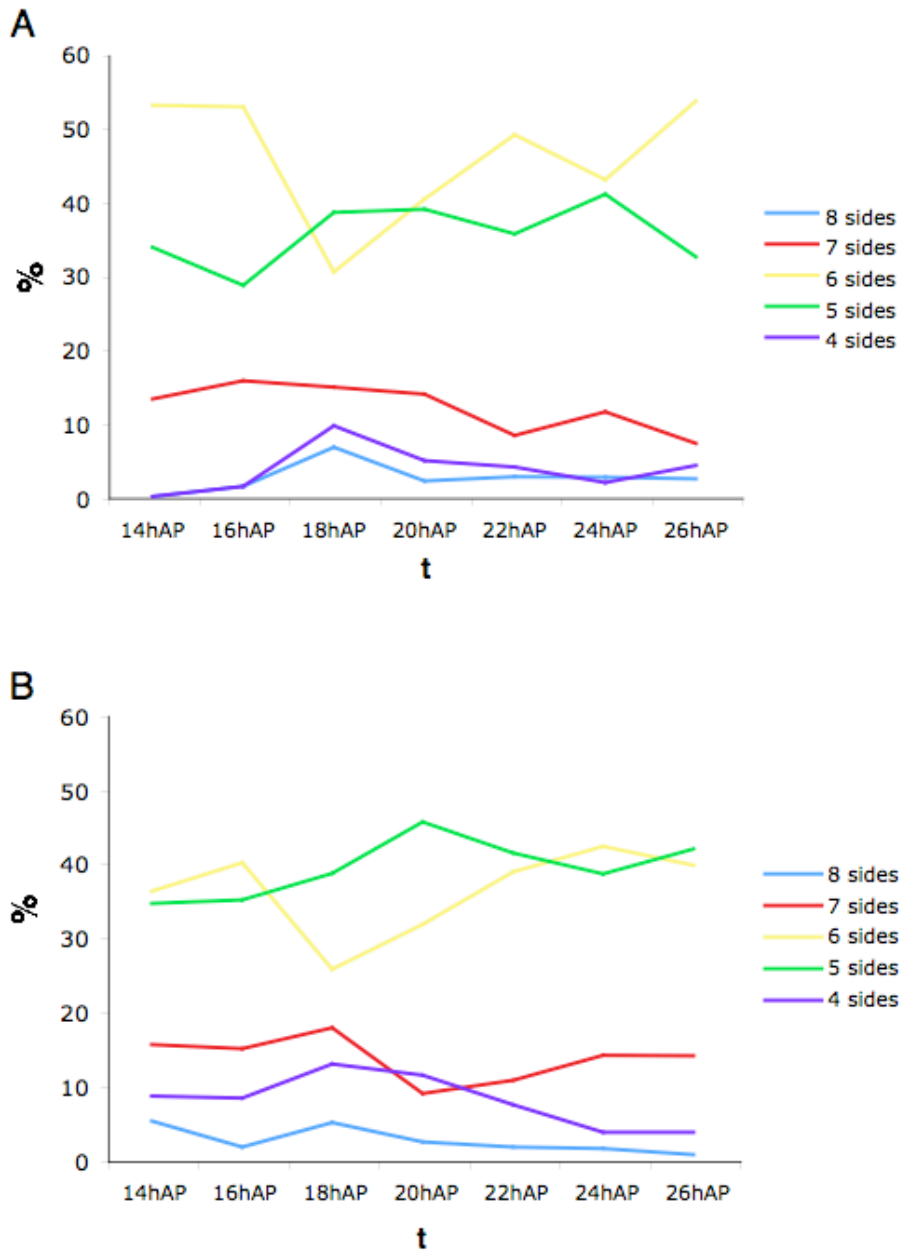

Figure 3.4 Polygon approximation for cells outside the midline (A) and in the midline (B) during development

The graphs show the polygon approximation percentage in the tissue during 12 h of development for outside midline (A) and midline (B). The graph shows the quantification of polygon approximation for one single notum in a region of 150 μm x 150 μm (n=300 cells), as a representative example.

3.3 Delamination during development of the notum

Using the constitutively expression of E-cadherin::GFP to follow apical junctional dynamics in the nota of wildtype animals during 12 h of development, we observed a significant level of regionalized epithelial cell delamination. This process is prevalent within the midline region, where 32.5 ± 13.6 % of cells underwent basal delamination, compared with 0.5 ± 0.3 % of cells in the surrounding tissue (mean ± s.d., n=4 pupae) (Fig. 3.5).

We analysed the distribution of delaminating cells in the whole notum for 4 different pupae and did not observe any simple rule regulating delamination in the tissue. The process is therefore likely to be stochastic. Several observations supported this hypothesis. First, the pattern of delamination varied between animals (Fig. 3.6) and was not symmetric across the midline. In addition, a variable proportion of midline cells left the tissue before and after division and, in many instances, only one of two sister epithelial cells underwent basal delamination (Fig. 3.6). Finally, cells delaminated from the tissue at variable time points over a 12 h period (Fig. 3.7). These observations rule out a simple role for cell lineage, position or developmental time; implying that delamination is a stochastic process.

Regionalised delamination therefore accompanies the topological rearrangement of the tissue to form a single, uniform monolayer epithelium. At the beginning of this process midline cells were anisotropic in shape. At the end, cells achieve an isotropic shape, suggesting a possible role for delamination in the developmental refinement of this tissue prior to terminal differentiation.

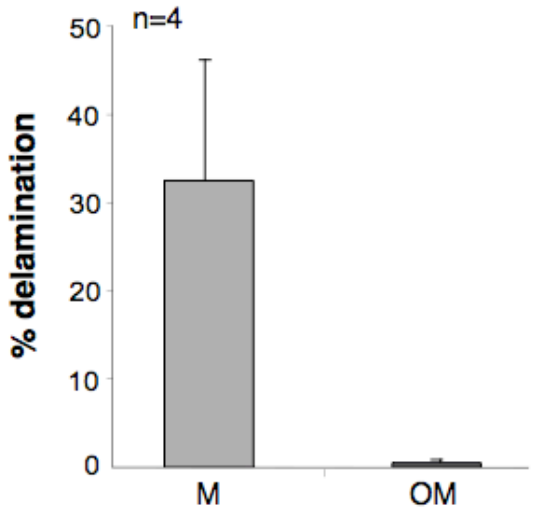

Figure 3.5 Delamination is prevalent within the midline of the notum

This graph shows the percentage of delaminating cells in the midline of the tissue (M) and outside the midline (OM). The percentage was calculated as the ratio between the number of cells, which delaminated in an 11h period and the total initial number of cells. The average and standard deviation were calculated between 4 different pupae. For each pupa, all the cells in a field of view were quantified (n=900). The midline was defined according to the shape of cells, including 4-5 rows of cells with elongated shape.

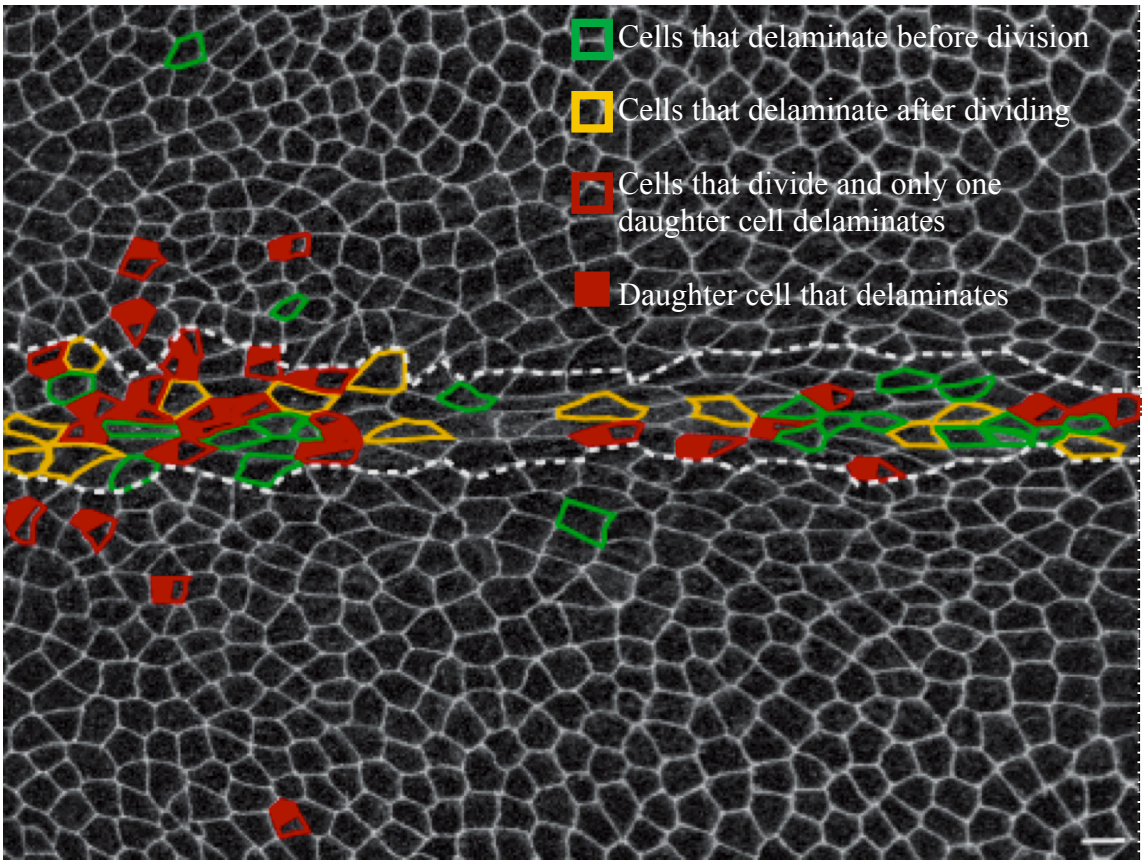

Figure 3.6 Delaminating cells have heterogeneous behaviour

E-cadherin::GFP notum at 14hAP. Cells delaminating between 14h and 26h AP were coloured according to their behaviour (see inset). Scale bar 10 μm.

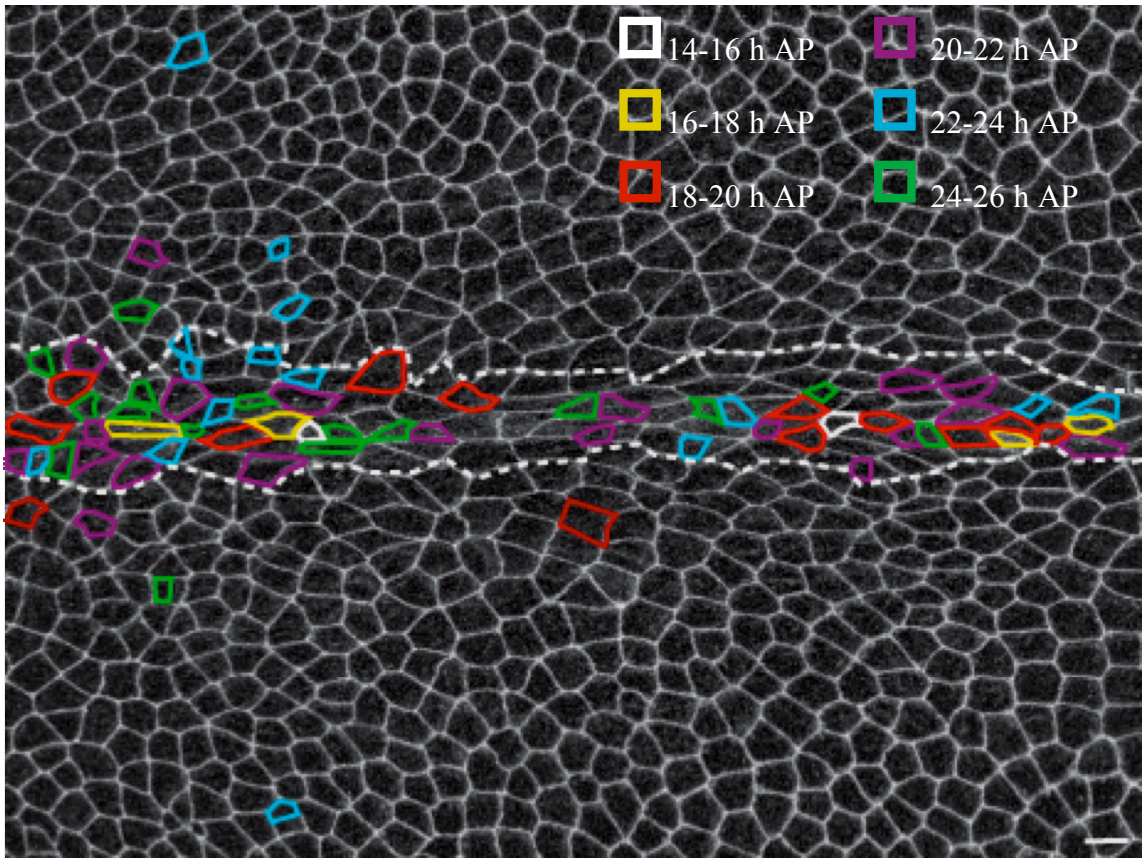

Figure 3.7 Cells delaminate during 12 h of development at different time points

E-cadherin::GFP notum at 14hAP. Cells delaminating between 14h and 26h AP were coloured according to time of delamination (see inset). Scale bar 10 µm.

3.4 Distribution of forces in the system

In order to understand how cells change their contacts, shape and position in the tissue, we analysed tissue mechanics in live organisms during development. The coordinated morphological and topological changes of single cells contribute on a larger scale to tissue morphogenesis. As cells grow, divide and change morphology, an intrinsic or resting tension develops within tissues and organs. This tension likely results from the contribution of force generation in individual cells that act in a coordinated fashion and external forces in the tissue (Kiehart et al., 2000). We analysed the distribution of forces in the developing notum by laser nano-dissection, which has frequently been used to study tissue mechanics during development. The relaxation of cell-cell interfaces after laser microsurgery is an indication of the distribution of forces in the tissue (Bertet et al., 2004; Hutson et al., 2003; Toyama et al., 2008).

To measure forces acting on cell-cell junctions in the developing notum, we used a multiphoton laser, which limits the ablated volume to very small regions. With short pulses, laser damage outside the focal volume is reduced since only a small amount of energy is deposited on the sample. In such a way it is possible to achieve sub-micrometer surgery that allows studies at a subcellular scale (Bertet et al., 2004). We focused on the plane of the adherens junctions and selected a small region of ablation (0.3 μm^2) in the centre of the junction, visualized by E-cadherin. The tissue was imaged every 2 s before and after laser ablation (with a 2 to 6 seconds delay following ablation) (Fig. 3.8). This enabled us to measure the vertex recoil, by calculating the increase in distance between the vertices after laser ablation. This vertex displacement is a measure of the resting tension along the junction, which is the result of the forces acting on that cell-cell contact (Bertet et al., 2004; Landsberg et al., 2009; Martin et al., 2009a; Rauzi et al., 2008).

To understand whether there was an anisotropic distribution of forces in the tissue, laser ablation was performed in the tissue for junctions in different directions (along the

anterior-posterior and dorsal-ventral axes). We then tested whether there was a difference in tissue mechanics in the midline, where cells have a distinct morphology early in development and delamination dominates, compared to junctions outside the midline. Each experiment was performed by simultaneous ablation of junctions within the midline and outside the midline, as an internal control. Moreover, the ablated cells were followed for up to 20 min after the cut to assess the extent of any damage. Cells were not irreversibly damaged and in all cells followed cell-cell contacts were re-established 10 min after the cut (Fig. 3.9).

The vertex displacement of junctions after laser ablation was measured by plotting a kymograph of the junction as a function of time (Fig. 3.10), and then by calculating the distance between the vertices for each time point. The vertex displacement was calculated at the initial phase of expansion, at 10 s and 16s after cut, extrapolated by the analysis of the kymograph and the quantification of vertex recoil velocity. These timepoints were chosen since at 10s there was a peak in the initial velocity, which started to decrese at 16 s. Vertex displacement is independent on junctional length (Fig. 3.11), so the measurements were not normalized for the initial length of the junctions.

Quantification of the vertex displacement over time following a junctional cut in the midline or outside the midline revealed a difference in local tissue mechanics in the two cases. At early stages of development, junctions outside the midline underwent significant vertex displacement following a laser cut, whereas vertices in the midline remained relatively unmoved (Fig. 3.12A and 3.13A). Junctions parallel and perpendicular to the anterior-posterior axis of the pupa showed a similar behaviour. In the case of perpendicular junctions, the vertex displacement in early pupae was 0.2 ± 0.3 μm at 10s and 0.3 ± 0.2 μm at 16s for midline junctions, 0.6 ± 0.2 μm at 10s and 0.7 ± 0.3 μm at 16s outside the midline (Fig. 3.12A), while for parallel junctions was 0.2 ± 0.2 μm at 10s and 0.4 ± 0.3 μm at 16s for midline junctions, 0.6 ± 0.4 at 10s and 0.7 ± 0.4 at 16 s outside the midline (Fig. 3.13A). By contrast, at 26h AP, when the tissue appeared to be at mechanical equilibrium, vertex displacement was found to be similar within and outside of the midline after laser cutting (Fig. 3.12B and 3.13B). In the case of

perpendicular junctions, the vertex displacement was 1.2 ± 0.6 μm at 10s and at 1.6 ± 0.5 μm at 16s for midline junctions, 1.2 ± 0.5 μm at 10s and 1.7 ± 0.8 μm at 16s outside the midline (Fig. 3.12B), while for parallel junctions was 1.2 ± 0.7 μm at 10s and 1.4 ± 0.7 μm at 16s for midline junctions, 1.2 ± 0.7 at 10s and 1.3 ± 0.7 at 16 s outside the midline (Fig. 3.13B).

These results suggest that, while at the beginning of tissue refinement cells in the midline appear to have different mechanical properties from cells outside the midline, tension is high and uniform later on during development.

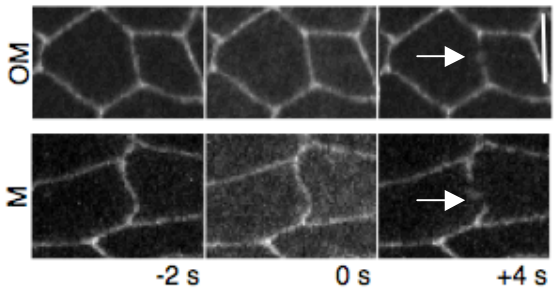

Figure 3.8 Time-lapse imaging during laser ablation

The tissue expresses E-cadherin::GFP. Images show the junction before laser cut (-2s), during cut (0s) and just after cut (+4s) for midline (M) and outside the midline (OM). Scale bar 5 µm.

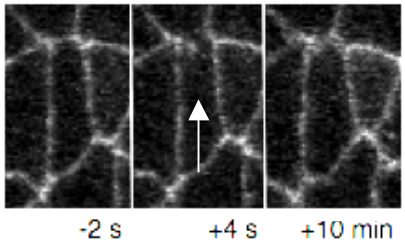

Figure 3.9 Cells are not irreversibly damaged after laser ablation, but are able to re-establish a junction

The tissue expresses E-cadherin::GFP. Images show the junction before laser cut (-2s), just after cut (+4s), as the junction is opening and after 10 min when the cell-cell contact has been re-established. Scale bar 5 µm.

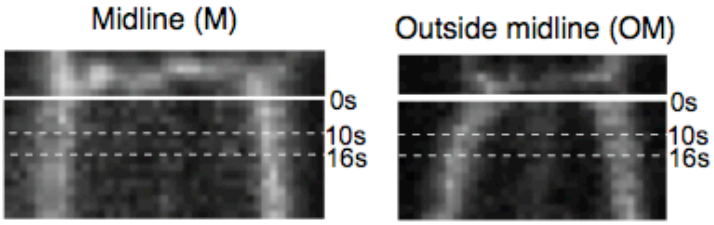

Figure 3.10 Kymograph analysis of vertex displacement

Images show the junction before the cut and the kymograph after the cut (0s). Dotted lines indicate 10s and 16s after cutting for a sample junction in the midline (M) and outside the midline (OM). Vertex displacement was calculated after plotting the kymograph, by measuring the distance between the vertices for each timepoint.

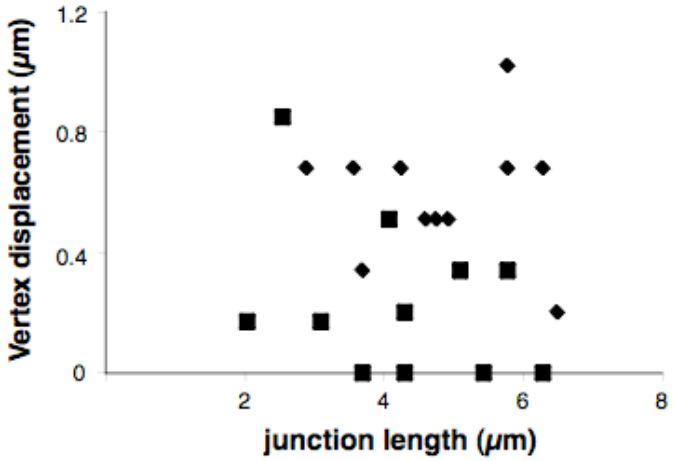

Figure 3.11 Vertex displacement does not correlate with junctional length

The graph shows a 2D plot of Vertex displacement versus junctional length. Each dot is a single junction. Squared dots indicate midline junctions, rhombi refer to junctions outside the midline. In both cases vertex displacement does not correlate with junctional length.

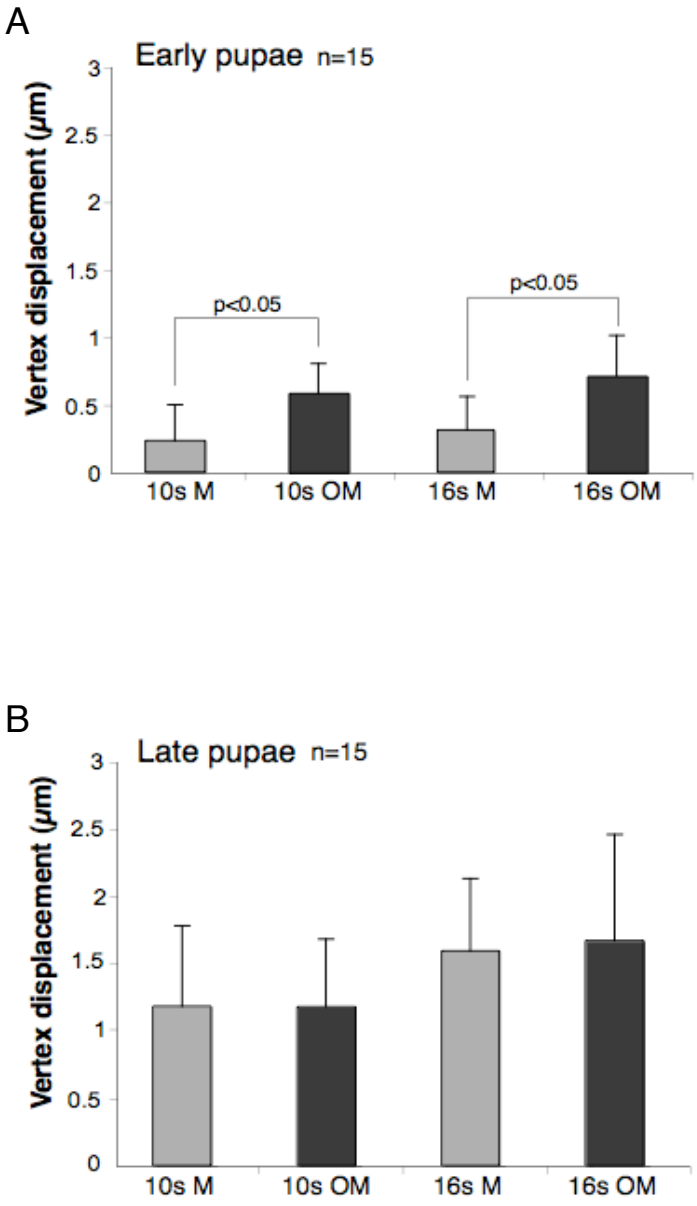

Figure 3.12 Vertex displacement quantification for cuts perpendicular to the anterior-posterior axis

Quantification of vertex displacement following a cut for single junctions perpendicular to the A-P axis of the animal. The graphs show the measurements after laser ablation for (A) early pupae (14h-16h AP) and (B) late pupae (24h-26h AP). Average and standard deviation for n=15 junctions from 5 different pupae. *P* value=0.003 both at 10s and 16s.

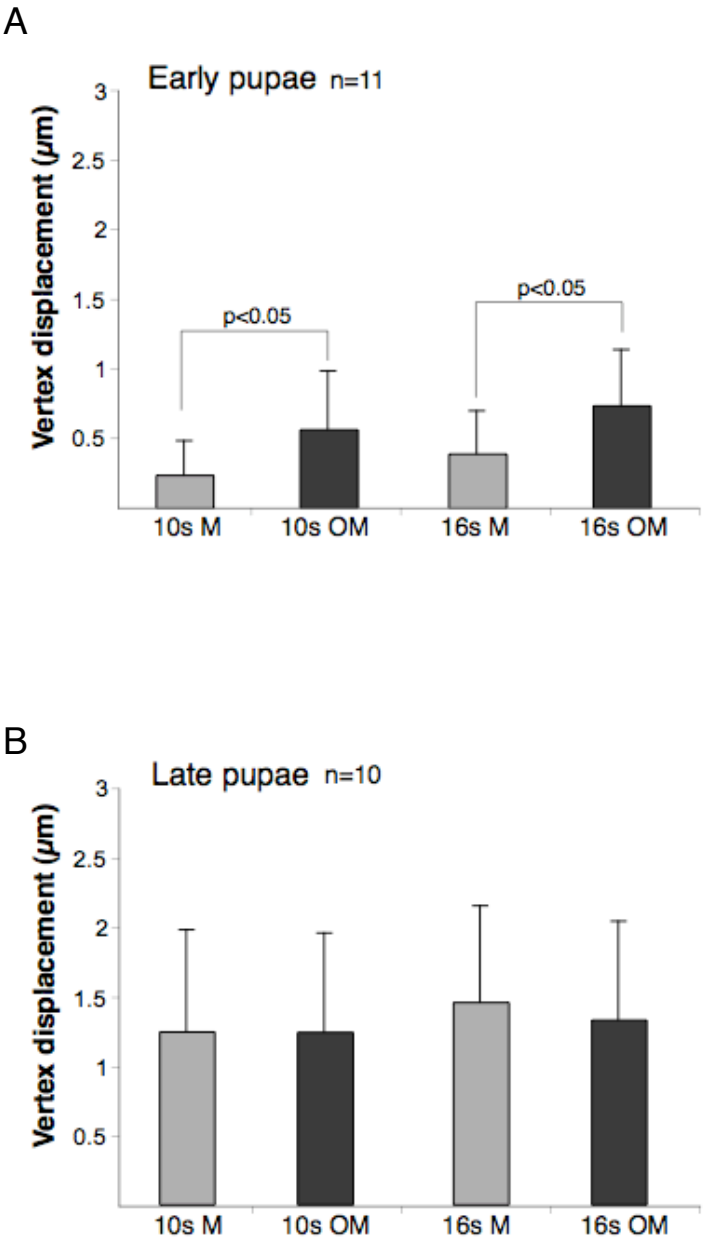

Figure 3.13 Vertex displacement quantification for cuts parallel to the anterior-posterior axis

Quantification of vertex displacement following a cut for single junctions parallel to the A-P axis of the animal. The graphs show the measurements after laser ablation for (A) early pupae (14h-16h AP) and (B) late pupae (24h-26h AP). Average and standard deviation for n=11 and n=10 junctions from 4 different pupae. *P* value=0.035 both at 10s and 16s.

3.5 Characterisation of individual cell contractility

Individual cell contractility is another important property that needs to be considered in developing epithelia in order to fully understand tissue mechanics and morphogenesis. To assess whether there was a difference in the tension generated by individual cells in the midline along the 2 axes, parallel and perpendicular to the midline, we decided to measure changes in apical area after laser ablation of adherens junctions connecting the cell to the rest of the tissue. In this way, the apical side of the cell could be isolated from the mechanical influence of junctions from its neighbours and its inherent apical contractility in different directions measured. After laser ablation, the apex of cells was reduced with similar speeds in both axes, parallel and perpendicular to the anterior-posterior axis of the animal. As a result, cells conserved their shape. Thus, elongated midline cells assumed an oval shape, while cells outside the midline assumed a more circular shape after laser-cutting (Fig. 3.14).

This analysis was then repeated for cells within the midline (n=5) and outside the midline (n=5), and results were quantified. The analysis of apical area changes, after the cell apex was isolated from its neighbours, revealed a heterogeneous cell behaviour (Fig. 3.15). Nevertheless, cells from the midline and outside the midline appeared to behave differently, although these results should be confirmed with a higher number of samples. During the first phase of loss of apical area, midline cells contracted less when isolated compared to cells outside the midline (Fig. 3.16). This could reflect the fact that cells outside and within the midline have distinct mechanics. Moreover, the 3 midline cells analysed relaxed back after cutting, starting to increase apical area between 240 s and 300 s. Cells outside the midline, however, were seen progressively decreasing in apical area at 300 s after laser-cutting and 2 cells started to relax back only 400 s after the cut (Fig. 3.15).

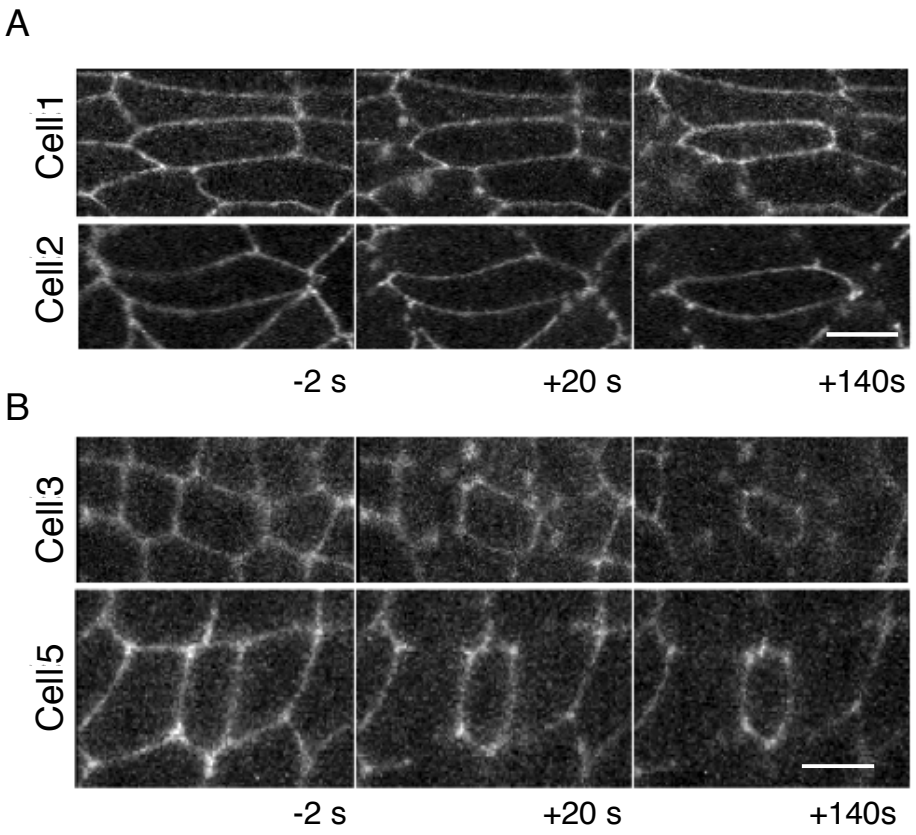

Figure 3.14 Cell contractility after laser ablation

The tissue expresses E-cadherin::GFP. Images show cells before laser cut (-2s), 20 s and 140 s after cut, when cells have been isolated and the apex is constricting. (A) midline cells number 1 and 2 (same as Fig. 3.15A). (B) Cells outside midline number 3 and 5 (same as Fig. 3.15B). Scale bar 5 μm.

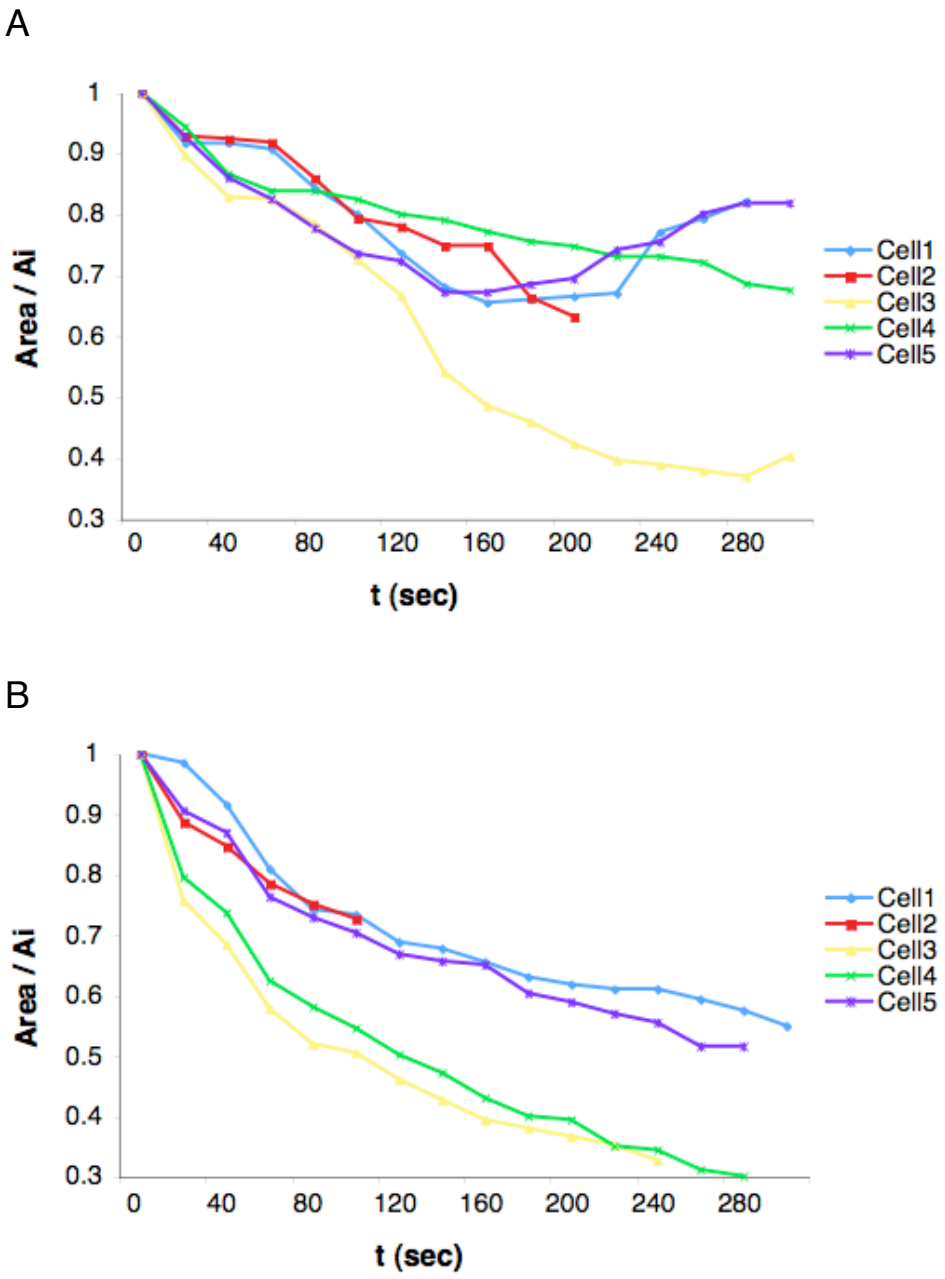

Figure 3.15 Area decrease quantification after laser nano-dissection

Quantification of decrease in area after cell apex has been isolated by laser nano-dissection. The graphs show the normalized area over the initial area for (A) midline and (B) outside midline cells. Each curve indicates a different cell (see inset).

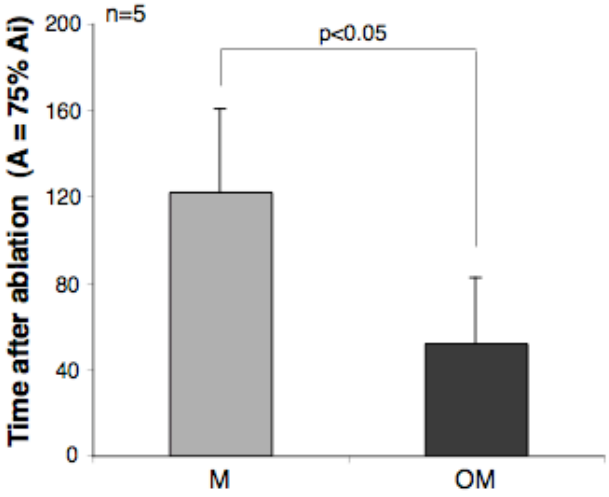

Figure 3.16 Midline cells decreased less in apical area after laser isolation

Average time for cells to decrease to 75% the initial area after cell apex has been isolated by laser nano-dissection in the midline and outside. In the midline, cell apical area contracts less. Number of cells = 5. *P* value is 0.013.

3.6 Myosin-II role in excitable cell contractility

Apical constriction of epithelial cells has been traditionally associated with Myosin-II cortical recruitment at cell-cell junctions, however recent studies have been shown that it is in fact driven by an apical medial actomyosin meshwork (Bertet et al., 2009; Bertet et al., 2004; Martin et al., 2009a). To understand the role of Myosin-II in tissue mechanics during development of the notum, we imaged the tissue marked with MyoII::GFP. In our movies, midline cells showed a meshwork of apical medial Myosin-II at 14h AP, together with junctional Myosin-II. Later in development at 26 h AP, Myosin-II was mainly localised along junctions (Fig. 3.17).

The analysis of the localisation and recruitment of Myosin-II, after laser ablation of junctions in the midline and outside the midline, suggested that the apical meshwork of medial Myosin-II could function in the response of midline cells to perturbation of the system over longer periods (Fig. 3.18). Midline cells started to constrict apically 200 s after laser cuts of single junctions, while we could not see any apical constriction outside the midline. In midline cells, apical constriction was concomitant with Myosin-II apical medial recruitment, a process similar to that previously reported for excitable pulsatile behaviour in other systems (Bertet et al., 2004; Martin et al., 2009a). After Myosin-II reached its highest intensity, the cells relaxed, increasing their apical area, and the junction was re-established. Thus, after disruption of tissue mechanics induced by laser nano-dissection, midline cells, which have high levels of apical Myosin-II, appeared more reactive and excitable than cells outside the midline. A potential explanation is that midline cells experience low tension along their junctions. Thus, following laser cut, cells sense a relative increase in tension, which could trigger activation of Myosin-II contractility. Then, the contracting cell pulls on neighbours, which in turn feel higher tension. This triggers the same Myosin-II dependent response.

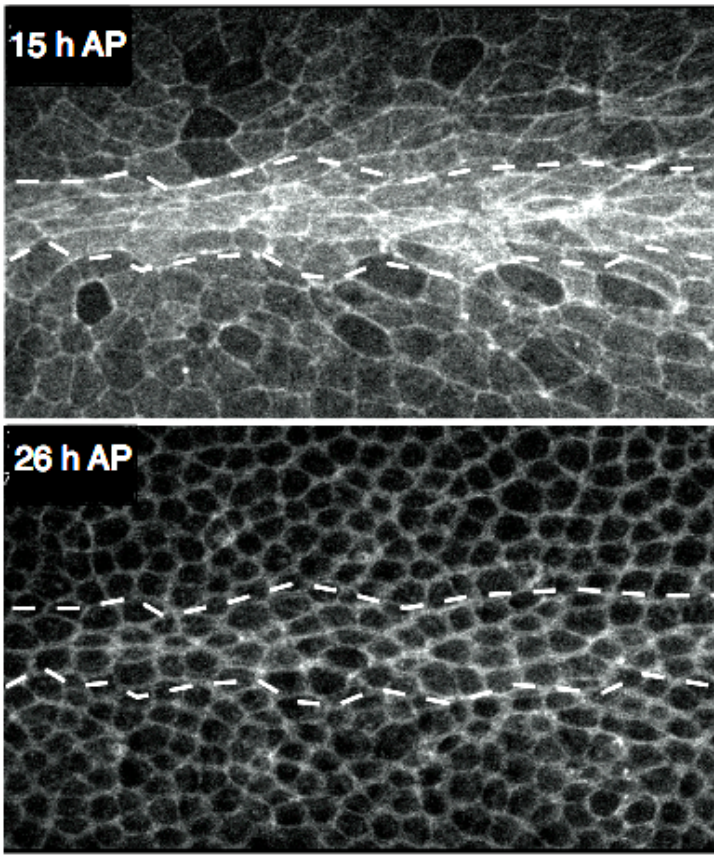

Figure 3.17 Midline cells showed junctional Myosin-II and a meshwork of apical medial Myosin-II

The figure shows stills from a 12h movie of the tissue marked with MyoII::GFP at 15 h AP and 26 h AP. The midline is indicated by the white dotted line.

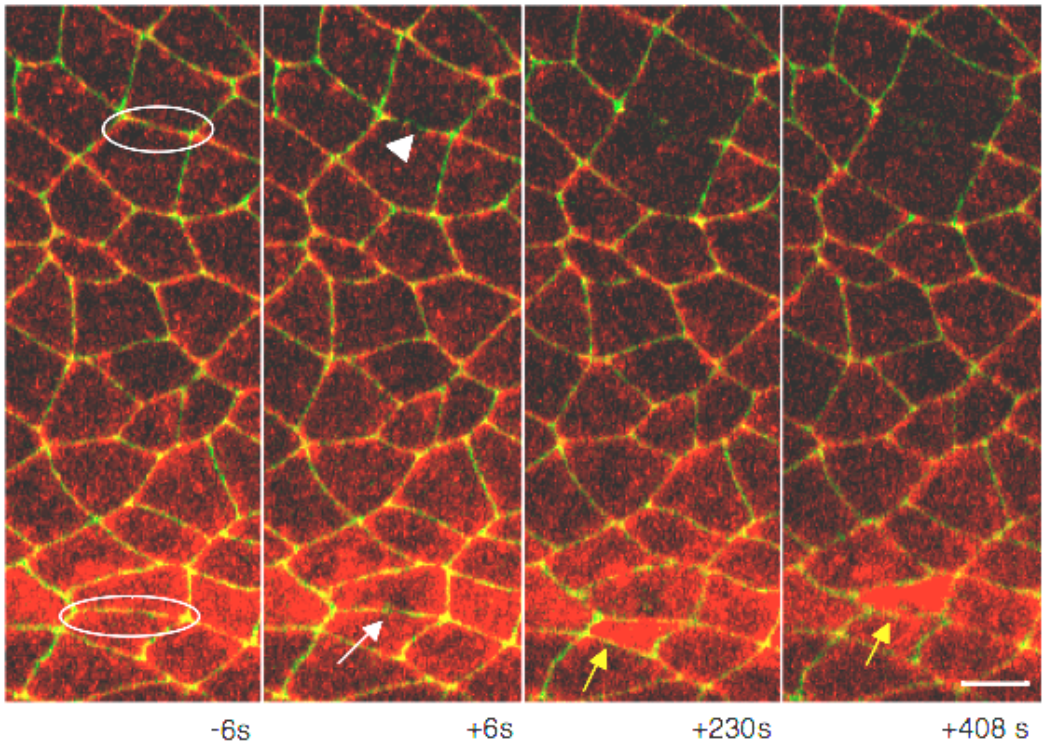

Figure 3.18 Midline cells appeared more reactive and excitable after perturbation induced by laser cut

The figure shows the tissue marked with E-cad::GFP and MyoII::Ch before laser ablation, 6 s, 230 s and 408 s after cutting (when the 2 cells showed the highest intensity of Myosin-II). The white arrow indicates the ablated junction within the midline, while the arrowhead indicates the ablated junction outside the midline. After ablation, midline cells transiently accumulate Myosin-II and constrict apically (indicated by the yellow arrows). They then pull on neighbours, which experience the same dynamic change in Myosin-II and apical area. Scale bar, 10 μm.

3.7 Conclusions

In this chapter, I characterised the model system used for my thesis project, the developing notum. The objective of my study was to investigate how a developing tissue achieves mechanical equilibrium in order to give the final shape of the adult epithelium. In this chapter I described the initial situation of the notum, early during morphogenesis (at 14 h AP), and its morphological and mechanical changes during 12 h of development. At 14 h AP, the midline of the notum is distinct from the rest of the tissue in terms of morphology, topology and tissue mechanics. Cells have an elongated shape and the number of 4-side cells is higher compared to outside the midline. This can be explained by the fact that cells, due to their anisotropic shape, have very long junctions along the A-P axis and very small junctions along the perpendicular axis. Thus, small junctions shrink to a vertex with a higher probability as a consequence of length fluctuation and topological rearrangements, resulting in a higher number of cells with few sides in the midline.

During this 12 h period of development, cell division, regionalised delamination and topological rearrangements of the tissue contribute to the formation of a single, uniform monolayer epithelium, which functions to support the flight muscles (Fernandes et al., 1996; Lee et al., 1995). The prevalence of cell delamination within the midline suggests a possible role for delamination in the developmental refinement of this tissue prior to terminal differentiation. This process could contribute to approach mechanical equilibrium in the developing dorsal thorax at late stages.

The initial situation of mechanical instability is reflected by distinct forces acting across the tissue, measured through laser ablation. In particular, this is represented by the difference in tissue mechanics between the midline and outside the midline of the tissue. Midline junctions showed a small vertex displacement after laser cutting, both in the parallel and perpendicular direction to the A-P axis of the notum, suggesting that this region may be under reduced tension. Thus, midline cells may experience distinct forces,

as suggested by nuclear shape and spreading along the Z plane. The initial shape of midline cells, however, does not reflect the forces acting on this region, since cells appear compressed from all directions. The initial form of the cells could be due to morphological events occurred after fusion of the two wing imaginal discs (Zeitlinger and Bohmann, 1999). The hypothesis that midline cells have distinct mechanics compared to the rest of the tissue is supported by laser isolation of cells from the tissue. Here, cells outside the midline, constrict apically for a longer time period and to greater extent compared to midline cells, before relaxing back. Cells which are not under tension show a higher sensitivity to any perturbation in the mechanical situation of the tissue, induced by laser ablation of junctions in this region. Thus, following laser cut, cells sense an increase in tension, which could trigger activation of Myosin-II contractility, which propagate in the neighbouring cells. Cells under isotropic tension instead seem to show a higher mechanical stability in reponse to perturbations. Another possible explanation of the behaviour observed after cell isolation could be due to the acto-myosin network, responsible for the contractility of cells after laser isolation. These results could reflect different localization and regulation of acto-myosin contractility, which pulls on adherens junctions generating apical constriction, in midline cells compared to cells outside the midline.

4. CELL DELAMINATION COUNTERBALANCES GROWTH IN THE DEVELOPING NOTUM

4.1 Introduction

Animal shape and size is controlled with extreme precision during development. Organs and tissues reach and maintain their form and size by coordinating three major processes: cell division, cellular growth (mass accumulation), and cell loss/survival. External factors such as nutrient availability and cell crowding can alter overall animal size, however local homeostatic interactions contribute to the achievement of the right shape and patterning of tissues. It has been previously shown that imaginal disc cells do not divide a fixed number of times, but they monitor their own growth and survival status relative to their neighbors (Johnston and Gallant, 2002). This kind of cell-cell communication responds to signals from the environment, such as nutrients availability, and promotes tissue plasticity and fitness in a changing environment (Bryant and Simpson, 1984; de la Cova et al., 2004; Johnston and Gallant, 2002). Tissue growth is promoted by Insulin/IGF Receptor (InR), PI3K and Target Of Rapamycin (TOR) pathways (Grewal, 2009; Wullschleger et al., 2006). The activation of PI3K and TOR pathways establish the basal growth rate of single cells in the tissue, and determine the final size of each organ and the animal as a whole.

The aim of this chapter is to characterise the mechanisms that contribute to the final shape and size of the developing notum, as the tissue achieves homeostasis. In particular we investigated how cell delamination and growth are coupled, by analysing how cell delamination responds to alterations in growth. Moreover, we studied the impact of environmental signals on the balance between cell loss and growth in the case of larval starvation, when the availability of nutrients is reduced.

4.2 Growth is regulated in the tissue by PI3K and TOR signaling pathways

Several groups have studied the role of insulin receptor (InR) in tissue size control in

Drosophila (Bohni et al., 1999; Chen et al., 1996; Leevers et al., 1996; Montagne et al., 1999; Weinkove et al., 1999). In particular, Leevers and her colleagues (Leevers et al., 1996) have shown that inhibition of PI3-kinase activity in the *Drosophila* wing disc reduces both cell size and number. Conversely, overactivation of PI3-kinase increases cell size, cell number and overall size. To alter overall tissue growth in the notum, we used RNAi to silence components of the PI3K and Hippo pathways. We used the *pnr*-GAL4 driver to induce dsRNA expression, since it defines the medial dorsal domain of the tissue. To increase growth in the tissue, several lines were used. Expression of the PI3K catalytic subunit p110 and silencing of PTEN, the phosphatidylinositol-3,4,5-trisphosphate 3-phosphatase, and of Warts, an inhibitor of the Hippo pathway, resulted in increased tissue growth. Conversely, expression of the tumor suppressors TSC1 and TSC2 and PI3K RNAi resulted in decreased growth. In addition, we silenced the ribosomal subunit r5S. However, in this case, the number of experiments was limited by the lethality of the RNAi. The only surviving animal showed reduction in growth.

4.2.1 PI3K activity affects cell size in the notum

Cell size in the tissue was quantified for all the lines tested, before the onset of division, by measuring: i) apical area, ii) tissue height. The average apical area within the *pnr* domain was significantly increased in p110 expressing tissues compared to the control and moderately increased in PTEN RNAi nota. However, increase in apical area was not observed in the case of Warts RNAi. Conversely, both TSC1 and TSC2 over-expression and PI3K RNAi led to a significant decrease in the apical area of the cells (Fig.4.1). Then, we measured the height of the tissue for all the lines tested. To quantify tissue height, nota were dissected from pupae at 16h AP and stained with DAPI and Phalloidin. For the analysis, xz slices were acquired from different regions of the tissue. Both upregulation of PI3K and the Hippo pathway caused an increase in tissue height, whereas inhibition of the PI3K pathway resulted in overall height decrease (Fig. 4.2). Together these data suggest that cell volume is significantly increased in tissues with increased PI3K activity (710.6 μm^3) and decreased when PI3K activity is inhibited (183.8 μm^3) compare to the control (358.4 μm^3). Warts RNAi, by contrast, leads to a cell density increase, but not a significant increase in cell volume (424.2 μm^3).

Significantly, in the case of both p110 overexpression and Warts RNAi, the overall increased growth resulted in folding of the tissue. In these regions, where cell density is increased, cells exhibited a smaller apical area (Fig. 4.3).

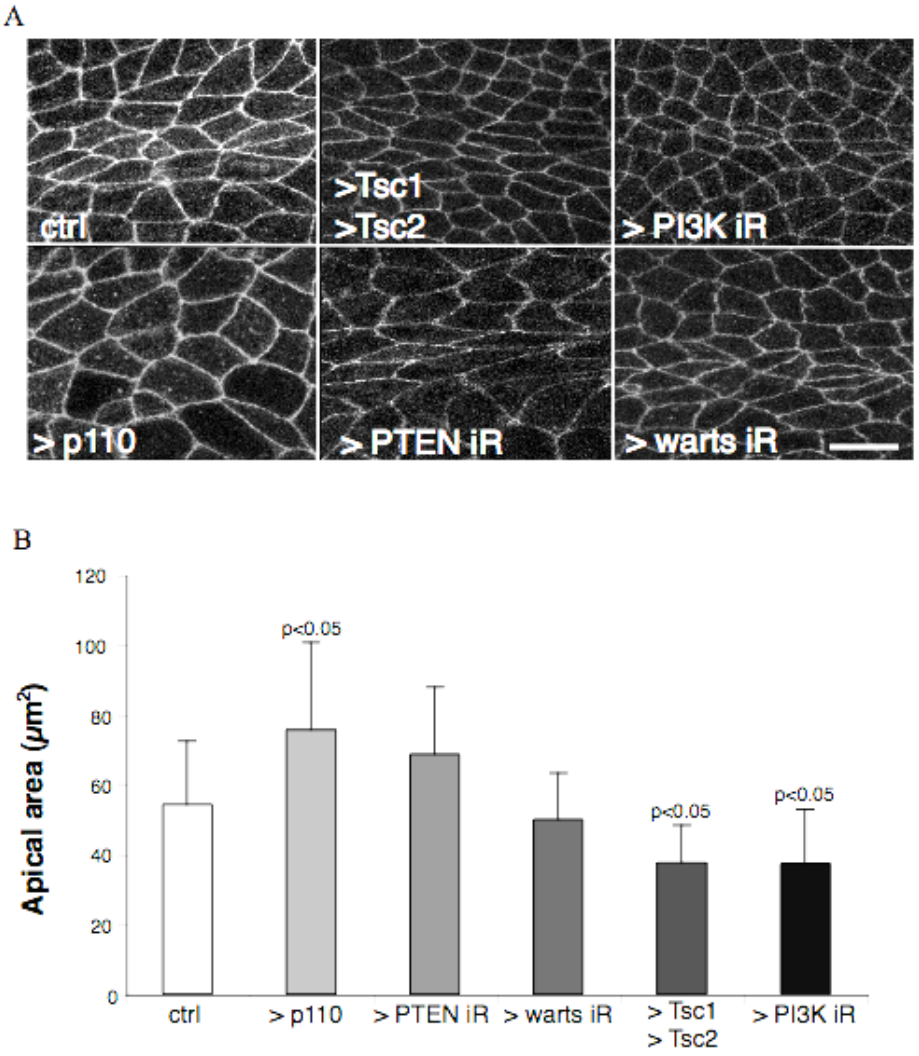

Figure 4.1 PI3K controls cell area in the notum

(A) E-cad::GFP expressing tissues from different lines. (B) Average apical area (n=20 different regions in the medial notum from 2 different pupae) for control and different mutant tissues. Scale bar, 10 μm. *P* values in order (0.03, 0.1, 0.5, 0.02, 0.03).

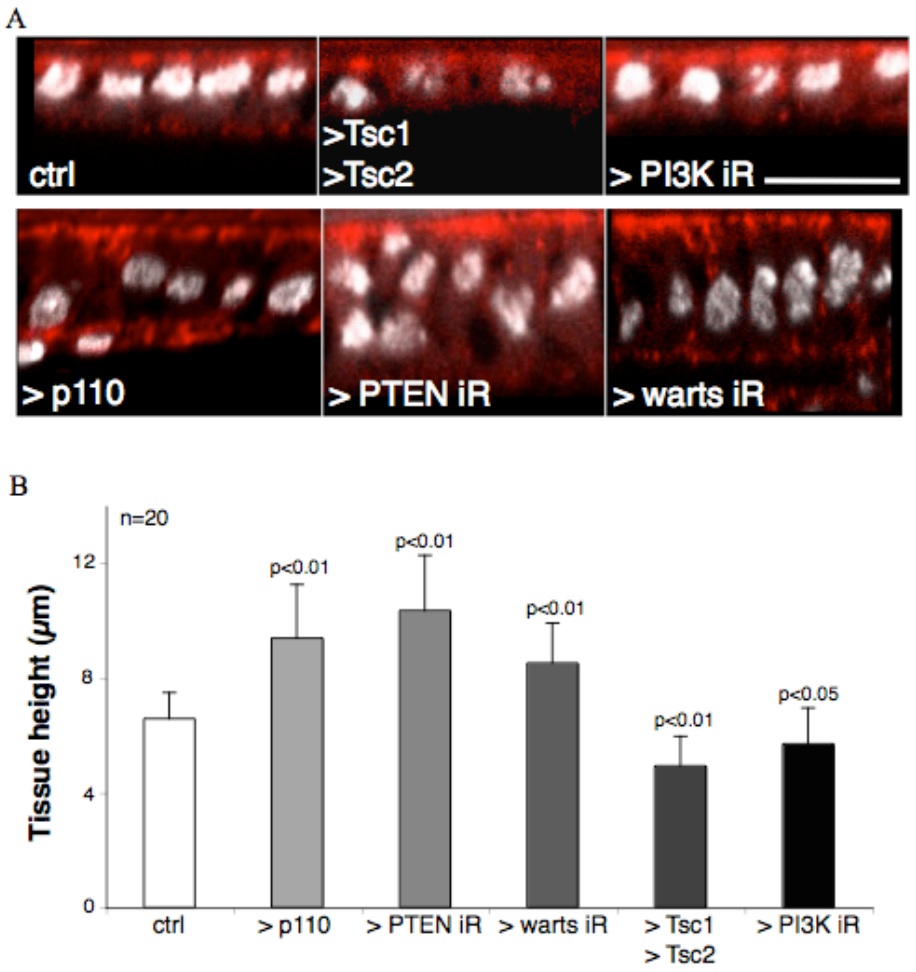

Figure 4.2 PI3K controls cell area in the notum

(A) xz axis of tissues stained with DAPI and Phalloidin. (B) Average tissue height (n=20 different regions from 4 different pupae) for control and different mutant tissues. The height is not uniform across the tissue, so each notum was divided in 5 regions and the height was measured. The *P* value refers to the height of different regions between different genotypes and takes into account the variability in height within each notum. Scale bar, 10 µm. *P* values in order (0.00001, 0.00001, 0.00001, 0.00001, 0.03).

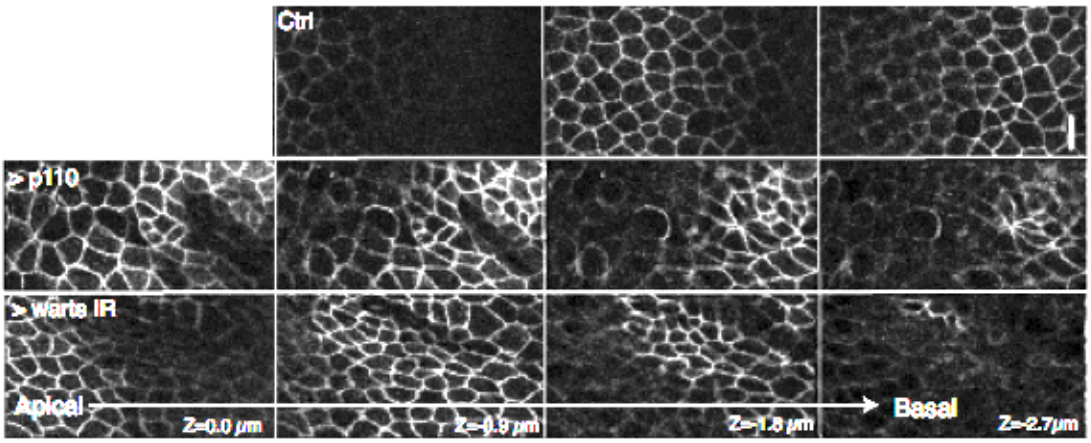

Figure 4.3 Increased growth by p110 expression and Warts iR in the notum results in tissue folding

xy planes of control, tissue expressing p110 PI3K and Warts iR marked with E-cadherin::GFP, for different z-slices. Scale bar, 10 µm.

4.2.2 Reduction in growth has an effect on tissue mechanics in early pupae

To test whether the changes in tissue growth lead to corresponding changes in tissue mechanics as predicted, we again used laser nano-dissection to measure tension across junctions in nota with increased and reduced growth. In tissues expressing p110 and Warts RNAi, the vertex displacement quantified for early pupae (14h-16h AP) after cutting (Fig. 4.4), was similar to the wildtype tissue (Fig. 3.11A). This can be explained by the fact that compression of cells within the layer is relieved by the buckling of cell layer out of the plane (Bertet et al., 2009) (Fig. 4.3). Due to the higher variability of the phenotype and lethality of PI3K RNAi and PTEN RNAi expression in the tissue, it was difficult to analyse vertex displacement in these lines. However, in animals expressing high levels of TSC1 and TSC2, where reduction in growth was most reproducible between different animals, junctional tension was high and uniform across the entire tissue in early pupae (Fig. 4.4). The graph in figure 4.4 shows analysis for junction perpendicular to the A-P axis of the tissue, however fewer cuts in the parallel axis revealed similar results. Thus, there appears to be a relationship between tissue growth, tissue mechanics and delamination.

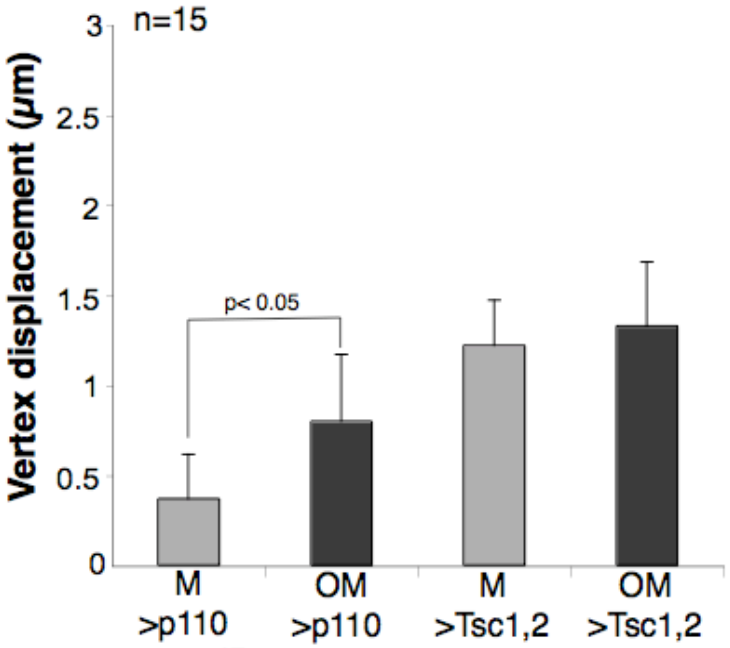

Figure 4.4 Decreased growth has an effect on tissue mechanics in early pupae

Quantification of vertex displacement after laser dissection of single junctions in early pupae for tissues expressing p110 and TSC1 and TSC2. The graphs show the measurements after laser ablation for early pupae (14h-16h AP) at 16s after laser cutting. Average and standard deviation for n=15 junctions from 5 different pupae. *P* value=0.01.

4.2.3 Cell growth and cell division are coupled in the notum

It has been previously shown that both PI3K and Hippo pathway upregulation increase cell number in the wing disc (Leevers et al., 1996; Tapon et al., 2002). Cell division was analysed in the case of increased and decreased growth, to understand whether cell density was affected in the tissue. During 12 h of development in the wildtype tissue, cells complete one wave of division, which starts in the tissue at 16h AP. Only few cells in the tissue divide twice during this time interval in the control. In the case of TSC1 and TSC2 expression, where the reduced growth phenotype was most reproducible, cell division started after 18 h AP, with 2h delay compared to the wildtype. In this tissue not all the cells completed the first wave of division, with ~10 % failing to divide in the 12 h period (n=500 cells, 3 different pupae). Thus, cell growth and cell division are related in the tissue. Conversely, in p110 overexpressing tissues, cell division started earlier in development. Around 15h AP cells were already dividing in the tissue and ~20 % of cells divided twice in 12 h. The phenotype was more variable in the other lines in which growth was increased. In the Warts RNAi tissue ~10 % of the cells divided twice in 12 h of development, with division starting at 16h AP (n=500 cells, 2 different pupae). Since warts RNAi expression did not lead to a substantial increase in cell volume, these data suggest that the effect on tissue buckling is the result of increased cell density.

4.3 Growth and cell delamination are coupled in the tissue

The lines tested for growth alteration in the notum were analysed for delamination rate, in order to understand whether delamination and growth were coupled in the tissue. In these pupae, changes in tissue growth in the notum led to a proportional effect on delamination rate.

In all cases, increased growth led to a corresponding increase in the rate of epithelial cell delamination, both within and outside the midline (Fig. 4.5 and 4.6). Under these conditions, rates of epithelial cell delamination were highest in crowded basal folds in

the epithelium that formed outside the midline as the result of tissue buckling (Fig. 4.7), where compressive forces would be expected to dominate. Conversely, delamination was significantly reduced in nota expressing p110 PI3K RNAi and following the expression of both TSC1 and TSC2 (Potter et al., 2001; Tapon et al., 2001) (Fig. 4.5 and 4.6), where growth was reduced, and was entirely absent in the rare surviving animals expressing RNAi targeting a subunit of the 5S ribosome, where growth was inhibited.

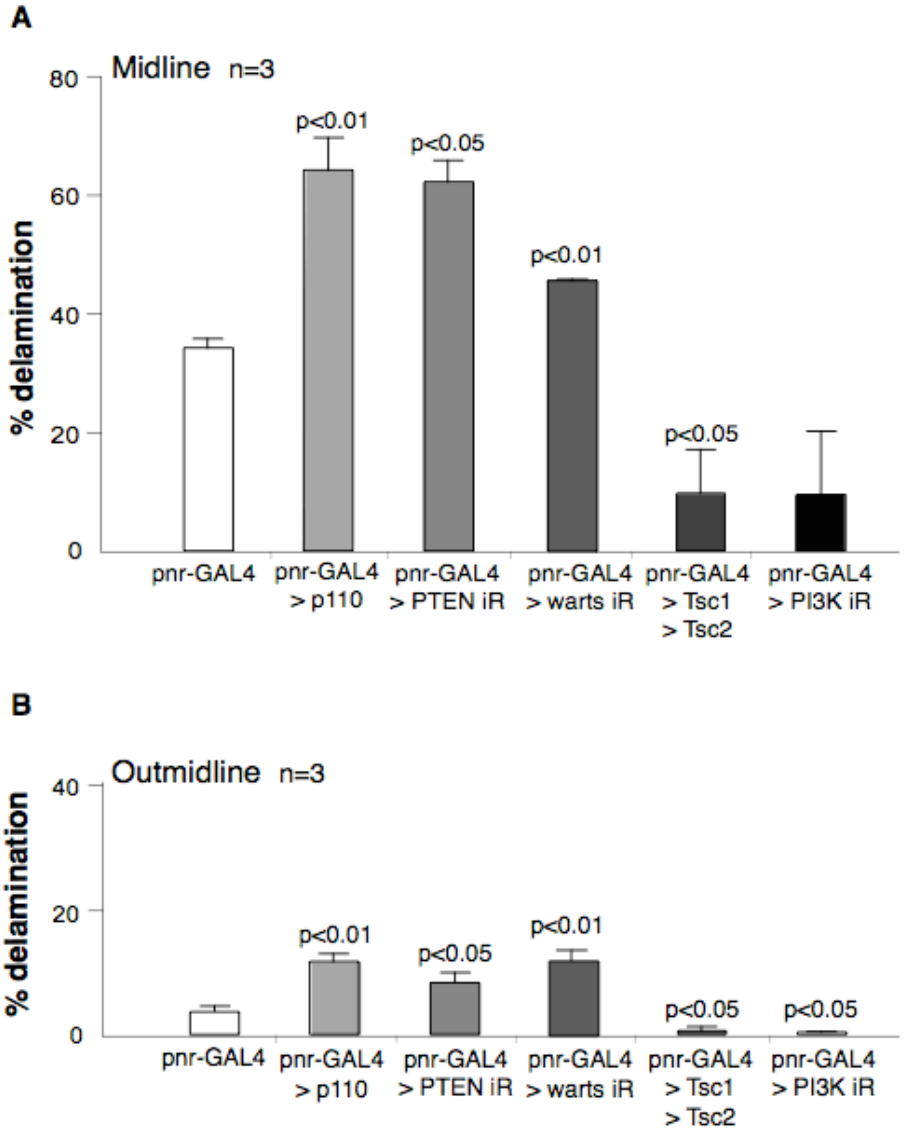

Figure 4.5 Delamination counter-balances tissue growth

Average rates of delamination (n=3 pupae) for cells in the midline (A) and outside midline (B) in control animals, in tissues where growth was increased (p110 PI3K expression, PTEN and Warts RNAi) and in nota with reduced growth (p110 PI3K RNAi, TSC1 and TSC2 expression). For each genotype all cells in a field of view (900 cells) for 3 different nota were quantified. The *P* value indicates the comparison with the control (Student t-test).

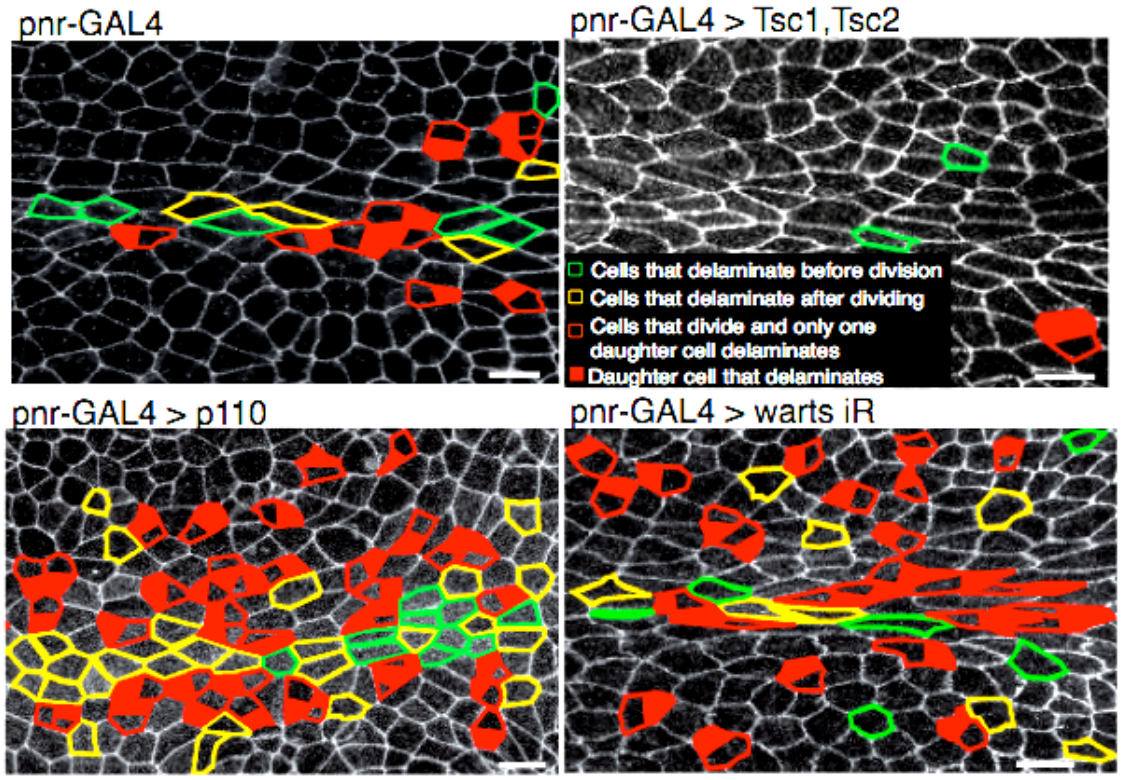

Figure 4.6 Delamination counter-balances tissue growth

Nota at 14h AP marked with E-cadherin::GFP. Cells delaminating were colored according to their behaviour (see inset). Scale bar, 10 µm.

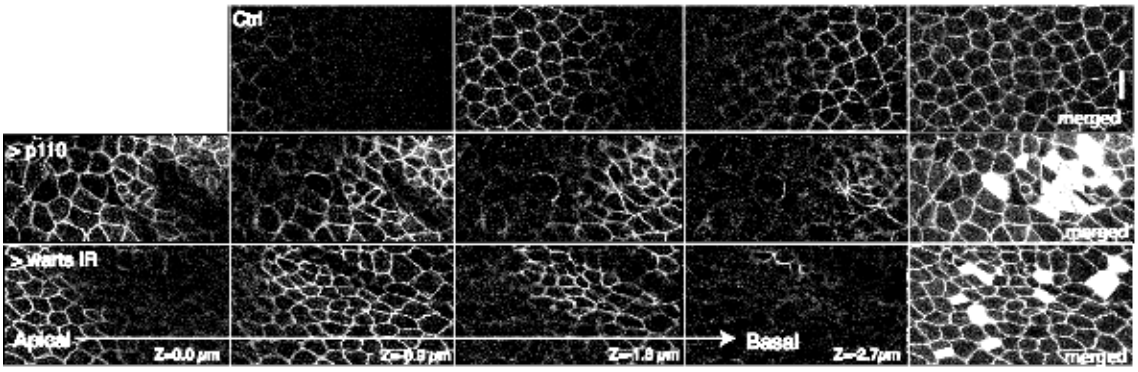

Figure 4.7 Cell delamination is highest in crowded basal folds in nota expressing p110 and Warts iR

xy planes of control notum, tissue expressing p110 PI3K and Warts iR marked with E-cadherin::GFP, for different z-slices. Cells delaminating from the tissue are coloured in white in the maximum Z projection. Scale bar, 10 µm.

4.4 Cell division is not required for delamination to occur

An effect on the timing and/or number of cell divisions in the tissue was observed in the lines tested, where growth was affected. As discussed in chapter 3, the onset of cell division during development resulted in topological changes in the epithelium, by introducing disorder in the tissue, and could influence tissue mechanics. To understand whether this process has an effect on cell delamination rate in the tissue, we overexpressed and silenced Cdc25 in the notum with the *pnr*-GAL4 driver. Cdc25 is a phosphatase that controls the progression through the cell cycle; by removing inhibitory phosphate residues from CDK1/cyclinB complex, Cdc25 promotes mitosis (Nurse, 1990).

The analysis of tissues overexpressing Cdc25, revealed a dramatic effect on the notum due to multiple divisions. The flies exhibited a severe thorax cleft phenotype, probably due to failed migration and closure of the 2 larval epithelia to give a continuous epithelium in the thorax. In these pupae, the midline was not properly sealed and the delamination rate could not be quantified (Fig. 4.8). In the case of Cdc25 RNAi however, despite the high temperature in which the flies were grown, the RNAi phenotype was mild, but led to a delay in the onset of division. Cell division was affected heterogeneously across the tissue, with 33.8 ± 12.4 % cells failing division in the midline and 55.5 ± 24.4 % cells outside the midline (mean ± standard deviation, number of nota = 3). Due to the high variability between different pupae and between different regions within the same tissue, we measured local correlations between cell delamination and division, in order to analyse the link between cell division and delamination in the system. If cell division has an effect on the latter process, cell delamination rates would be expected to correlate to the local division rate. However, cell delamination continued unabated in regions where cell division was inhibited (Fig. 4.9), suggesting that it is not required for delamination.

Taking advantage of this system to study the effects of delamination independently of division, we analysed the polygonal distribution of cells over time in Cdc25 RNAi

tissues, in which division is partially inhibited and delayed compare to the wildtype, to understand whether cell delamination contributes to achieve topological order in the system (Fig. 4.10). In Cdc25 RNAi tissues, the onset of division is 20-22 h AP (16 h AP in the wildtype), but cells delaminate from the tissue before the onset of division. Interestingly, in the midline of the tissue, the number of hexagonal cells increases between 14 h and 20 h AP. During this time interval, cells do not divide but delaminate from the tissue, and the latter process could be responsible for the increased order in the epithelium, measured by the increase in hexagonal packing. However, when division starts at 20 h AP, disorder is introduced into the tissue, and the number of hexagonal cells drops in favour of cells with fewer or higher number of sides.

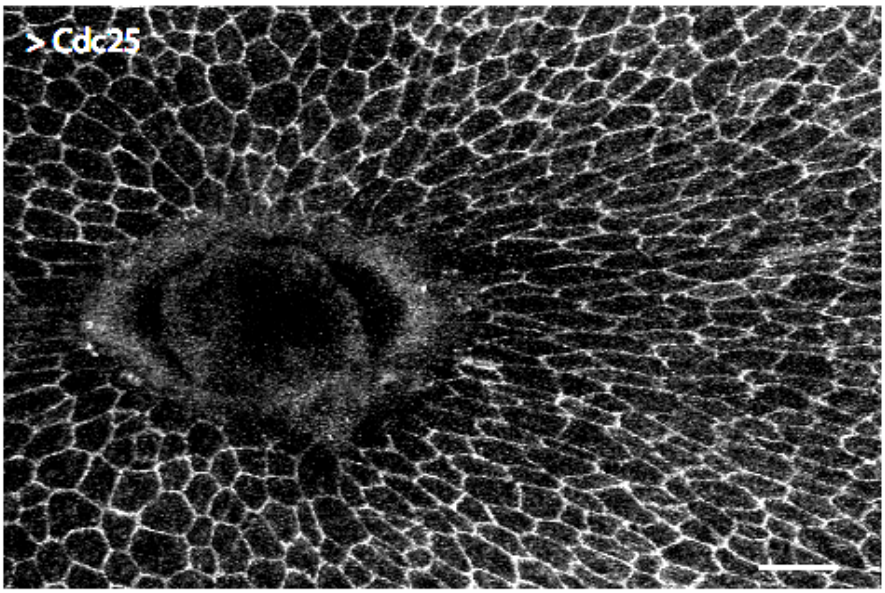

Figure 4.8 Cdc25 expression causes a thorax cleft phenotype in the notum, likely due to enhanced division

Cdc25 expressing tissue marked with E-cadherin::GFP. Scale bar, 10 μm.

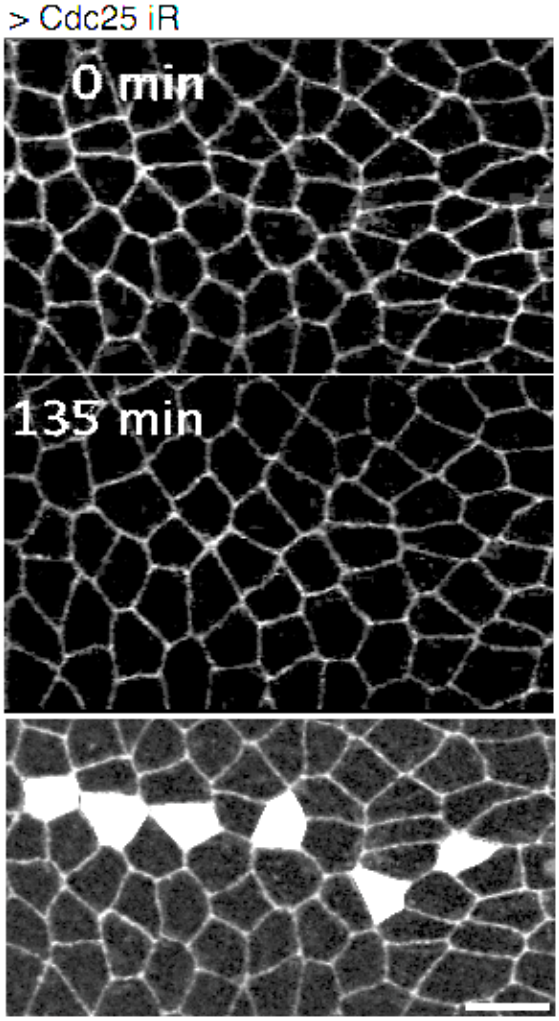

Figure 4.9 Cells delaminate in regions of Cdc25 iR tissues where division is completely inhibited

Tissue marked with E-cadherin::GFP expressing RNAi for Cdc25 at timepoint 0 and after 135 min. During this time interval cells do not divide but cells delaminate (coloured in white in the still). Scale bar, 10 μm.

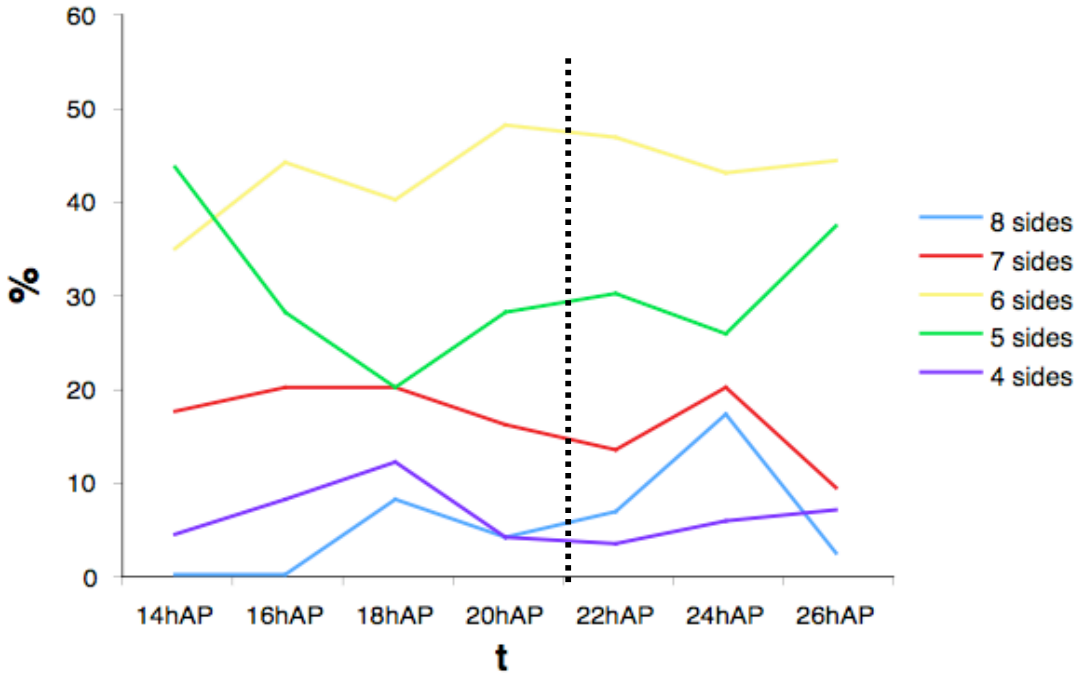

Figure 4.10 Polygon distribution for cells in the midline during development in Cdc25 iR

The graph shows the polygon distribution in the tissue during 12 h of development, for Cdc25 iR tissue. Note that in Cdc25 iR tissues cell division is delayed and start at 21-22h AP (indicated by the dashed line). This graph shows the polygon distribution for one representative notum for a region of 150 μm x 150 μm.

4.5 Cell delamination is a non-cell autonomous process

In all the cases discussed above, cell delamination was analysed in the midline and outside the midline, in the same cells in which growth was increased or decreased. To test whether this link between PI3K signaling, growth and delamination is cell autonomous, ND638-GAL4 was used to drive the expression of p110 PI3K, which most reproducibly increased growth in the tissue, and TSC1 and TSC2, which led to a significant decrease in cell size. ND638-GAL4 is expressed in the lateral dorsal thorax of the fly (Gerlitz et al., 2002), faraway from the midline of the tissue (Fig. 4.11). We then analysed the distribution and rate of delamination in the notum, to understand the effect of changes in tissue growth distally in the tissue and whether the process is cell autonomous.

TSC1 and TSC2 expression under the ND638-GAL4 promoter did not drive any change in delamination in the midline or outside compared to wildtype tissues (Fig. 4.12). In this case, however, there appeared to be no change in the width of the notum, so it is likely that tissue mechanics is not altered in the notum. In the case of p110 PI3K expression, distal increase in growth did not have any effect on midline delamination (Fig. 4.12), however ~ 4 % of cells delaminated at the boundaries where p110 was expressed (150 cells), and no cells delaminated in the control in this region. This led to a reduction in the width of the notum, which could lead in some delamination across the boundary. This result suggested that i) tissue mechanics is not transmitted over a long range in the tissue, but only on neighbouring cells and ii) the effect of increased growth is non-cell autonomous, since cells delaminated at both sides of the boundaries (Fig. 4.13).

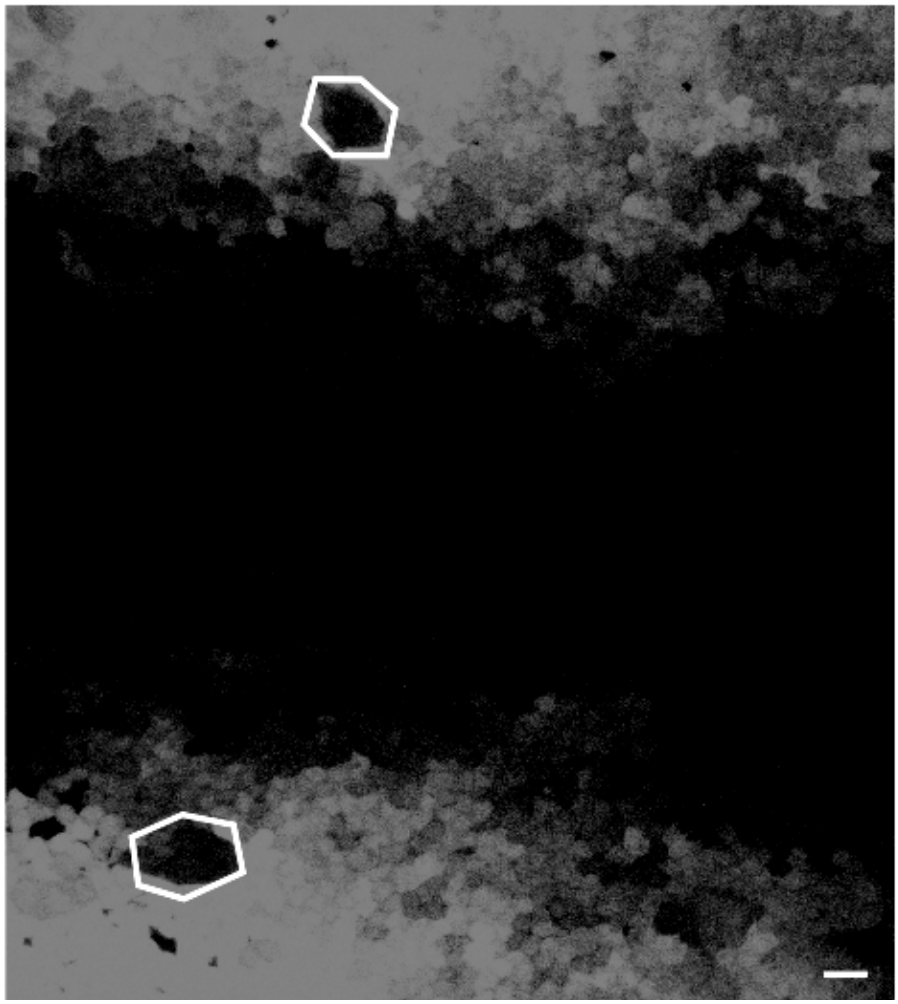

Figure 4.11 ND-GAL4 expression domain

GFP is expressed under the ND638-GAL4 domain (laterally in the notum). The size of the tissue is 220 μm x 270 μm. ND638-GAL4 expression domain is defined by the macrochaetes (indicated inside the white polygons). Scale bar, 10 μm.

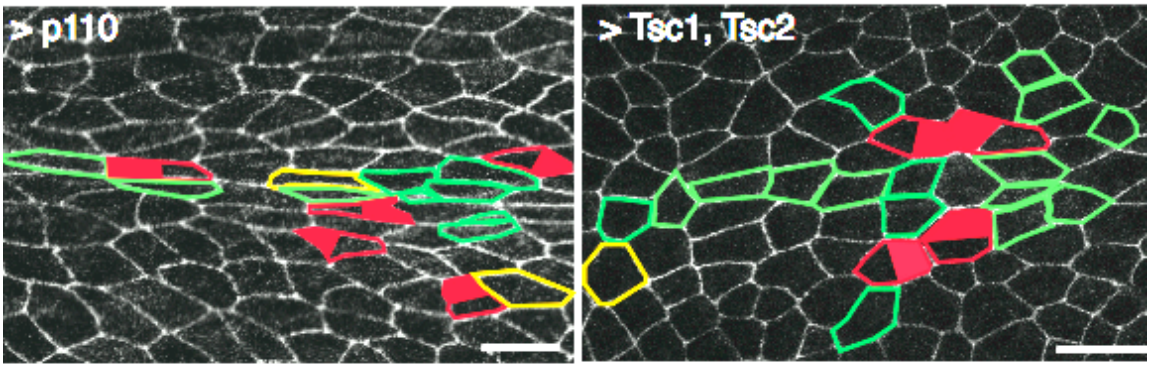

Figure 4.12 Midline delamination rates are unaffected in nota with distal changes in growth

Tissue marked with E-cad::GFP expressing p110 PI3K and TSC1 and 2. Delaminating cells are coloured with different colours according to their behaviour (see inset of Fig. 4.6). Scale bar, 10 µm.

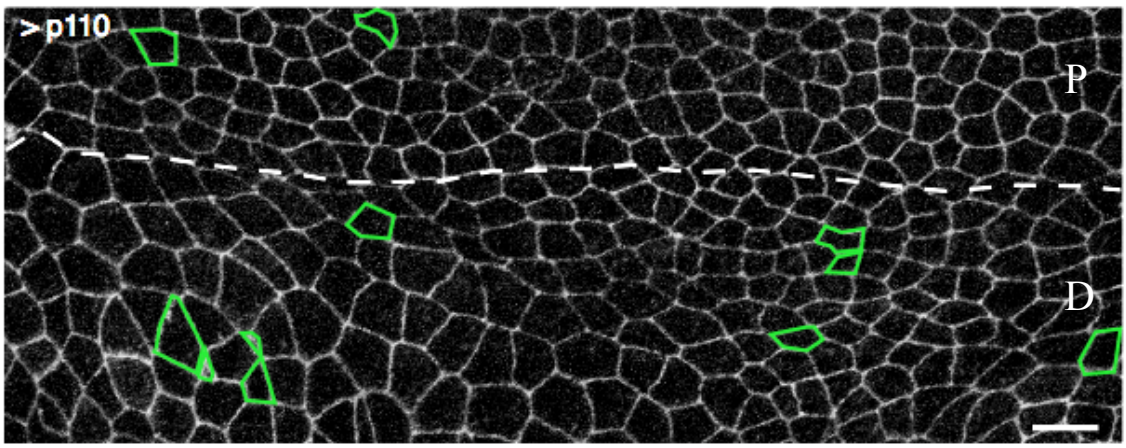

Figure 4.13 Non-autonomous delamination in response to changes in growth

Tissue marked with E-cad::GFP expressing p110 PI3K. The white dotted line indicates the boundary with ND638-GAL4 expression domain (expressed distally (D)). Delaminating cells are coloured with different colours according to their behaviour (see inset of fig. 4.6). Scale bar, 10 µm.

4.6 Starvation: cell delamination is a robust mechanism in homeostasis achievement

As an additional test for a link between tissue growth and delamination, we imaged starved pupae, since external factors, such as nutrient availability, control tissue size and the size of the whole animal in *Drosophila.* Larvae were grown in low nutrients food and the notum development was analysed to understand whether homeostatic interactions are conserved in different environmental conditions. The size of the adults after starvation was variable between ¾ and ½ the size of larvae grown in standard food, however starved animals showed a very conserved tissue patterning. Bristles were regularly spaced and the number of bristle rows was preserved. By imaging the tissue with E-cad::GFP, it was possible to measure the distance between the macrochaetes in the notum as an estimation of the size of the tissue, and analyse cell number and area in starved pupae (Fig. 4.14). The distance between macrochaetes was 165.5 ± 6.1 μm in the pupae after starvation, more than 30% less compared to the control (245 ± 7.3 μm). However, cells were 20 % smaller in area (41.8 ± 7.68 μm^2) compared to the control cells (51.3 ± 12.7 μm^2), and macrochaetes were separated by about 31 cells in the former group, 38 in the latter. The analysis after nutrients restriction revealed that the process of growth-dependent delamination is extremely robust during development. In the starved pupae, 38.7 ± 13.7 % of the cells delaminate from the midline, and 1.55 ± 0.6 outside (n=2 animals) (32.5 ± 13.6 and 0.5 ± 0.3 respectively in the control).

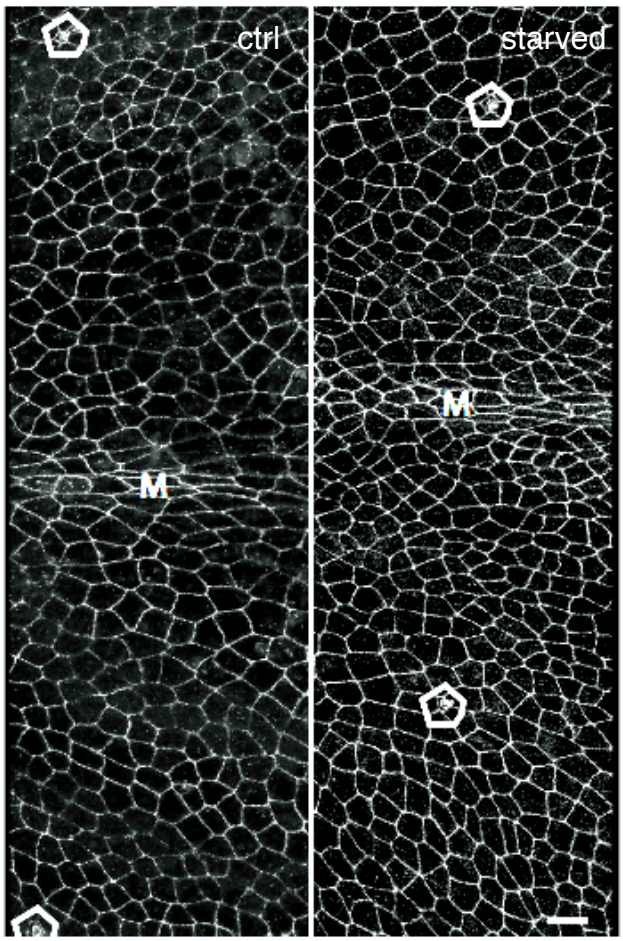

Figure 4.14 The notum is smaller in starved animals with fewer smaller cells

Starved and control tissues marked with E-cad::GFP. The macrochaetes are indicated inside the white polygon. M indicates the midline. Scale bar, 10 μm.

4.7 Conclusions

The development of tissues and organs is finely regulated to reach their final shape and size in the adult. To maintain form and size, cell growth and loss are precisely balanced. This mechanism is extremely conserved, even when external signals, such as nutrient availability, alter overall size of the animal. In the developing notum, when larvae are starved, the tissue size is smaller, without any alteration in the correct patterning of the adult epithelium. This is achieved thanks to the correct balance between cell loss and growth.

In the developing notum, cell growth is counter-balanced by regionalised cell delamination, in a region of the tissue where cells appear overcrowded. The midline is formed by the fusion of the two wing imaginal discs to give a continuous epithelium, which results in a subtle furrow. Increase in growth across the whole tissue by PI3K upregulation enhances this effect, so that the tissue buckles as the result of increased tissue pressure. In these folds, many cells delaminate. Conversely, when growth is inhibited in the tissue, tension is high and uniform in the whole notum, reducing cell delamination. This suggests a direct link between local tissue mechanics and delamination. The process of growth-dependent delamination appears non-cell autonomous. In the case of regionalised increased growth, only neighbouring cells respond to increased crowding, by delaminating across the boundary. This suggests that compressive forces are felt locally in the epithelium and are not transmitted across the whole tissue. However, we were unable to test whether a global increase in tension would be transmitted and what are the effects of such a treatment.

5. REGULATION OF CELL DELAMINATION

5.1 Introduction

In this chapter, we investigate three possible mechanisms that are likely to regulate delamination in this system: i) cell death, ii) cell competition and iii) endocytosis of AJs.

First, we analysed whether cell delamination in the developing notum is due to a mechanism that eliminates dying cells and contributes to tissue refinement (Manjon et al., 2007; Solon et al., 2009; Toyama et al., 2008). To do so, we imaged the tissue marked with His::RFP and basal membrane markers and looked at the hallmarks of apoptosis, such as pyknotic nuclei and membrane blebbing. Delaminating cells exhibited the hallmarks of apoptosis only after losing their entire apical domain, when they were basally extruded from the tissue. This suggests that cell death is a consequence and not a cause of delamination. To test this, we then analysed whether the process is blocked when over-expressing an antiapoptotic protein, DIAP1.

Second, we tested the role of cell competition in regulating this process of cell delamination. This phenomenon describes a situation in which slowly dividing cells are eliminated from a population of more rapidly dividing cells (Morata and Ripoll, 1975). To do so, we silenced key regulators that have been shown to trigger competition induced-death of cells in the tissue, including p53, JNK and Fwe (Mesquita et al., 2010; Moreno et al., 2002; Rhiner et al., 2010).

Third, since apical constriction of delaminating cells requires junction disassembly for junctions to decrease in length, we analysed the role of endocytosis and E-cadherin recycling. Cdc42 could be a possible candidate involved in junction recycling during delamination, since cells lacking Cdc42 showed defects in AJs endocytosis, loss of apical material and increased delamination (Georgiou et al., 2008).

5.2 Delaminating cells show hallmarks of apoptosis after losing their entire apical domain

We first analysed whether cell delamination in the developing notum is due to a mechanism that eliminates dying cells and contributes to tissue refinement (Manjon et al., 2007; Solon et al., 2009; Toyama et al., 2008). Rosenblatt *et al*. (Rosenblatt et al., 2001) described apoptotic cell extrusion as a common mechanism in development to eliminate dying cells, which exhibit pyknotic nuclei and blebs, in order to maintain an intact epithelium. To do so, we simultaneously tracked nuclei and the apical junctions to determine the fate of cells undergoing basal delamination. When the tissue was marked with His::RFP, it was only possible to see the first signs of cell death after the loss of apical junctions, as the nuclei of cells lacking all junctions became visibly condensed and pyknotic (Fig. 5.1A).

Using the basal marker Resille::GFP to visualise delaminated cells trapped underneath the epithelium, it was clear that following delamination these cells started blebbing, before being removed by circulating macrophages in 20-30 minutes (Fig. 5.1B).

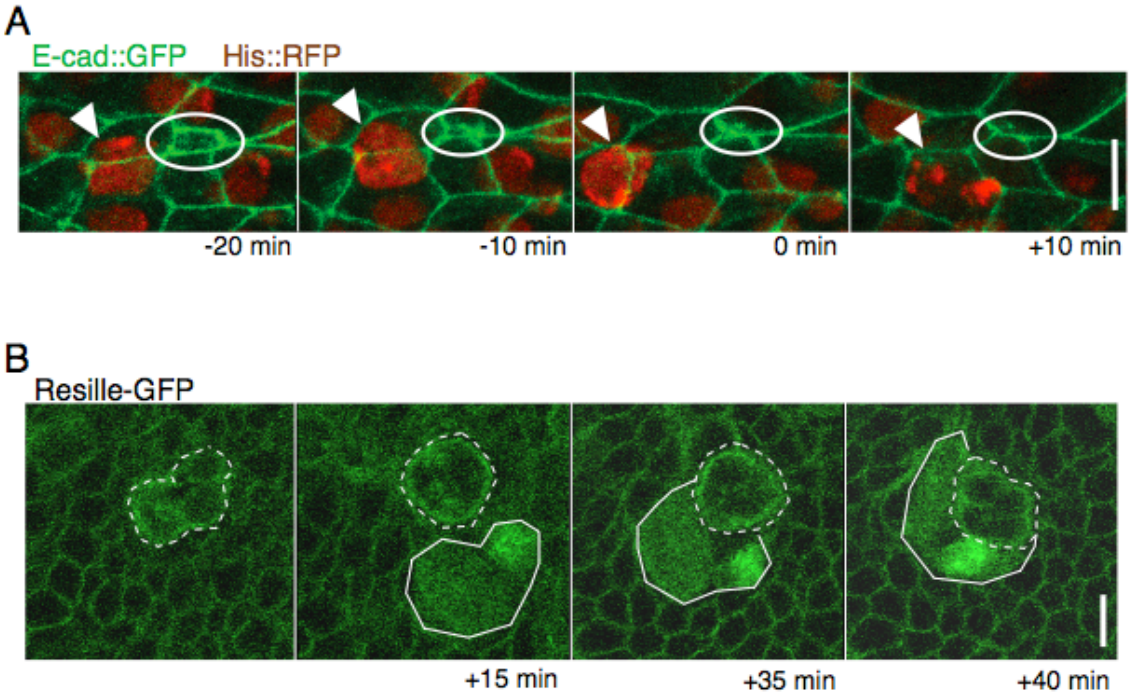

Figure 5.1 Delaminating cells show hallmarks of apoptosis after losing their entire apical domain

(A) The image shows a delaminating cell marked with E-cadherin::GFP and His::RFP. Its apex (white circle) and nucleus (arrowhead) are indicated. (B) Delaminated cells are rapidly phagocytosed by circulating macrophages from the basal side of the epithelium. Timelapse of basal side of the tissue imaged with Resille::GFP. A cell extruded from the tissue is blebbing (indicated by the dashed line). The cell is phagocytosed by a circulating macrophage (indicated by the white line). Scale bar, 10 μm.

5.3 Diap1 overexpression has a modest inhibitory effect on cell delamination

In many tissues cell death plays a role in homeostasis achievement during development, counteracting proliferation. In order to understand the role of programmed cell death in midline delamination, DIAP1 was expressed in the developing notum to suppress apoptosis within the tissue (Brand et al., 1994). The line was tested with a strong promoter, Act5c-GAL4. First, DIAP1 overexpression was verified by staining with anti-DIAP1 antibody. Second, inhibition of cell death was analysed by imaging with Resille::GFP and by quantifying the time of survival of delaminated cells underneath the epithelium, before being cleared by macrophages (Fig. 5.2). The antibody staining confirmed DIAP1 increased expression relative to the control (Fig. 5.2A). This induced a higher but variable survival of cells underneath the epithelium (Fig. 5.2B). In addition, inhibition of apoptosis induced a small but reproducible reduction in overall rates of midline cell delamination (23.4 ± 5.6 % versus 34.2 ± 1.54 % in the control).

These data suggest that DIAP1 overexpression is not sufficient to prevent delamination or to prevent extruded cells to undergo apoptosis, even though DIAP1 overexpression seems to cause cells to persist underneath the epithelium, perhaps by delaying the onset of apoptosis and/or their ability to be recognized by macrophages.

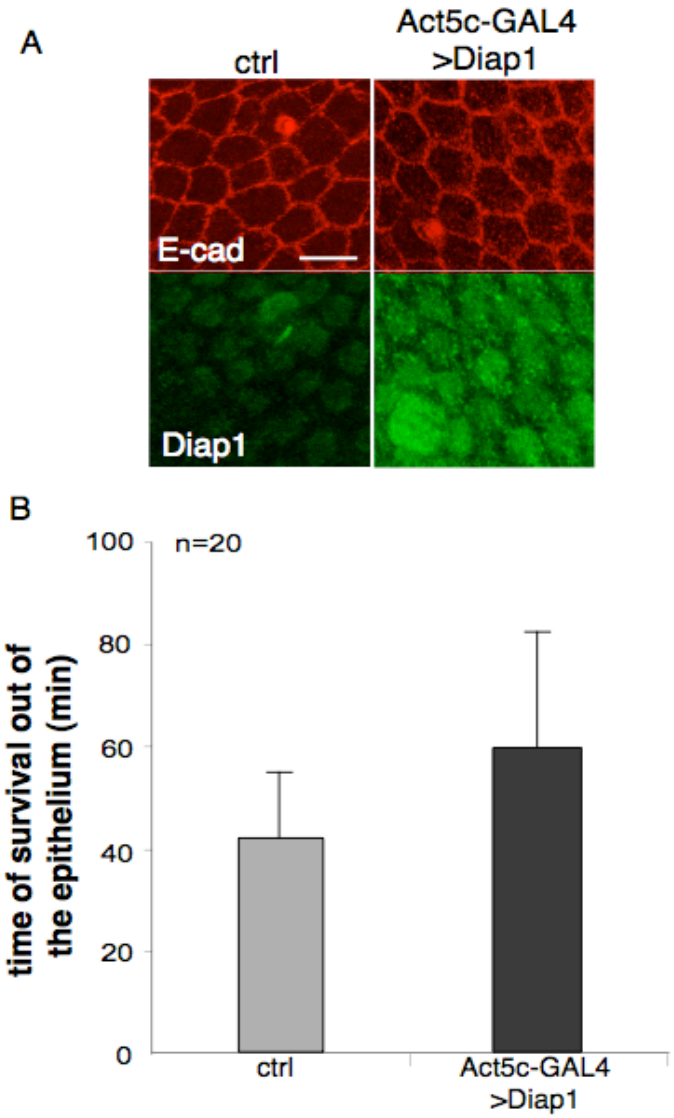

Figure 5.2 Increased DIAP1 expression induces a variable but higher survival of cells underneath the epithelium

(A) Tissue overexpressing DIAP1 and control stained for E-cadherin and DIAP1. Scale bar, 10 µm. (B) Time of survival of delaminated cells underneath the epithelium before being cleared from the tissue in control and DIAP1 overexpression (n=2 pupae). *P* value is 0.06.

5.4 The role of cell competition in epithelial cell delamination in the notum

Cell competition is emerging as an important mechanism that contributes to tissue growth and homeostasis. This process results when neighboring cells within a growing tissue sense metabolic or growth rate differences. As a response, apoptosis is triggered in the metabolic 'weaker' cells (Johnston and Gallant, 2002; Moreno et al., 2002). JNK and Fwe have been shown to be the major effectors of this process, triggering apoptosis in 'loser' cells (Mesquita et al., 2010; Moreno et al., 2002; Rhiner et al., 2010). The JNK pathway is activated in many stress-induced processes, and eliminating JNK activity prevents some "weaker" cells from dying in some systems. More recently, Flower (Fwe), a cell membrane protein, conserved in multicellular animals, has been shown to be necessary and sufficient to decide cell fate during cell competition (Rhiner et al., 2010). If Fwe is lost in an entire tissue, cell competition cannot occur and suboptimal cells may accumulate. Finally, p53 was shown to play a role in triggering a non-cell autonomous response in cell competition (Mesquita et al., 2010).

Since JNK signaling was shown to mediate apoptosis of extruded cells (Gibson and Perrimon, 2005), puc-LacZ expressing nota were stained with anti-ß Galactosidase antibody to analyse the expression of JNK in midline cells. These stainings revealed high levels of JNK signaling along the midline (Fig. 5.3). This observation suggests that JNK signaling could be involved in cell extrusion and can be tested by interfering with this signaling pathway, silencing JNK in the tissue.

The expression of RNAi with the *pnr* promoter led to defects in thorax closure, since JNK is required for migration and sealing of the wing discs leading edge at the midline to give the notum in the pupa (Zeitlinger and Bohmann, 1999). Adults showed a severe thorax cleft phenotype, therefore midline cell delamination was difficult to quantify. However, the analysis on milder lines revealed that delamination continued unabated in nota with JNK RNAi expression (Fig. 5.4).

The same was observed in tissues expressing p53DN (Fig. 5.4), in which delamination rate (30.9 ± 8.34 %) was similar to the control (34.2 ± 1.54 %).

In the case of Fwe iR, however, a small reduction in delamination rate was observed (19.8 ± 1.44 %). Interestingly, this modest inhibition was similar to the one observed in Diap1 overexpressing tissues, when blocking apoptosis.

This result suggests the existence of a population of weaker cells in the tissue, in which apoptosis is triggered.

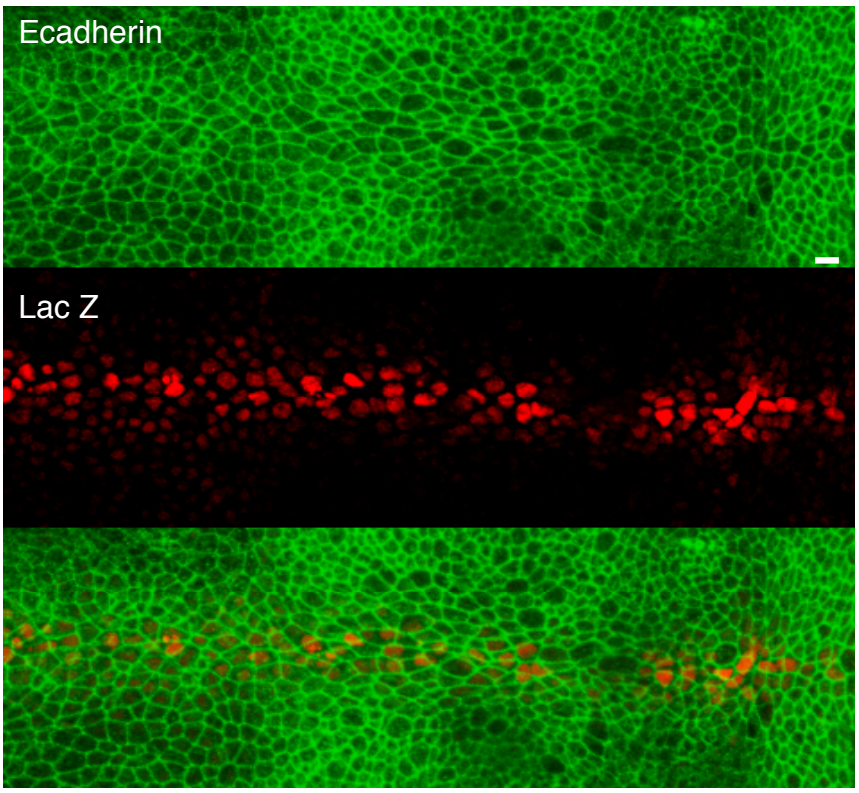

Figure 5.3 Puc is expressed in the midline

The figure shows Puc expression along the midline of the notum. Puc-LacZ expressing tissues were stained for E-cadherin (green), LacZ (in red). The scale bar is 10 μm.

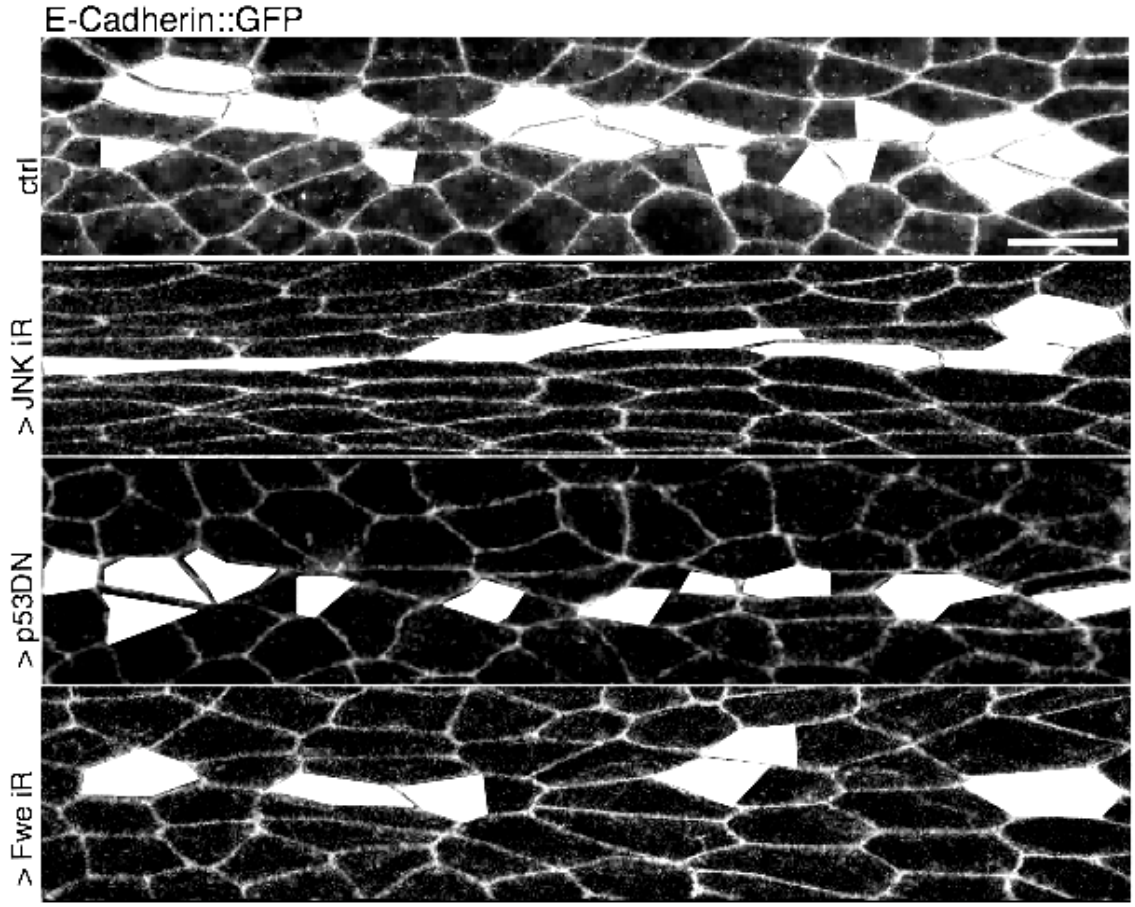

Figure 5.4 Midline cell delamination is independent of cell competition

As expected for a process independent of apoptosis, delamination from the midline was not completely inhibited in nota expressing RNAi targeting JNK, p53 and Flower. Z-projection of midline region from control, JNK RNAi, p53DN and Fwe RNAi expressing tissues. Cells delaminating over 12h are colored in white. Scale bar, 10 μm.

5.5 A possible role for endocytosis in epithelial cell delamination

Fluctuations in junction length, mediated by adherens junction disassembly and assembly, maintain the integrity of the tissue, as it is actively remodelled (Fristrom, 1988). This requires active junction remodeling, probably through endocytosis and E-cadherin recycling. Interestingly, in the midline junctions appear to rapidly change their shape, often appearing convoluted, suggesting a different rate of E-cadherin delivery and removal at AJs in this region (Fig. 5.5). This could contribute to the process of delamination, which requires junction dynamics.

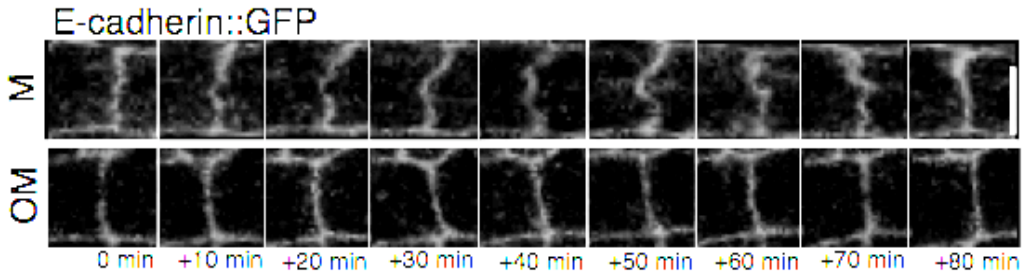

Figure 5.5 Midline junctions appear often convoluted and change their form rapidly over time

Junctions between cells in the midline of the notum are convoluted. Timelapse of junctions in the midline (M) and outside the midline (OM), visualized with E-cad::GFP. Scale bar, 5 μm.

This idea was suggested by the analysis of *cdc42* mutants, which showed a possible link between defects in endocytosis and epithelial cell delamination in the notum. Cdc42 is a Rho-family GTPase, which has been implicated in the regulation of actin filament dynamics (Rohatgi et al., 2000), in the control of epithelial cell polarity and junctional organization, and in vesicle trafficking (Balklava et al., 2007; Garrett et al., 2000; Schafer, 2002; Sokac et al., 2003). Defective junctional organisation was observed in *cdc42* mutant cells accompanied by apical constriction, junctional discontinuities, abnormal junctional extensions and isolated E-cadherin rich puncta (Georgiou et al., 2008).

Junctions were analysed through live imaging thanks to E-cadherin::GFP under the control of a ubiquitous promoter and in some cases cell delamination was observed (Fig. 5.6). Confocal images and EM showed ectopic junctional material accumulating in *cdc42* mutant cells, leading to convoluted junctions. An endocytosis assay using TRITC-labelled dextran demonstrated that in *cdc42* mutant cells endocytosis was compromised. A significant reduction of dextran-labelled endosomes was observed compared to the wildtype cells and only few junctional puncta and extensions were found colocalising with endocytic markers, implying that ectopic junctional structures were not internalised (Fig. 5.7). These data suggested that in mutant clones a failure to remove AJs could lead to AJs instability, loss of apical material and subsequent epithelial cell delamination.

To analyse if Cdc42-mediated endocytosis of AJs was involved in midline cell delamination, RNAi for the Rho-GTPase was expressed in the tissue under *pnr*-GAL4 promoter. These tissues did not exhibit the severe junctional effects previously observed in *cdc42* null mutant clones (Fig. 5.8A), but groups of cells outside the midline in the tissue showed apical constriction. In these regions, a higher number of cells delaminated from the epithelium (14.2 ± 4.2 %) (Fig. 5.8B). However, midline cell delamination remained unaffected (30.3 ± 3.5 %). Thus, Cdc42-mediated endocytosis does not appear to be required for midline cell delamination.

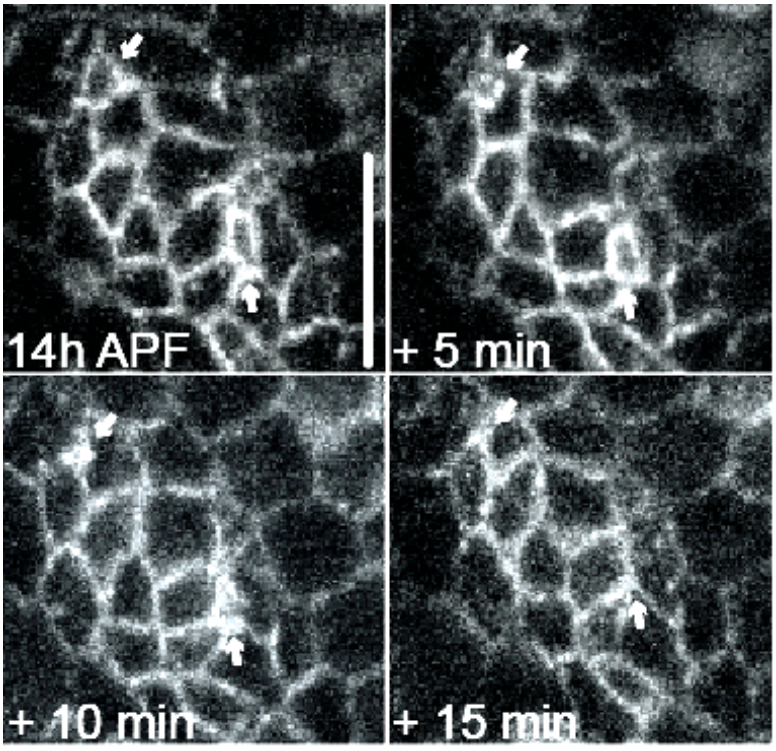

Figure 5.6 Cell delamination in *cdc42* mutant clones

Progressive apical constriction and delamination of *cdc42* mutant cells (arrows). APF=after puparium formation. Scale bar, 10 μm.

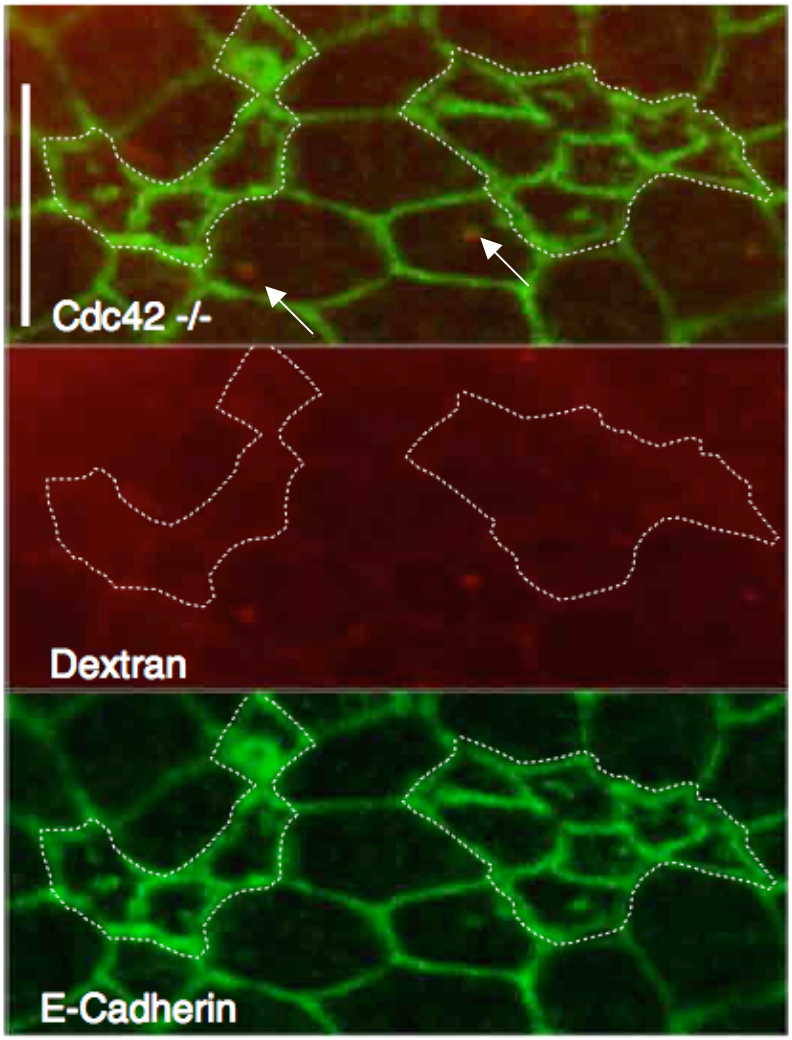

Figure 5.7 Endocytosis is compromised in *cdc42* mutants

In a 20 min TRITC-Dextran uptake assay, few Dextran-labeled endocytic structures are observed within *cdc42* mutant clones, labeled as negative marked clones (GFP not shown for clarity of the image) indicated inside the white dashed line. Outside the clone, E-cadherin spots colocalize with Dextran (indicated by the arrows). In *cdc42* mutant cells, almost all E-cadherin puncta and tubules lack Dextran staining. Scale bar, 10 μm.

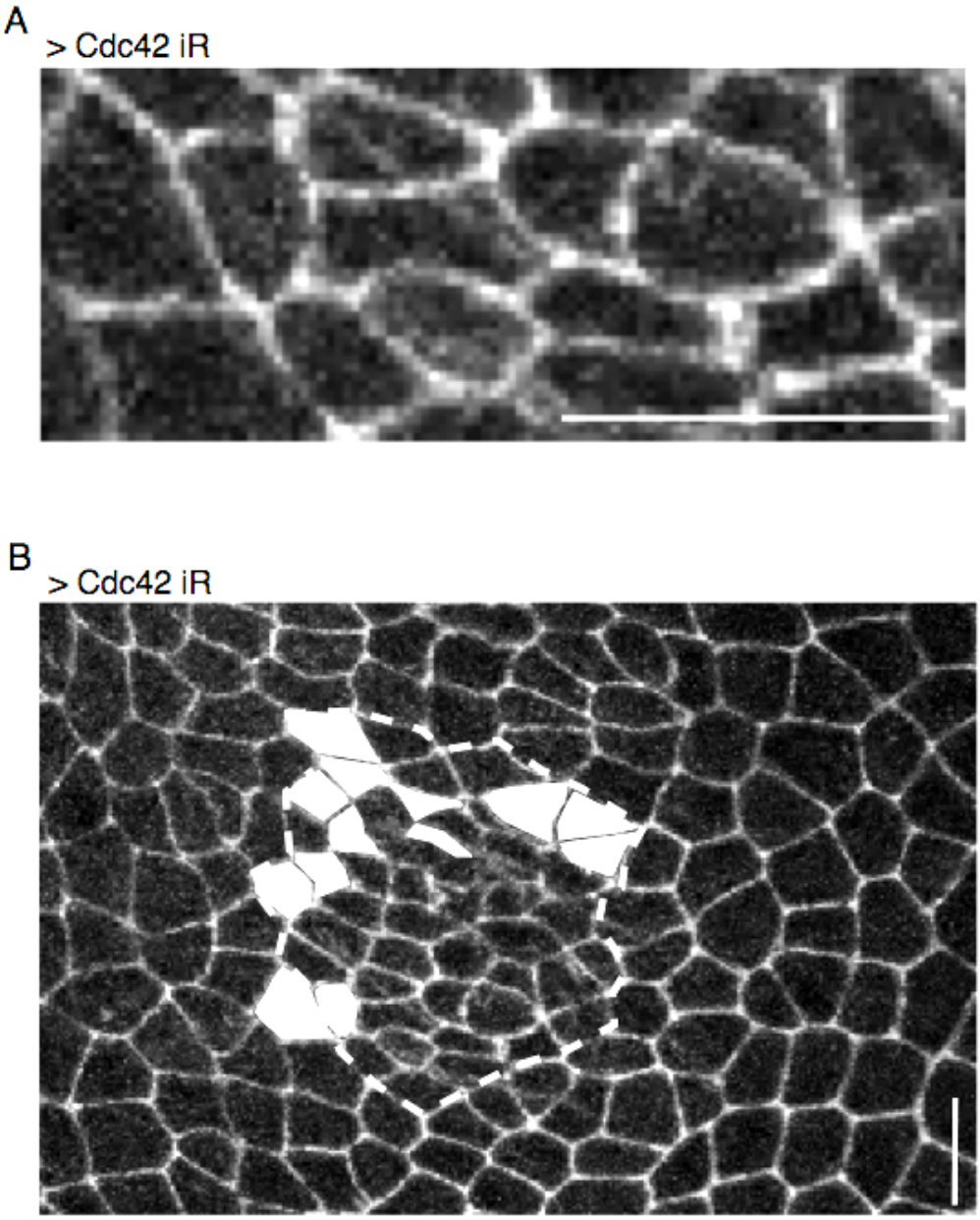

Figure 5.8 Cdc42 iR nota showed regionalized apical constriction but no severe junctional defects

Cdc42 iR tissue marked with E-cadherin::GFP. (A) The tissue did not show any severe junction abnormality. (B) Region characterized by apical constriction (inside the white dashed line). Cells delaminating are coloured in white. Scale bar, 10 μm.

5.6 Conclusions

In this chapter, we analysed possible candidates regulating midline cell delamination. In particular, we investigated the role of cell competition, cell death and Cdc42-mediated endocytosis in the process. To test the role of cell competition, we used RNAi lines against JNK and Fwe. The RNAi expression was not tested in these lines, however a phenotype has been described in the literature. In the case of Fwe knockdown, it has been shown to block apoptosis of outcompeted cells (Rhiner et al., 2010). The role of JNK in cell competition is less clear, although inhibition of JNK has been reported to rescue a small fraction of 'loser' cells from dying (de la Cova et al., 2004). The role of Cdc42-mediated endocytosis was tested by generating clones and by silencing Cdc42 in the whole tissue. The RNAi line used to silence Cdc42 was reported in the VDRC stock centre to have a phenotype in the adult, but it was not tested with an antibody.

Cell competition is the result of cell-cell interaction between two different populations of cells. Cells with a slower metabolism are outcompeted by the others, and apoptosis is triggered in the loser cells (de la Cova et al., 2004). JNK, Fwe and p53 play a role in driving a non-cell autonomous response in cell competition (Mesquita et al., 2010; Moreno et al., 2002; Rhiner et al., 2010). In the developing notum, delamination seems to be independent on p53 and JNK. Fwe however, had a modest inhibitory effect on midline cell delamination. This highly conserved protein has been shown to be necessary and sufficient to induce apoptosis during cell competition.

The analysis of the role of programmed cell death in the process of cell delamination, revealed that some cells die through apoptosis in the tissue, and are then extruded. When DIAP1 overexpression was tested, it seemed to have a modest inhibitory effect on cell delamination, similar to the one seen in Fwe RNAi tissues. Moreover, it had a variable effect on the survival of cells underneath the epithelium, so that cells survive longer before being cleared by macrophages.

Two hypotheses could explain the modest effect of DIAP1 overexpression and Fwe iR on cell delamination:

i) In the majority of cases, extrusion triggers the apoptotic cascade, in a process similar to anoikis;

ii) DIAP1 overexpression and Fwe RNAi levels were not high enough to prevent apoptosis in these cells.

Finally, Cdc42-dependent endocytosis of AJs did not seem to play a role in this process, since Cdc42 RNAi expression did not inhibit midline cell delamination in the notum.

The analysis of possible regulators of midline cell delamination in the tissue suggests that cell competition, apoptosis and Cdc42 mediated endocytosis do not play a major role in this process. However, due to the limitations of the techniques used, this should be tested further before ruling out the possibility of a role of these processes in midline cell delamination.

6. MECHANISMS OF CELL DELAMINATION

6.1 Introduction

Having been unable to unambiguously identify the molecular machinery regulating midline delamination, we looked in more detail at the mechanisms by which cells leave the tissue. In particular, we analysed the behaviour of AJs, since the first event observed in epithelial cell delamination was apical constriction.

First, we carried out a computational model of epithelial mechanics, which was developed in collaboration with Aida Mehonic, to understand whether tissue mechanics and junctional dynamics alone could explain the process of midline delamination, The model was based on mechanical properties of cells (line tension, contractility and compressibility of cells) and simulated the notum situation, where the overall area remains constant. This approach allowed us to better understand the likely role of tissue mechanics in epithelial cell delamination, since junction dynamics were sufficient to induce cell delamination in simulations.

Second, we analysed junction dynamics in vivo during apical constriction. The analysis of junction behaviour revealed the existence of two distinct mechanisms of delamination in the tissue. To understand whether these two different behaviours correspond to distinct signaling pathways, we analysed the effect of apoptosis inhibition and cell growth upregulation on the ratio between the two mechanisms in the system.

Finally, we analysed the role of Myosin-II in cell delamination, since an actin-myosin ring was shown to drive epithelial cell extrusion of apoptotic cells (Rosenblatt et al., 2001).

6.2 A computational model of the notum

To gain insight into the role of mechanics in driving delamination, a computational model of the epithelium was developed in collaboration with Aida Mehonic and Tom Duke (unpublished data). The approach adapted previous models (Farhadifar et al., 2007; Graner and Glazier, 1992; Hufnagel et al., 2007; Kafer et al., 2007) and simulated the notum situation, where the overall area of the tissue remains constant. The model was based on the following dominant mechanical forces in the tissue: line tension of junctions due to cell-cell adhesion and cell membrane tension; contractility due to cortical acto-myosin; and limited cell compressibility. It was able to simulate growth-induced crowding, junctional dynamics and cell rearrangements (Fig. 6.1A). Dynamics were modeled by stochastic movement of the vertices and junctional rearrangements were modeled to allow for topological changes observed in the tissue in which cells exchange neighbors, known as T1 transitions (Fig. 6.1) and cell delamination (Fristrom, 1988).

The mechanical forces acting within the tissue are modeled by the work function W specified in Fig. 6.1A. The work function and the parameter values are adapted from the model described by Farhadifar *et al.* (Farhadifar et al., 2007), which simulate a growing wing disc epithelium. However, in the case of the notum, the tissue size is fixed, so we imposed continuous boundary conditions using a 2-dimensional box. This box was also used to fix the total area A_{tissue} available to the cells, which as a result compete for available space, with N_0=240 cells in fixed rectangular area $A_{tissue}= N_0A^0$. This is described by the compressibility term, which expresses the difference between the area of the cells and their preferential area. In the model we quantify the degree of increased growth using a parameter K and model over-crowded tissue by increasing the value of the preferential cell area A^0; these new parameter values correspond to a tissue that would have the same value of the work function, and hence the same equilibrium configuration. The second term in the equation describes the tension along the junction, which is a function of the junction length itself. Finally, the third term in the equation models the acto-myosin contractility in epithelial cells. The value of work function W

changes dynamically over time according to the position of the vertices. As the tissue evolves, cells can exchange neighbors through a process known as the T1 transition. The Farhadifar model (Farhadifar et al., 2007) was implemented by monitoring the tissue for junctions shorter than a given threshold value; in that case a vertex move reduces the junction length to zero and exchange cell neighbors. This procedure allows for reversible changes in the topology of the tissue. A second kind of topological change can occur when a cell is extruded from the tissue. This was modeled by removing any cell that has only 3 junctions and whose apical area is smaller than the threshold value of $A_0/4$, a value based upon the observed onset of the fast phase of delamination.

As discussed in chapter 4, cell delamination appears to counter-balance tissue growth to achieve the homeostasis of the epithelium during development. The simulations indeed revealed that delamination is both favoured by an anisotropic cell organisation and contributes to the development of an increasingly isotropic cell organisation as the system moves towards equilibrium (Fig. 6.1C). The model was then used to test the effects of tissue growth on delamination rates by changing the preferred apical cell area A^0. In these simulations, a high prefered area A^0 equivalent to high growth rates resulted in crowding-induced delamination, while a low A^0 reduced delamination (Fig. 6.1B). Finally, it was possible to reproduce the behavior of cells within the midline (with anisotropic geometry and crowded) and outside the midline (isotropic geometry and no crowding) (Fig. 6.1D), and the junctional changes that accompany relaxation of the tissue to mechanical equilibrium. Significantly, this computational analysis demonstrated that tissue mechanics are sufficient to explain delamination and its prevalence in the crowded midline of the notum, without the need to invoke a specific signalling event triggering cell loss.

In this chapter, we compare the model and data from the *in vivo* analysis to determine the path of crowding-induced delamination. In simulations, spontaneous fluctuations in the length of individual cell-cell junctions drove a stochastic series of neighbor exchange events as individual cell-cell junctions shortened into vertices (Fig. 6.1E), leading to random delamination events across the tissue. This reduced overall tissue crowding. Interestingly, we observed similar processes in vivo.

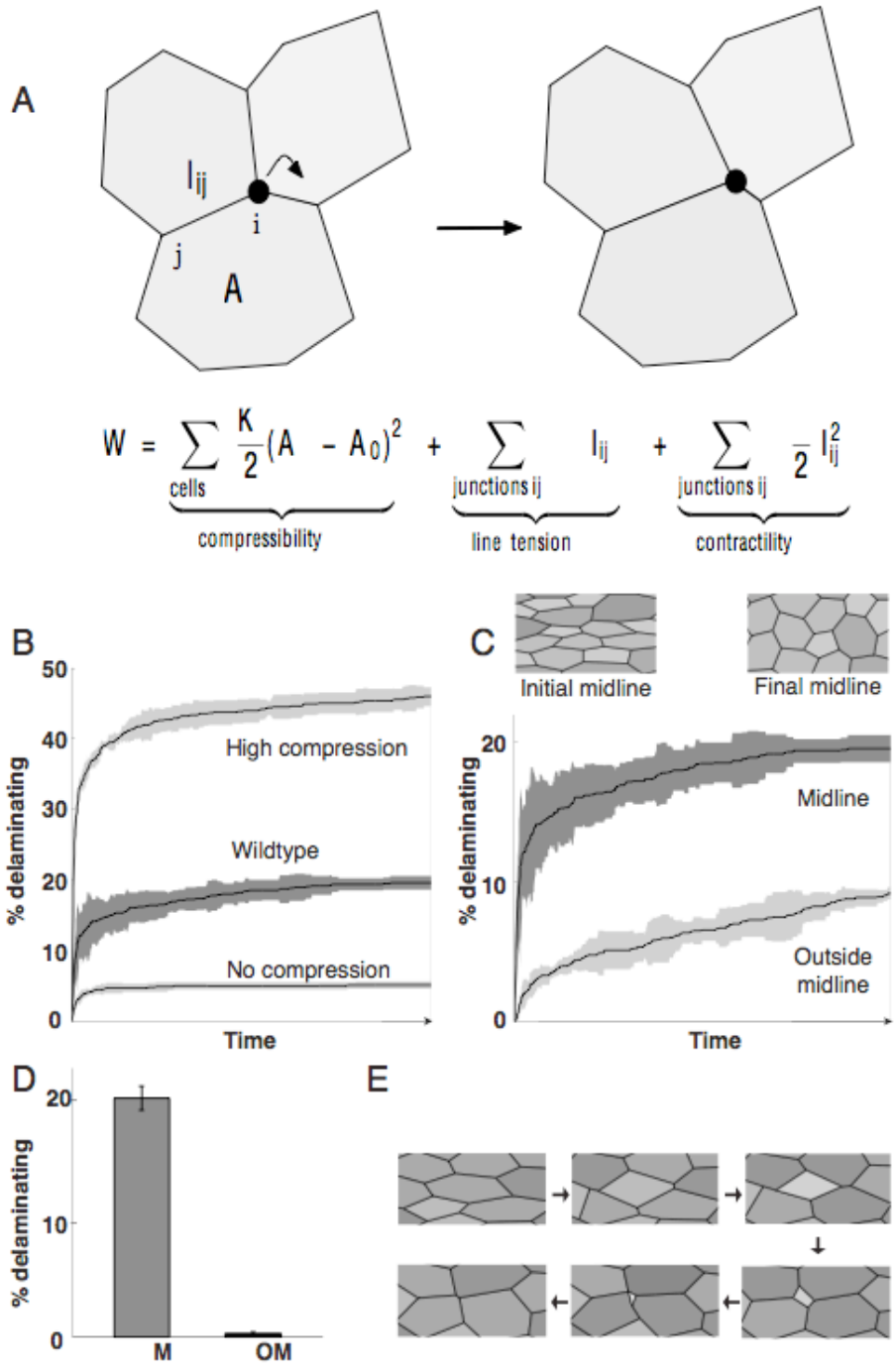
A
l_{ij}
i
j
A
$W = \sum_{\text{cells}} \frac{K}{2}(A - A_0)^2 + \sum_{\text{junctions ij}} l_{ij} + \sum_{\text{junctions ij}} \frac{1}{2} l_{ij}^2$
compressibility
line tension
contractility
B
% delaminating
High compression
Wildtype
No compression
Time
C
Initial midline
Final midline
% delaminating
Midline
Outside midline
Time
D
% delaminating
M
OM
E

Figure 6.1 Topological rearrangements drive a stochastic process of delamination in tissues under mechanical pressure

(A) An earlier mechanical model of epithelial mechanics(Farhadifar et al., 2007) was adapted to study the role of forces in epithelial cell delamination based upon mechanical forces that act in the apical plane: junctional line tension (Λ), contractility of cortical acto-myosin (Γ) and limited cell compressibility (K) based upon a target area (A^0). The tissue evolves by small stochastic displacements of the vertices, biased towards changes that lower the work function, *W*. (B) Cumulative proportion of cells delaminating from a modele of wildtype tissue (midline) and a tissue with high or low growth as a function of time. Data was averaged over 6 simulations. (C) The effect of cell geometry on delamination. Stills show initial and final cell configurations for the midline simulation; values of parameters correspond to the wildtype tissue. The midline was modeled with an anisotropic geometry and crowding, while outside the midline with isotropic geometry and no crowding. (D) Final proportions of cells delaminating: a comparison between simulations of wildtype tissue within and outside of the midline. (E) As a cell is extruded in a simulation, it progressively loses junctions as its apical area diminishes.

6.3 Two different junction dynamics could be distinguished in delaminating cells

In the model simulations, spontaneous fluctuations in the length of individual cell-cell junctions drove a stochastic series of neighbor exchange events as individual cell-cell junctions shortened into vertices, leading to random delamination events across the tissue. By imaging the junctions with E-cad::GFP, it was possible to analyse *in vivo* the dynamics of single junctions in delaminating cells. Two different mechanisms could be distinguished according to junction behaviour.

First in crowded regions of the notum, cells suffered the loss of individual junctions via a series of T1 transitions (Bertet et al., 2004; Blankenship et al., 2006; Irvine and Wieschaus, 1994), accompanied by the progressive loss of apical cell area over an extended and variable period (Fig. 6.2A, B), as seen in simulations. T1 transitions appeared to occur randomly in the tissue as the result of fluctuations in junction length (Fig. 6.3), thus leading to the preferential loss of smaller cell-cell junctions and a partial loss of apical cell area. Once a critical threshold was reached, where a cell retained a relatively small apical domain and between 3 to 4 neighbours, it then suffered a rapid loss of apex and underwent delamination within a short and reproducible timeframe (~10 min). The analysis of individual junctions during the process revealed that single junctions behave independently (Fig. 6.4).

Second, a small subpopulation of epithelial cells delaminated via a distinct mechanism of apical constriction without concomitant changes in neighbor relationships over a period of 30-40 min (Fig. 6.5). This led to the formation of rosette-like intermediates resembling those accompanying the extrusion of dying epithelial cells (Rosenblatt et al., 2001). The analysis of junction dynamics showed that they decrease in a coordinated fashion (Fig. 6.6).

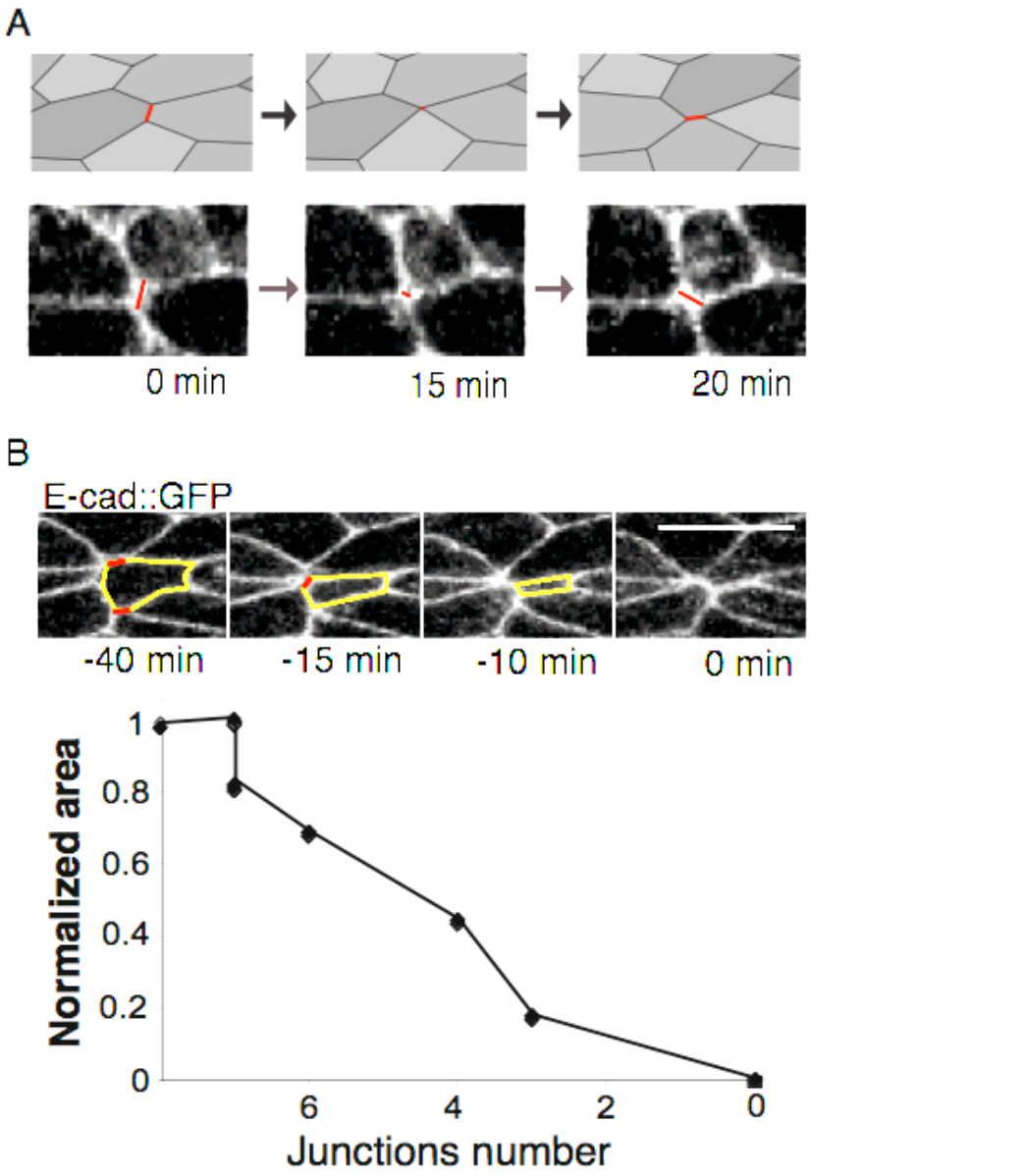

Figure 6.2 Cells delaminate losing individual junctions via a series of T1 transitions
(A) Cell losing junctions through T1 transitions in the epithelial model and from in vivo data. (B**)** A midline wildtype cell (yellow perimeter) and a plot to show the relative timing of the loss of apical area and neighbours as it delaminates. Junctions disappearing between frames are indicated in red. Scale bar, 10 μm.

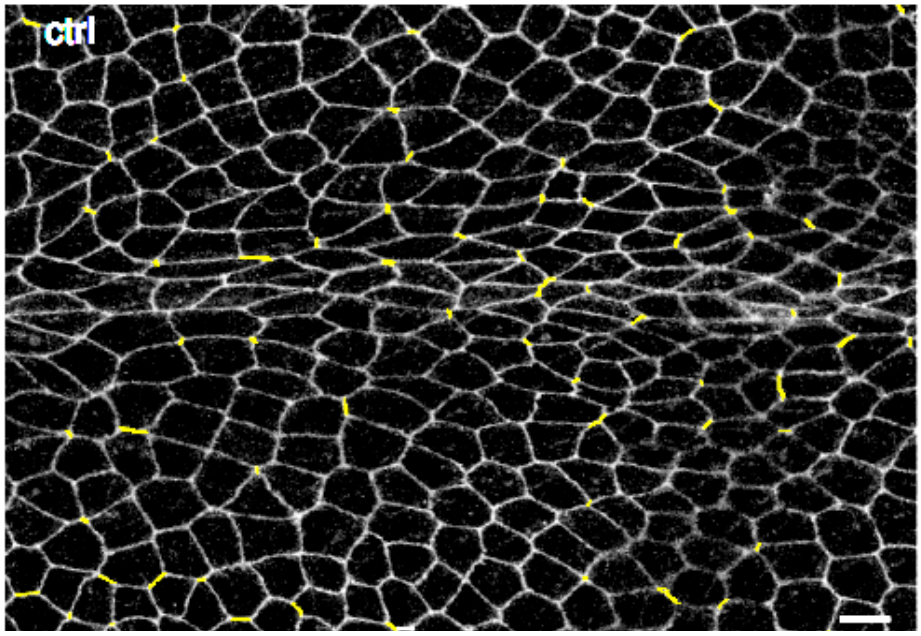

Figure 6.3 T1 transition map in the tissue

Wildtype tissue marked with E-cad::GFP. Junctions undergoing T1 transition before the onset of division are marked in yellow in the figure. Scale bar, 10 μm.

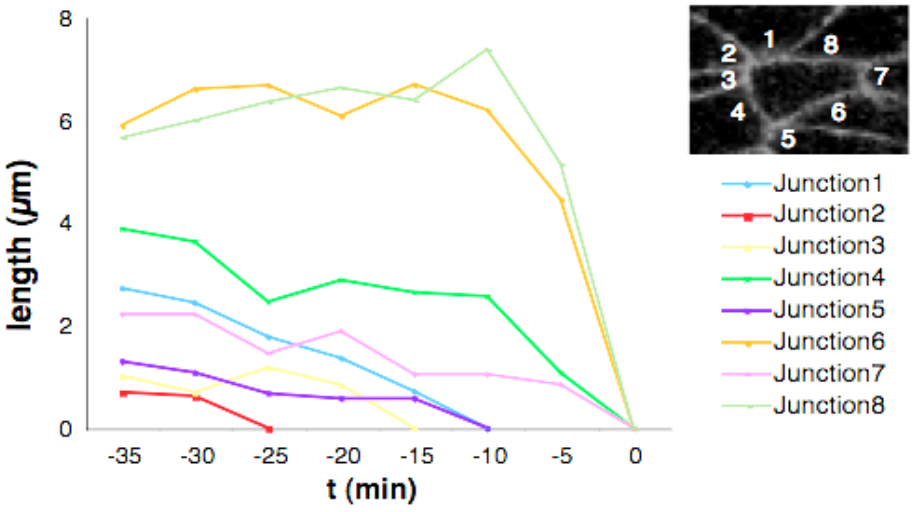

Figure 6.4 Single junctions decrease independently during T1-driven delamination

Quantification of single junction length over time. Each coloured curve corresponds to a junction, indicated in the figure by the relative number. Time 0 is the time when the apex of the cell disappears from the tissue.

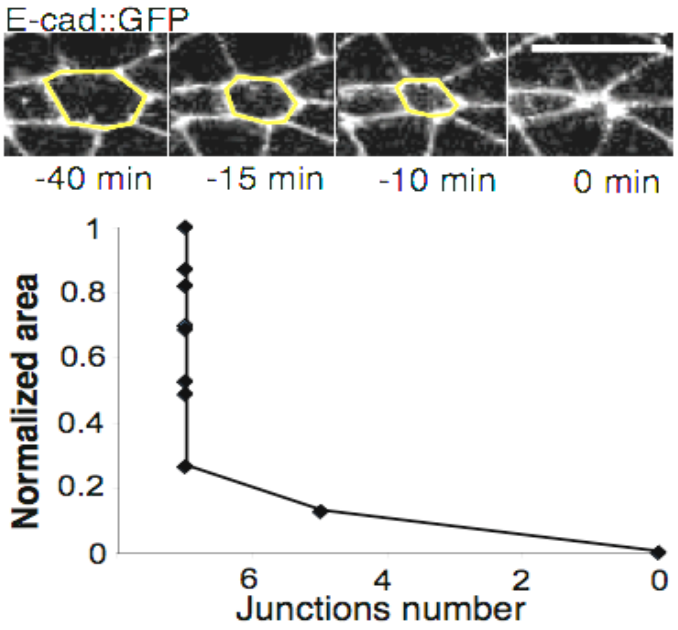

Figure 6.5 A small subpopulation of epithelial cells delaminated via the formation of rosette-like intermediates

A cell (yellow perimeter) delaminating from the midline via rosette formation and the plot showing area decrease over junction number. Scale bar, 10 µm.

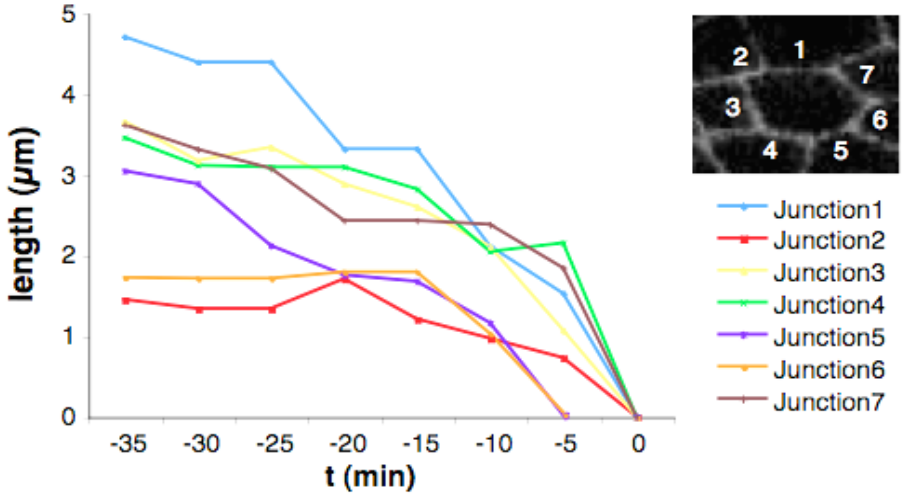

Figure 6.6 Junctions decrease in a coordinated fashion via rosette-like intermediates

Quantification of single junction length over time. Each coloured curve corresponds to a junction, indicated in the figure by the relative number. Time 0 is the time when the apex of the cell disappears from the tissue.

6.4 Delamination via serial junctional loss is independent of apoptosis

In chapter 5, we showed that inhibition of apoptosis through DIAP1 overexpression induced a small but reproducible reduction in overall rates of midline cell delamination (23.4 ± 5.6 % versus 34.2 ± 1.54 % in the control) (Fig. 6.7A). The analysis of junction dynamics in delaminating cells in DIAP1 overexpressing tissue showed that this decrease appeared to result from the selective inhibition of delamination via rosette-like intermediates (Fig. 6.7B). Thus, this suggests that delamination via rosette-like intermediate is dependent on apoptosis.

The same reduction in overall midline delamination rates was observed in Fwe RNAi tissues. However, in these tissues a subpopulation of cells delaminated via rosette-like intermediates (30% of delaminating cells), as in the control.

As a final test of the role of cell death in midline delamination, we irradiated developing pupa with UV light to induce ectopic cell death. This caused a higher number of cells to leave the tissue through the formation of a rosette intermediate (Fig. 6.8B). These cells underwent apical constriction without concomitant changes in neighbour relationships over a period of 40 min (Fig. 6.8A).

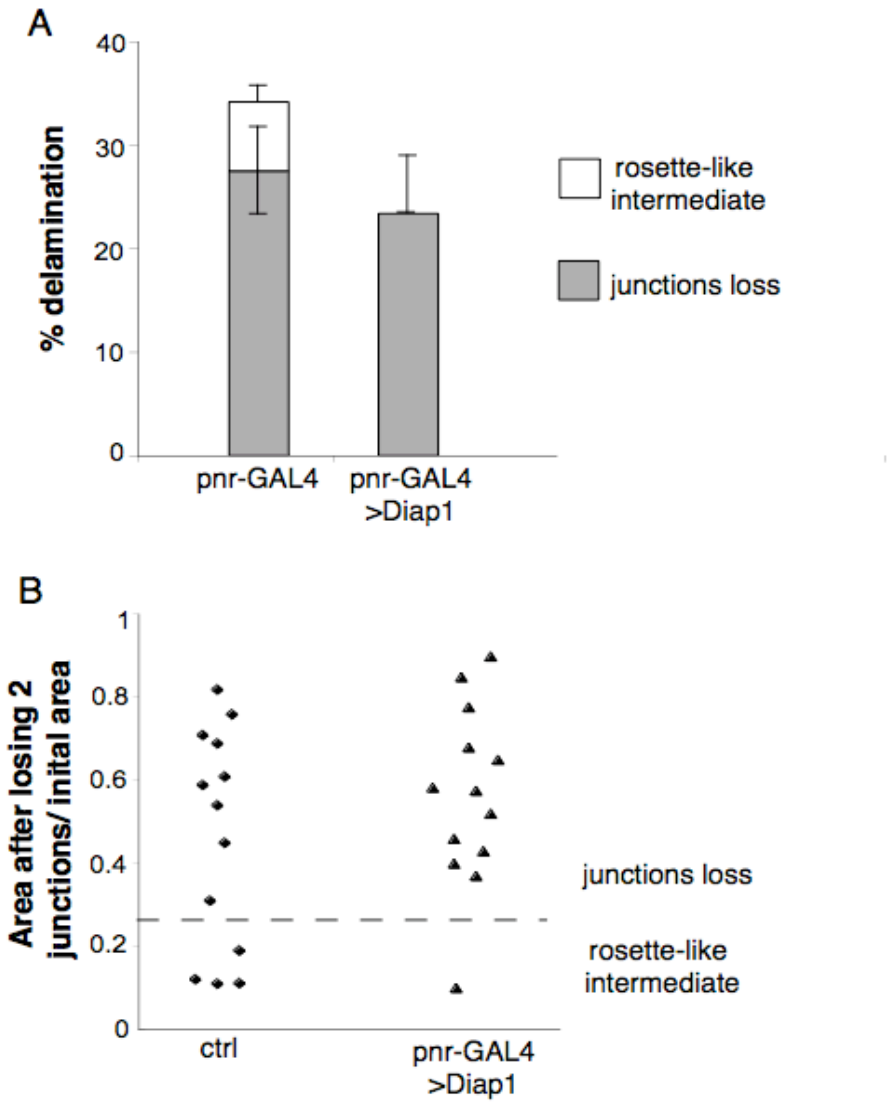

Figure 6.7 Inhibition of apoptosis induced a reduction in delaminating cells via rosette-like intermediate

(A) % midline delamination (n=3 pupae) for control pupae and following DIAP1 overexpression. White bars indicates cells that delaminate via a rosette intermediate and gray bars indicate cells that delaminate by losing junctions. (B) Plots shows the area of delaminating cells (n=13 each) after they have lost 2 junctions or 1 in the case of 5 side-cells as a fraction of their initial area in the control and in tissues expressing DIAP1. Cells above the dotted line delaminate by serial junctional loss, cells below the dotted line delaminate through the formation of rosette-like intermediates.

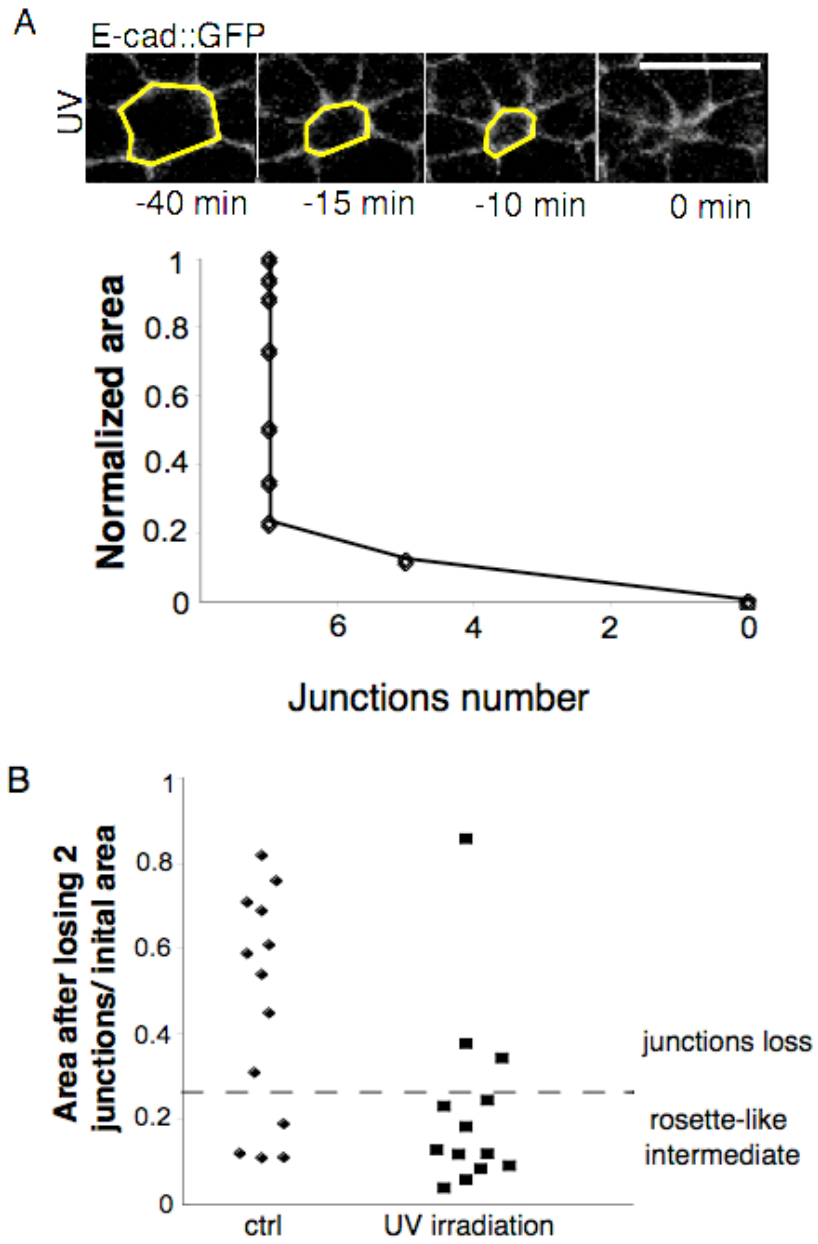

Figure 6.8 Most cells delaminate via rosette-intermediate after UV irradiation induced apoptosis

(A) A delaminating cell (yellow perimeter) after UV irradiation and the graph of area decrease vs junction number. (B) Plot shows the area of delaminating cells (n=13 each) after they have lost 2 junctions or 1 in the case of 5 side-cells as a fraction of their initial area in the control and UV irradiated tissue. Cells above the dotted line delaminate by serial junctions loss, cells below the dotted line delaminate through the formation of rosette-like intermediates. Scale bar, 10 µm.

6.5 The effect of growth on the two mechanisms of delamination

In chapter 4, we analysed the effect of cell growth on cell delamination. In particular, p110 overexpression and Warts RNAi had a different effect on cell growth. Both the PI3K and Hippo pathway upregulation increased tissue pressure and cell density, but only p110 overexpression had an effect on apical cell size. In both cases, however, delamination was massively increased compared to the control.

In the developing notum, two types of cell delamination were distinguished according to junction behaviour. Thus, we analysed what is the proportion of the two different mechanisms in tissues where growth was increased.

In p110 overexpressing tissues, the ratio between the two mechanisms of delamination was similar to the wildtype, so that PI3K upregulation increased delamination via rosette like-intermediates and via junctional loss (Fig. 6.9). In the case of Warts RNAi, however, delamination via rosette-like intermediates was significantly increased, to 50 % of delaminating cells (Fig. 6.9). This suggests that Warts RNAi likely increases the number of cells dying as the result of increased density in the tissue.

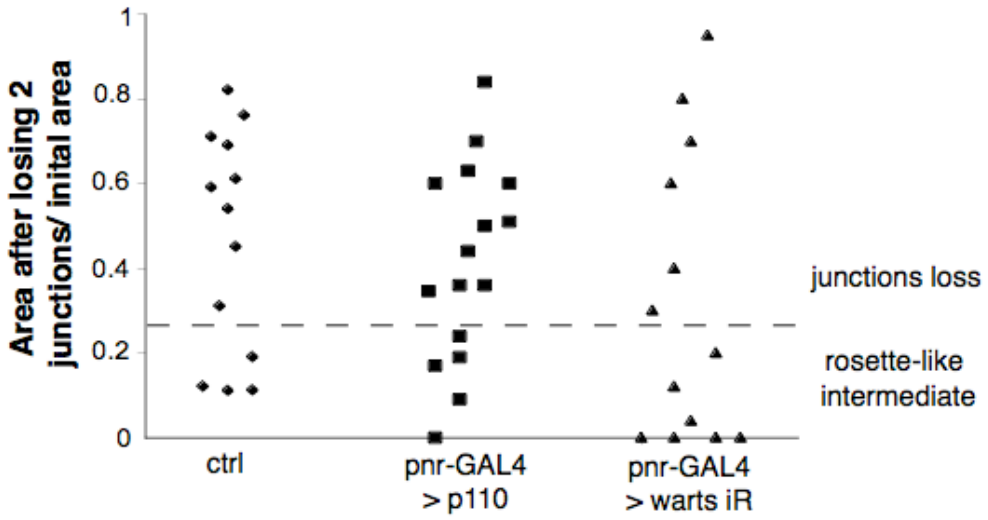

Figure 6.9 Growth increase and junction behaviour in delaminating cells

Plot shows the area of delaminating cells (n=15) after they have lost 2 junctions or 1 in the case of 5 side-cells as a fraction of their initial area in the control, p110 overexpression and Warts iR tissues. Cells above the dotted line delaminate by serial junctions loss, cells below the dotted line delaminate through the formation of rosette-like intermediates.

6.6 The final step of cell delamination is driven by a distinct mechanism Myosin II-dependent

The majority of cells leave the tissue via serial junctional loss, which occurs in a variable amount of time for different cells. The analysis of junction dynamics revealed that junctions fluctuate in length during this process (Fig. 6.4), with high probability of small junctions of shrinking to a vertex. When the cell retains a relatively small apical domain and between 3 to 4 neighbours, it then suffers a rapid loss of apex and undergoes delamination within a short and reproducible timeframe (~10 min). In this last phase, the analysis of junction dynamics revealed that they do not oscillate anymore in length, but rapidly decrease (Fig. 6.4). To understand if a different mechanism was triggering the final apical loss of the cell out of the epithelium, we imaged the tissue marked with Myosin-II::Cherry, since acto-myosin was previously shown to drive apoptotic cell extrusion from tissues (Rosenblatt et al., 2001). Rosenblatt *et al*. showed that early apoptotic epithelial cells trigger formation of an actin and myosin ring in the live neighboring cells surrounding it. Rho-dependent contraction of this ring then squeezes the dying cell out of the epithelium (Rosenblatt et al., 2001).

Here, when delaminating cells became 3 or 4 sided and had less than 25% of their initial apical area, Myosin-II was seen coalescing around the apices of surrounding cells (Fig. 6.10A). Myosin-II intensity was measured after background subtraction in order to correct for bleaching of the sample. The analysis of Myosin-II intensity approximately correlated with apical area decrease (Fig. 6.10B), indicating that it may generate the force to drive the last phase of apical loss in delaminating cells. To test this hypothesis, we used laser nano-dissection to ablate Myosin-II cables around the apex of delaminating cells. A laser cut in these fibers led to a rapid increase in apical area, indicating that Myosin-II provides the force for this final apical constriction in cell delamination (Fig. 6.11). Moreover, these cells were imaged for 20 minutes after laser cutting, but did not disappear as expected for delaminating cells showing Myosin-II accumulation (Fig. 6.11). Therefore, Myosin-II appears to drive the final apical extrusion of delaminating cells from the tissue.

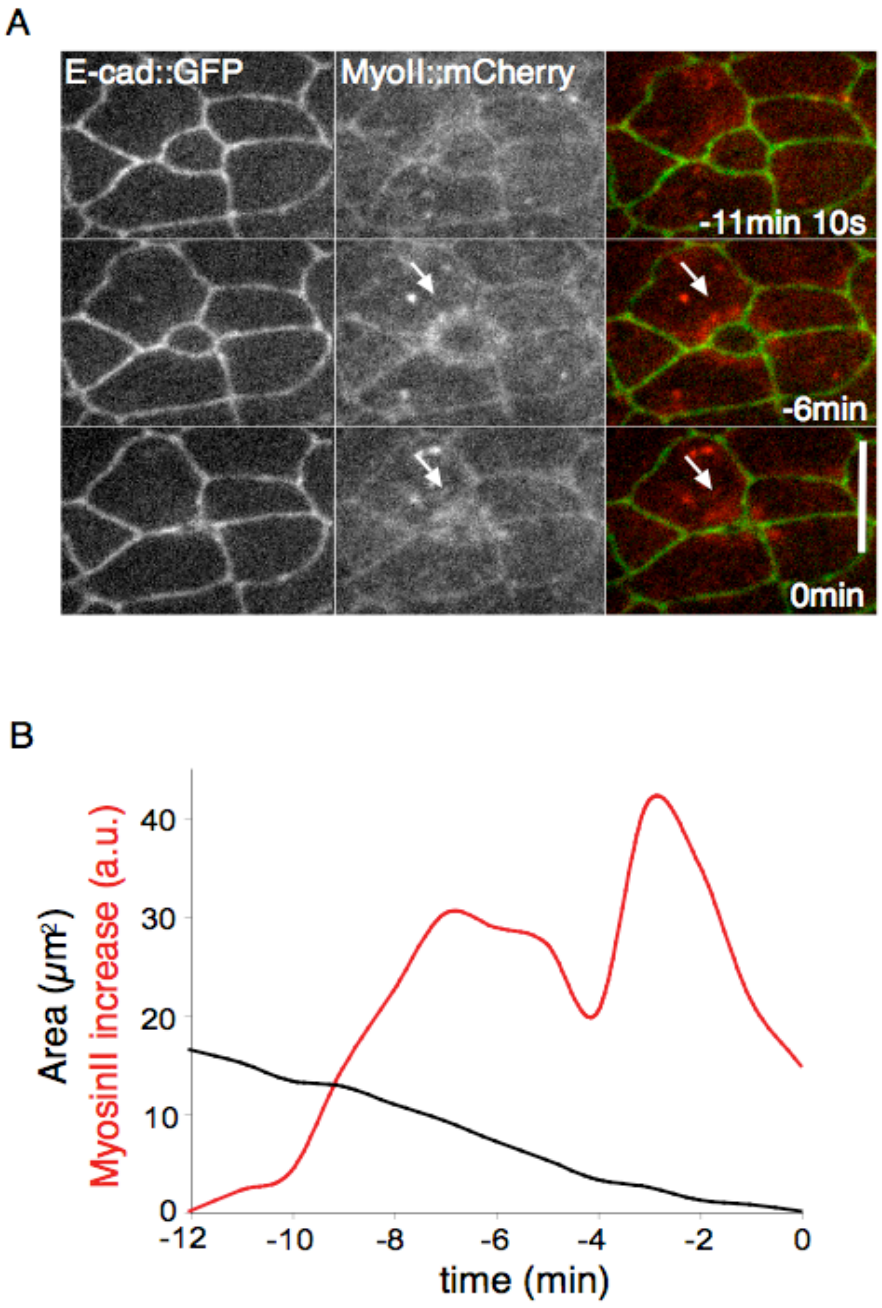

Figure 6.10 Myosin-II coalesces around the apex of delaminating cells in the last phase of apical loss

(A) Tissue marked with E-cadherin::GFP and MyoII::Cherry. Myosin-II ring is indicated by the arrows. Scale bar, 10 μm. (B) The graph shows the apical area decrease (black curve) and Myosin-II intensity (red curve) over time. Myosin-II pixel intensity was quantified with Image j by drawing a region (fixed area over time) all around the apex of the delaminating cell.

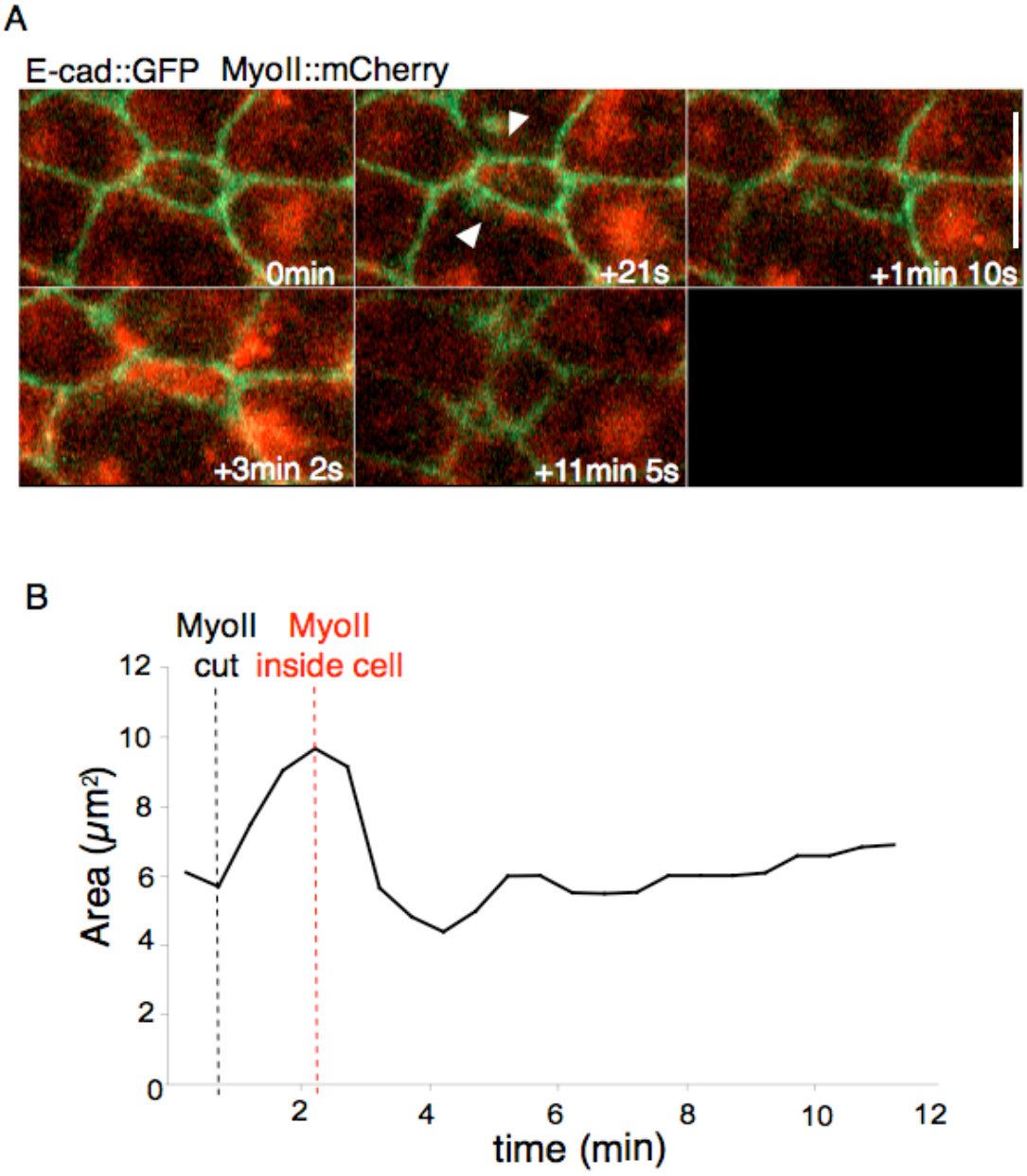

Figure 6.11 Myosin-II drives the final phase of apical loss

(A) Tissue marked with E-cadherin::GFP and MyoII::Cherry. Myosin-II ablation points are indicated by the arrows. Scale bar, 10 µm. (B) The graph shows the apical area oscillation (black curve) over time. Dotted lines indicate Myosin-II cut and accumulation inside the cell.

6.7 Myosin-II localizes at the junctions of extruded cells after UV irradiation-induced apoptosis

Myosin-II was shown to drive the extrusion of apoptotic cells (Rosenblatt et al., 2001). This is important to maintain an intact epithelial barrier. Rosenblatt *et al*. showed that early apoptotic epithelial cells trigger the formation of an actin and myosin ring in the live neighboring cells surrounding it. Rho-dependent contraction of this ring then squeezes the dying cell out of the epithelium (Rosenblatt et al., 2001).

To understand whether there was any difference in localization and timing of accumulation of Myosin-II in the case of apoptotic-induced extrusion compare to the process of midline delamination described in this thesis, we irradiated pupae with UV light in order to induce apoptosis in the notum. We then imaged the tissue marked with E-cadherin::GFP and Myosin-II::Cherry 2 hours after irradiation. Many cells were extruded from the epithelium and some of them exhibited loss of E-cadherin from the contacts with neighbouring cells (Fig. 6.12). In apoptotic cells, Myosin-II accumulated early during this process of cell extrusion at the junctions of the dying cell (Fig.6.12).
In conclusion, the analysis of Myosin-II localization showed a different behaviour of the contractile acto-myosin ring in the case of apoptotic cells compare to live cell delamination. In the latter process, Myosin-II accumulated only in last phase of apical loss in the neighbouring cells. In the case of apoptotic-induced extrusion, Myosin-II accumulated early during this process at cell-cell junctions, which was previously shown to drive extrusion (Rosenblatt et al., 2001).

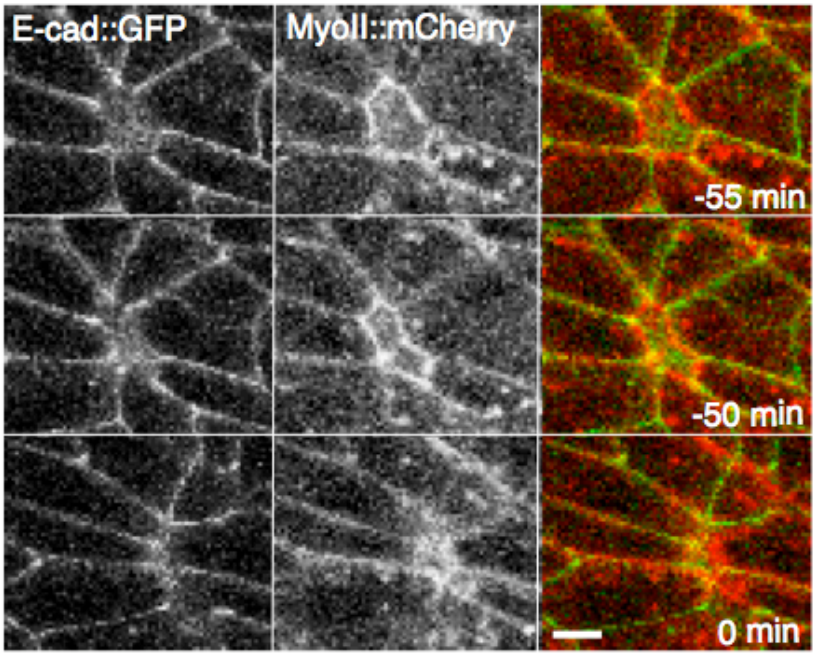

Figure 6.12 Myosin-II localizes at the junctions of extruded cells after UV irradiation-induced apoptosis

Tissue marked with E-cadherin::GFP and MyoII::Cherry. Myosin-II (in red) localizes at the junctions of the dying cell, which shows loss of E-cadherin from the adherens junctions. Scale bar, 10 μm.

6.8 Conclusions

The analysis of junction dynamics revealed the existence of two types of behaviours in the tissue. A small population of cells delaminates by the formation of rosette-like intermediates, by gradually losing apical area but not junctions over time. This mechanism of cell delamination is specifically inhibited by DIAP1 overexpression. Interestingly, this type of behaviour is observed when apoptosis is induced by UV irradiation in the tissue.

In the majority of cases, cells leave the tissue by stochastically losing junctions over time via neighbour exchange events. Delamination via serial junctional loss is apoptotic-independent and is enhanced when growth is increased in the tissue by upregulation of PI3K signalling. Interestingly, Warts RNAi increased the proportion of cells leaving via rosette-like intermediates, probably increasing the number of cells dying as the result of increased density in the tissue, despite the fact that cells with low level of Warts were shown to have high levels of DIAP1 (Udan et al., 2003).

Growth-dependent delamination appears to be a two step-process. First, in an epithelium competition between cells undergoing random topological rearrangements causes some to suffer the progressive loss of junctions and apical area. Then, once a cell has a small apex and fewer than 5 neighbors, the final apical constriction is driven by the action of an apical Myosin-II belt that forms within its 3-4 neighbors. Interestingly, Myosin-II localisation in this process appears to be distinct from the accumulation of Myosin-II after UV irradiation-induced apoptosis in the tissue. In this case, Myosin-II accumulates from the beginning of apical loss at the junctions of the extruded cell.

7. DISCUSSION

7.1 Introduction

The aims of this thesis were to identify the mechanisms that contribute to tissue refinement in developing epithelia. In particular, how tissues balance proliferation and cell loss in order to regulate their size and shape. Importantly, tissue shape is robust and conserved, even when size is reduced.

To understand the complex process of homeostasis achievement in developing epithelia, global perturbations in growth were analysed using the *pnr*-GAL4 driver, which is expressed in a wide domain in the medial part of the notum. Then, to understand the cell autonomous interactions between growth and cell loss, the system was perturbed using ND638-GAL4 driver, expressed in the lateral domain of the tissue. The effect of these changes in growth was quantified on the midline of the tissue, which is not included in the ND638 domain and where the majority of cells delaminate. Finally, to understand the robustness of this homeostatic mechanism, smaller animals following starvation were analysed. In starved animals, despite the tissue being smaller compared to animals grown in standard food conditions, bristle spacing and tissue form were conserved.

Through this work, I have identified a novel mechanism of live cell delamination, which counter-balances tissue growth to relieve over-crowding in the achievement of tissue homeostasis. A vertex model of epithelial mechanics recapitulates this process of delamination and suggests a role for tissue pressure. Based on these findings, crowding-induced stochastic cell delamination is likely to be a generic mechanism that buffers epithelia against variations in growth.

These findings have implications for our understanding of tumor progression. Cells delaminate as the result of tissue crowding. Apoptosis is then activated following the loss of cell-cell apical contacts, in a process similar to anoikis (Emoto, 2008). Thus, cells in hyperplastic tissues are likely to delaminate from the epithelium. Metastasis then results from cell survival underneath the epithelium, despite the loss of contacts with the neighbouring cells.

7.2 Live cell delamination is a 2-step process that counter-balances tissue growth in the achievement of tissue homeostasis

Midline cell delamination suggested the existence of a possible mechanism of cell loss, which acts to relieve tissue overcrowding. This seems to be the case of the midline of the tissue, where cells experience different forces. To test if this process was responsive to tissue mechanics, I increased growth-induced tissue crowding in the notum, by up-regulating PI3K signaling (Weinkove et al., 1999) or through inhibition of Hippo pathway signaling (Halder and Johnson, 2011). In both cases a significant increase in cell loss was observed across the whole tissue. Conversely, when growth was inhibited, delamination dramatically decreased from the midline of the tissue. Moreover, this process appears non-cell autonomous because increase in growth in regions outside the midline, caused delamination across the boundary of the p110 expression domain. These data support the idea that delamination responds to tissue mechanics.

The analysis of delamination kinetics revealed a 2 step-process that is accompanied by progressive loss of apical area (Fig. 7.1A). In the first phase, cells stochastically lose junctions over time, through topological rearrangements called T1 transitions. In a situation of increased crowding, determined for instance by increased growth, loss of junction is accompanied by loss of apical area. This appears to be stochastic, since: i) there is a variable distribution of delaminating cells in space and time between different animals, ii) there is a large variation in the time for a cell to delaminate (between 40 and 90 minutes). Moreover, cells can be rescued by immediate delamination by cutting Myosin-II cables.

However, when a delaminating cell has a small apex and few sides, it rapidly loses its apical domain in a reproducible time interval of 10 minutes, and junctions decrease in length in a coordinated fashion. Myosin-II accumulates around the apex of the delaminating cell forming a cable around the junctions in the neighbouring cells (Fig. 7.1A), to trigger the rapid final apical loss. Interestingly, in the computational model, cells show these 2 distinct phases of delamination. In a situation of crowding, cells

delaminate by serial loss of junctions accompanied by decrease in apical area. However, when a cell is small with few sides, cell delamination had to be implemented in the model due to the high energetic cost of eliminating the cell by noise alone. This could explain Myosin-II recruitment *in vivo*, which could generate the force necessary to drive the final extrusion. This could be due to pressure that delaminating cells appear to exert on their neighbours as they resist apical loss, causing neighbours to actively respond by accumulation of Myosin-II cables apically around the cell-cell interface. In movies it appears that Myosin-II accumulates once the cell has reached a small circular apex, suggesting that this geometry may play a role in self-reinforcing Myosin-II recruitment. However, it is possible that Myosin-II accumulation at this stage is driven by cell-cell biochemical signaling rather than purely by tissue mechanics.

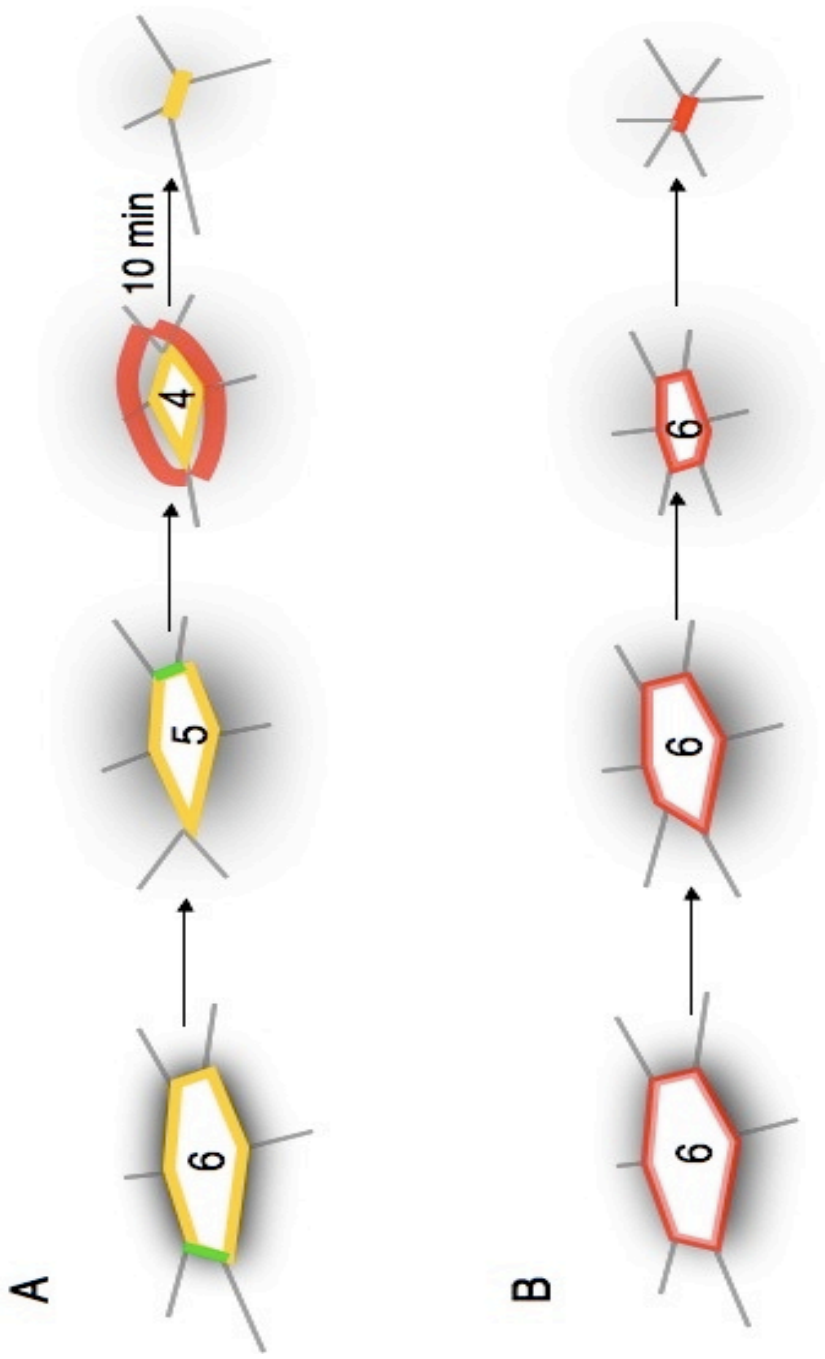

Figure 7.1 Live cell delamination and apoptotic cell extrusion

(A) The figure shows our model for mechanism of live cell delamination. In green are indicated the junctions that shrink into a vertex during the process. (B) Mechanism of apoptotic cell extrusion. Myosin-II accumulation is indicated in red in the figure, localised around the delaminating cell apex in (A) and at the junctions in (B).

7.3 Force generation and transmission during morphogenesis of the notum

The problem of how tissues organise, change shape and acquire complex forms during morphogenesis has long been studied. Several theories have emerged to explain these rearrangements. Complex morphogenetic processes are now thought to arise as the result of basic principles of cell-cell communication and cell shape changes (Fristrom, 1988; Rauzi and Lecuit, 2009). The most common processes that determine tissue remodeling in different species are tissue elongation, bending and invagination, which are driven by the coordinated deformation of single cells (Fristrom, 1988). These changes are conserved in evolution and likely reflect simple physical rules. In 1917 D'Arcy Thompson described the tendency of cells to assemble in epithelial sheets by following mathematical rules (Thompson, 1917). Cells, like bubbles, organize following the geometrical principle of surface minimization. According to this rule, they adhere to each other to form three-way vertices at an angle of 120°, leading to hexagonal tissue packing. This configuration is the most stable and requires less energy, being near a condition of mechanical equilibrium. Interestingly, like bubbles, when isolated from tissues through trypsinization, cells become round. Thompson proposed the theory that cells minimize their surface tension by minimizing contacts with their neighbours. The result is a hexagonal configuration, which is prevalent in most epithelial tissues (Thompson, 1917).

Adhesion between cells is clearly important in the regulation of tissue surface tension, which is mediated by the formation of homophilic interactions of E-cadherin at the *zonula adherens* (Lecuit and Lenne, 2007). These molecules associate in a complex with several binding partners in order to mediate adhesion between adjacent cells. More recently, cortical tension emerged as an additional player (Lecuit and Lenne, 2007; Rauzi et al., 2008). The contractile network, constituted by the acto-myosin cytoskeleton, generates movement and force by Myosin-II mediated contraction of anti-parallel actin fibers (Rauzi et al., 2008). The interplay between AJs and this contractile network allow different cell shape changes and cell-cell contact remodeling. The role of

these molecules in surface tension transmission has been tested by laser ablation experiments of cutting single junctions. For example, Rauzi *et al*. showed through laser cutting that vertices relaxation depends on Myosin-II accumulation at the junctions, during germ band elongation (Rauzi et al., 2008). Surface tension was highest at AJs where Myosin-II was predominantly localised.

Another property has been proposed to contribute to generate the force necessary for tissue morphogenesis. Cells, in contrast to bubbles, resist to deformation because of their elastic properties, which measure the deviations from a preferred size of the cell (Farhadifar et al., 2007; Hufnagel et al., 2007; Kafer et al., 2007). In our model of epithelial tissue mechanics based on the Farhadifar model (Farhadifar et al., 2007), elastic properties are expressed by the compressibility (function of the area) and line tension (function of the perimeter) terms. *In vivo*, we tested the forces acting on the notum during development by laser ablation. Vertex displacement was measured after nano-cutting. Vertex recoil indicates not only Myosin-II mediated contractility of single junctions, but also the resistance of single cells to the local forces acting on these junctions, since cells appeared to have a preferred size. These factors contribute to the cellular viscoelastic properties, which define the resistance of a cell to deformation when a stress is applied (Paluch and Heisenberg, 2009). Few methods have been developed to measure these physical properties of the cell. The majority of them consist on measuring the dynamic of cell deformation in isolated cells after stretching or compressing a cell with micropipette (Hochmuth, 2000), atomic force microscopy (Wu et al., 1998) or 'optical stretcher' (Guck et al., 2001). However, laser ablation is the only technique used to estimate cellular viscoelasticity *in vivo* in embryos or tissues. Following these experiments, the cell has been described as a viscous drop surrounded by a contractile cortex. Thus, vertex recoil after laser ablation is a measure of the cell deformation, which results from local tissue mechanics, not only of Myosin-II contractility and line tension along the cell-cell contact, as previously shown (Rauzi et al., 2008). According to our results, the kinetic of vertex displacement after laser cutting suggested that junctions within the midline of the tissue have peculiar mechanics and the distance increase between the vertices after ablation is very small (0.5 μm in 16 s). In addition,

the tension along each junction does not seem to correlate with junction length, probably due to the softness of the tissue ablated.

In the case of the midline of the notum, laser ablation experiments of single junctions after cutting cell-cell interfaces in a direction parallel and perpendicular to the anterior-posterior axis of pupae, revealed that cells within the midline are subjected to different tissue mechanics on both directions compared to outside the midline, since vertex displacement in midline junctions was significantly less compared to the outside. This result could be explained by three different hypotheses: i) different forces acting on midline junctions (compression or pulling); ii) 3D conformation of the tissue (slight furrowing at the midline); iii) different adhesive properties between cells within and outside the midline, resulting in a softer or stiffer tissue.

In the case of the first hypothesis, the results of laser ablation rule out the possibility of midline cells to be pulled, as initially deduced by their elongated shape. If midline cells were pulled along their long axis, a higher vertex displacement would be expected in the long axis compared to their short axis. Therefore, these results suggest that compressive forces could act on both axes in midline cells. However, two alternative explanations could be proposed. First, the slight furrowing of the midline could affect tissue mechanics, then midline cells could have different physical properties compared to cells outside the midline. The small vertex displacement of midline cells could be due to midline cells being softer compared to the rest of the tissue, perhaps due to different adhesive properties of these cells.

It is debated how forces are transmitted across epithelial tissues during development. An additional physical property that could influence tissue mechanics is range of mechanical influence in the epithelium. In particular, the analysis of laser ablation experiments in the wildtype notum (Fig. 7.2) and ND638-GAL4 expression of p110 suggested that forces are not transmitted over a long range in the tissue. In the case of p110 PI3K expression, distal increase in growth did not have any effect on midline delamination but drove cells to leave the tissue at the boundaries where p110 was

expressed. This indicates a local effect of increased crowding in the tissue. Similarly, after laser ablation of single junctions, cell deformation was only seen in the first 2 rows of cells close to the cut, which decreased in area as the result of relaxation of the junctions (Fig. 7.2). Thus, together with cortical tension and cortical elasticity, range of mechanical influence should be taken into account when studying tissue mechanics in morphogenesis.

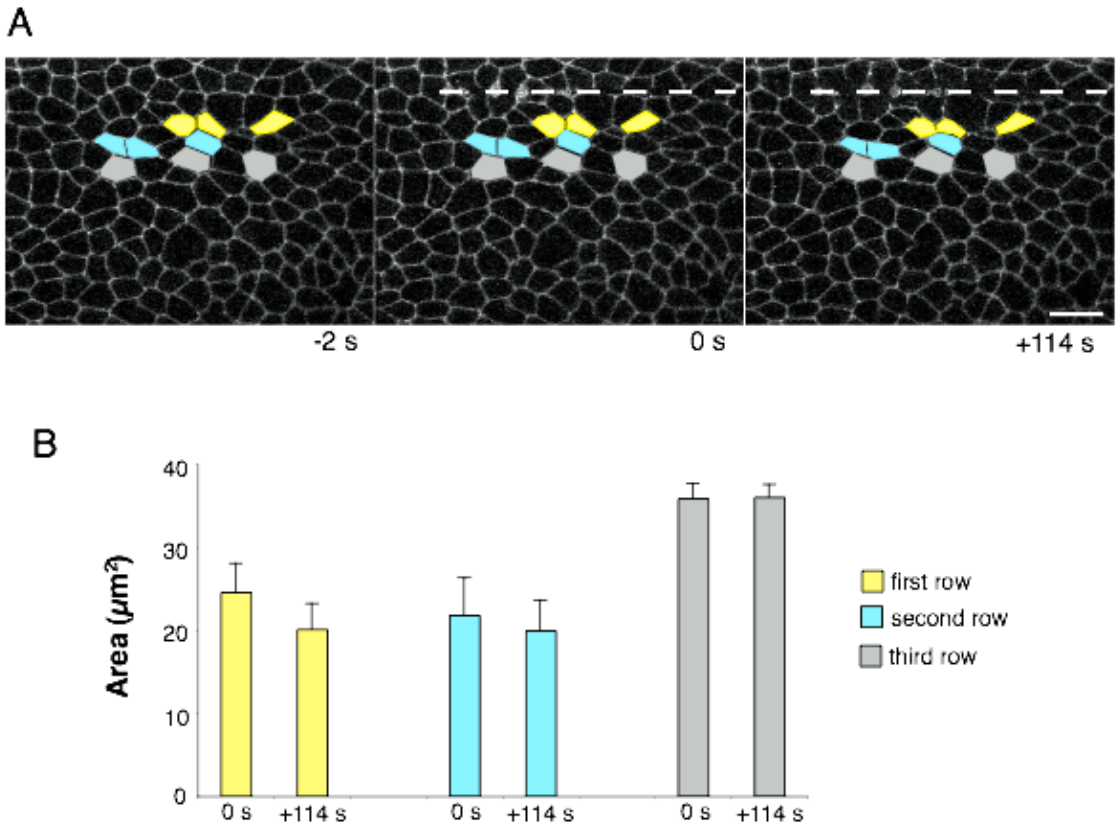

Figure 7.2 Tension relaxation after laser ablation is transmitted in the tissue only in the first 2 rows of cells next to the cut

(A) The figure shows stills from a movie during laser ablation of the notum. The white dashed line indicates the cut (0 s). Cells from the first row next to the cut are coloured in yellow, from the second and the third in light blue and grey respectively. Scale bar, 10 μm. (B) Average cell area (± st.dev.) before and following laser ablation (+114 s) in the first three rows of cells next to the cut (colours as in the figure (A)).

7.4 Tissue proliferation: the problem of uncoupling cell size, cell division and developmental time in the notum of *Drosophila*

One of the principle regulators of organ and tissue size during development in *Drosophila* is the PI3K signaling pathway. Components of the PI3K signaling pathway have been implicated in regulation of different processes during development, including cell growth (increase in cell mass), cell division and differentiation, which all occur at specific developmental times (Weinkove et al., 1999). Modulation of the activity of p110 and AKT has been shown to affect cell size in wing imaginal discs of *Drosophila* (Leevers et al., 1996). Moreover, null mutations in the downstream component DS6K and overexpression of the pathway inhibitor PTEN both decrease cell size in developing imaginal discs (Gao et al., 2000; Montagne et al., 1999). Similar observations were made in this study of the notum. The analysis of cell number in animals in which these proteins were overexpressed or knocked down, also revealed an effect on cell division, which was relatively mild compared to the effect on cell size. Thus, over-expression of p110 resulted in a modest increase in cell number in the notum as well as in wing imaginal discs, as previously reported (Leevers et al., 1996; Weinkove et al., 1999), and a significant increase in cell size. It is tempting to speculate that the effects of PI3K signaling on translation initiation, promoting protein synthesis (Dufner and Thomas, 1999), could result in faster accumulation of G1 cyclins to the critical levels, required to promote cell cycle progression (Evans et al., 1983). Several observations support this idea. Flow cytometry analysis suggested that PI3K signaling pathway influences progression through different phases of the cell cycle. The proportion of cells in G1 is reduced, while the one in S and G2-M phase is increased (Gao et al., 2000; Weinkove et al., 1999). Thus, growth and division are coupled in epithelial tissues. This coupling is particularly evident for Hippo pathway perturbations, since in Warts RNAi tissues cell size is constant despite variations in cell number. Conversely, cell division does not affect growth, as seen in Cdc25 RNAi experiments (Neufeld et al., 1998).

The effect of PI3K signaling pathway on cell division rates could affect cell fate specification and differentiation, modulating developmental time. In particular, analysis

of PI3K, PTEN, Tor, TSC1 and S6K in the development of *Drosophila* eye revealed that increased PI3K signaling activity causes precocious differentiation, while down-regulation of this pathway delays differentiation (Bateman and McNeill, 2004). Developmental timing in nota of PI3K mutants was calculated using SOP lineage cell differentiation as a marker. Although in p110 overexpressing nota, the onset of cell division was earlier in development compared to the wildtype, SOP lineage cells differentiation timing was similar compared to the control. A similar timing was observed also in PTEN RNAi, PI3K RNAi and r5s RNAi tissues. However, in TSC1 and 2 overexpression tissues, P1 cell differentiation was severely delayed, for ~10 hours, resulting in fewer smaller P1 cells in the adult dorsal thorax. Thus, some components of the pathway have an effect on developmental timing.

Because growth, cell cycle and developmental timing are regulated by common signaling pathways, it is difficult to uncouple these events. For instance, timing may have an impact on the regulation of delamination in animals over-expressing TSC1 and TSC2. This appears not to be the sole explanation for the decrease in delamination, since r5s RNAi and PI3K RNAi reduced delamination but did not affect developmental timing. However, it would be a good idea to further study the effect of developmental timing on cell delamination in nota overexpressing 4EBP, cyclinD/cdk4 or Myc, since in the eye they were shown to affect cell growth but not cell differentiation (McNeill et al., 2008).

Cell division does not seem necessary for cell delamination to occur in the tissue, since cells delaminate from the tissue before the onset of division in the developing notum. Moreover, this process does not correlate locally with cell delamination when division is locally inhibited by Cdc25 RNAi. However, a possible effect on cell delamination cannot be completely ruled out, since cell division increases the rate of neighbour exchange events in the tissue.

7.5 Live cell delamination is not triggered by cell competition mechanisms

Cell competition is an homeostatic process in which cells with a slow metabolism are eliminated from an epithelial tissue by a population of faster dividing cells (Morata and Ripoll, 1975). It is thought to be an important mechanism in the regulation of tissue size in morphogenesis. Despite epithelial cell delamination in the notum being a regionalised process at the midline of the tissue, where cells appear morphologically different, midline cells do not appear to be eliminated from the tissue as the result of cell competition. JNK and Fwe have been shown to be the major effectors to trigger cell death of 'loser' cells (Moreno et al., 2002; Rhiner et al., 2010). Although the role of JNK in cell competition is not totally clear, Fwe is thought to be necessary and sufficient to mediate cell competition induced-death (Rhiner et al., 2010).

In the midline of the notum, the JNK pathway is activated during thorax closure and results in midline cells Puc expression. The analysis of Puc expression in the midline of the tissue revealed that JNK pathway could be active after thorax closure, triggering midline cell death. However, the expression of JNK RNAi did not block epithelial cell delamination and was independent of cell death. It has been previously reported that in the case of cell competition triggered by different levels of Myc, JNK inhibition could not completely block cell death, which was triggered by Hid (de la Cova et al., 2004). Moreover, in *tkv* mutant clones, inhibition of JNK did not stop cells being eliminated from the tissue (Adachi-Yamada et al., 1999; Gibson and Perrimon, 2005).

Fwe was shown to be the main trigger of cell competition, upstream of caspase activation. If it is lost in an entire tissue, cell competition cannot occur and 'losers' cells accumulate (Rhiner et al., 2010). Expression of Fwe RNAi in the notum did not block cell delamination. However a modest decrease in the percentage of cells delaminating was observed. Thus, although cell competition does not seem to be the main process triggering cell delamination, it may contribute to some cell death in the tissue.

Importantly however, inhibition of apoptosis by DIAP1 over-expression did not completely block cell delamination, but induced a 30% decrease in the number of delaminating cells, indicating the existence of a small subpopulation of cells in the tissue that are extruded as a consequence of apoptosis activation. This process has been previously described in the literature in *Drosophila* during dorsal closure (Muliyil et al., 2011), in tracheal system development (Baer et al., 2011) and in zebrafish embryogenesis (Cole and Ross, 2001). In these cases, the apoptosis of delaminating cells appears to be necessary and sufficient to drive cell delamination. Thus, antiapoptotic protein over-expression in these systems suppresses completely or nearly cell delamination (Muliyil et al., 2011). Mithocondrial fragmentation appears to precede the activation of the apoptotic cascade and the inhibition of this event blocks delamination of AS cells, affecting the completion of dorsal closure (Muliyil et al., 2011). In addition, other stresses could lead to elimination of cells from epithelial tissues. Disruption of cell-cell contacts has been proposed to trigger the detachment and the following activation of the apoptotic cascade in delaminating cells (Gibson and Perrimon, 2005). Moreover, loss of apical determinants triggers apoptosis in the embryonic epidermis of *Drosophila* through the activation of JNK signaling (Kolahgar et al., 2011).

Apoptotic cells are extruded from an epithelial monolayer through the formation of rosette-like intermediates, where neighbouring cells take the place of the dying cells. This process is mediated by the contraction of an acto-myosin ring, which forms early on during extrusion (Rosenblatt et al., 2001). A similar process was observed to eliminate apoptotic cells in the notum, and it was distinct from live cell delamination in terms of junction dynamics and Myosin-II localisation (Fig. 7.1). In the case of live cell delamination, cells lose their apical domain by serial loss of junctions, which shrink into a vertex (Fig. 7.1A). In the case of apoptosis induced extrusion instead, cells are eliminated by the formation of a rosette-like intermediate (Fig. 7.1B). Moreover, Myosin-II accumulates around the apex of delaminating cells only in the last phase of apical constriction (Fig. 7.1A), while apoptotic cells show junctional Myosin-II around their apex from the beginning of the process of extrusion (Fig. 7.1B), and in some cases loss of E-cadherin at the junctions.

7.6 Outlook and future perspectives

In this thesis, I described a novel process of live cell delamination, which appears to be a two-step mechanism that results from gradual apical loss. First, the delaminating cell loses junctions over time, then when the cell is small and with few sides, Myosin-II accumulates around the apex triggering the final apical loss. It was not possible to identify molecular signals, which if inhibited could stop delamination, other than growth inhibition. However, the model proposed in this thesis predicts that cell delamination is likely to be driven by topological rearrangements that occur stochastically in the tissue. To test the role of T1 transitions in driving epithelial cell delamination, cortical rigidity could be increased. Preliminary results suggest that increasing Myosin-II activity by expression of MYPT-75D RNAi, results in higher rigidity of the tissue and a decrease in number of T1 transitions compared to the control (Fig. 7.3). MYPT-75D is a specific regulatory subunit of PP1β, which activates the myosin phosphatase activity (Vereshchagina et al., 2004). In the future, the analysis of tissues expressing MYPT-75D or equivalent perturbations, would enable to test the role of T1 transitions in cell delamination.

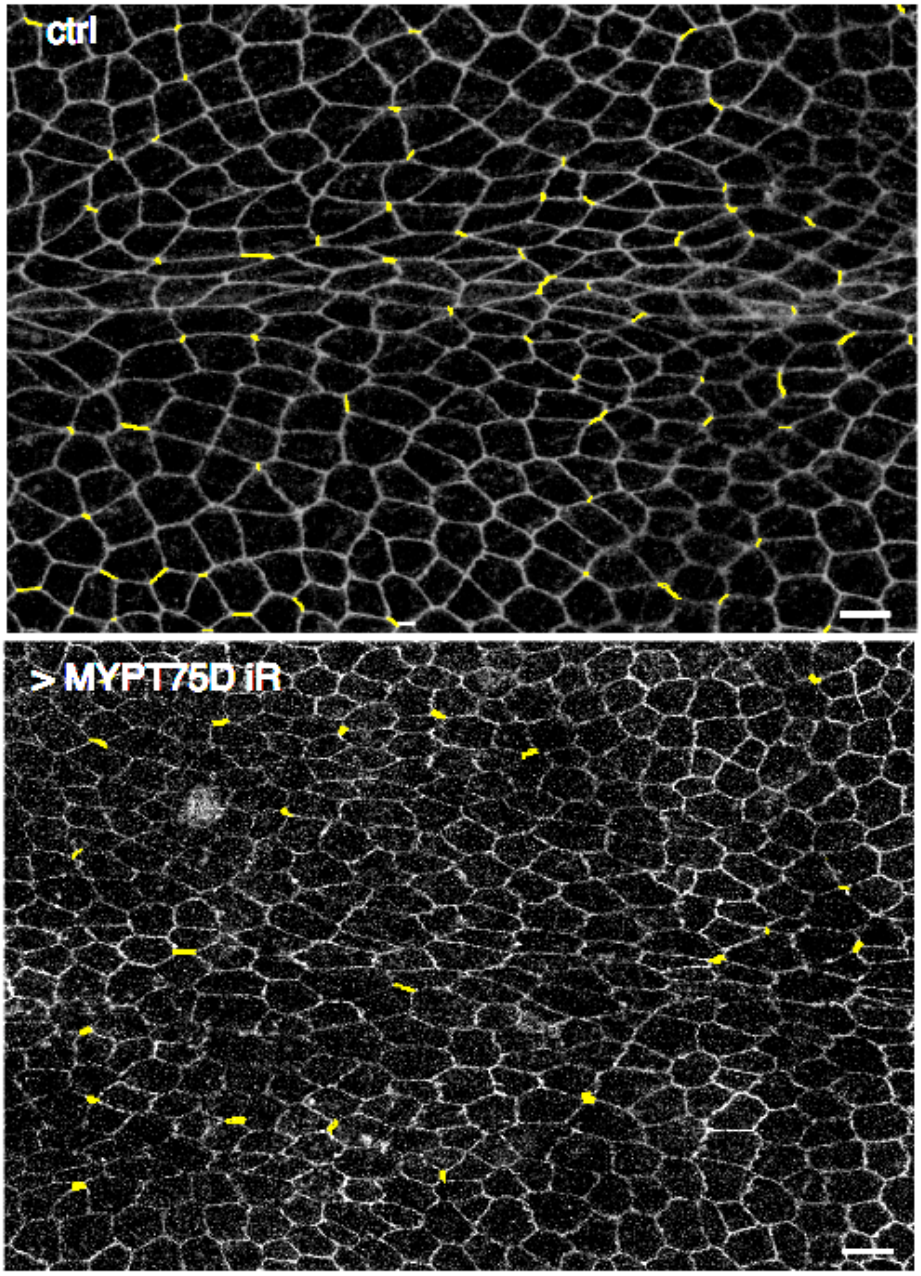

Figure 7.3 MYPT-75D RNAi nota show a decrease in T1 transitions

The figure shows the junctions undergoing T1 transitions before the onset of division for control and MYPT-75D RNAi tissues, indicated in yellow. Scale bar, 10 μm.

Delaminating cells become pyknotic after losing their apical domain, suggesting the possibility of the existence of a survival signaling mechanism triggered by the adhesion to neighbouring cells, in a process like anoikis (Emoto, 2008). This may be key to the process of metastasis. In the future, it would be important to identify the molecules responsible for the regulation of cell death following delamination. Cytoskeleton components would be likely candidates, since in anoikis substantial evidence exists that both signaling molecules and apoptosis regulators are associated with the cytoskeleton (Vachon, 2011). Disruption of anchorage-dependent apoptosis would enable cell survival underneath the epithelium. These cells could then divide and migrate in the body, providing a new model for tumor progression.

Finally, it would be interesting to investigate the role of the basal lamina and how apical and basal signals are coordinated in epithelial cell delamination. This work suggests that the initial event could be apical constriction, but this could determine further basal rearrangements in the delaminating cell.

8. BIBLIOGRAPHY

Adachi-Yamada, T., Fujimura-Kamada, K., Nishida, Y. and Matsumoto, K. (1999). Distortion of proximodistal information causes JNK-dependent apoptosis in Drosophila wing. *Nature* **400**, 166-9.

Adachi-Yamada, T. and O'Connor, M. B. (2002). Morphogenetic apoptosis: a mechanism for correcting discontinuities in morphogen gradients. *Dev Biol* **251**, 74-90.

Agnes, F., Suzanne, M. and Noselli, S. (1999). The Drosophila JNK pathway controls the morphogenesis of imaginal discs during metamorphosis. *Development* **126**, 5453-62.

Aldaz, S., Morata, G. and Azpiazu, N. (2003). The Pax-homeobox gene eyegone is involved in the subdivision of the thorax of Drosophila. *Development* **130**, 4473-82.

Alessi, D. R., James, S. R., Downes, C. P., Holmes, A. B., Gaffney, P. R., Reese, C. B. and Cohen, P. (1997). Characterization of a 3-phosphoinositide-dependent protein kinase which phosphorylates and activates protein kinase Balpha. *Curr Biol* **7**, 261-9.

Alessi, D. R., Kozlowski, M. T., Weng, Q. P., Morrice, N. and Avruch, J. (1998). 3-Phosphoinositide-dependent protein kinase 1 (PDK1) phosphorylates and activates the p70 S6 kinase in vivo and in vitro. *Curr Biol* **8**, 69-81.

Aplin, A. E., Howe, A. K. and Juliano, R. L. (1999). Cell adhesion molecules, signal transduction and cell growth. *Curr Opin Cell Biol* **11**, 737-44.

Artavanis-Tsakonas, S., Rand, M. D. and Lake, R. J. (1999). Notch signaling: cell fate control and signal integration in development. *Science* **284**, 770-6.

Attwell, S., Roskelley, C. and Dedhar, S. (2000). The integrin-linked kinase (ILK) suppresses anoikis. *Oncogene* **19**, 3811-5.

Baer, M. M., Bilstein, A., Caussinus, E., Csiszar, A., Affolter, M. and Leptin, M. (2011). The role of apoptosis in shaping the tracheal system in the Drosophila embryo. *Mech Dev* **127**, 28-35.

Balklava, Z., Pant, S., Fares, H. and Grant, B. D. (2007). Genome-wide analysis identifies a general requirement for polarity proteins in endocytic traffic. *Nat Cell Biol* **9**, 1066-73.

Bardet, P. L., Kolahgar, G., Mynett, A., Miguel-Aliaga, I., Briscoe, J., Meier, P. and Vincent, J. P. (2008). A fluorescent reporter of caspase activity for live imaging. *Proc Natl Acad Sci U S A* **105**, 13901-5.

Barrett, K., Leptin, M. and Settleman, J. (1997). The Rho GTPase and a putative RhoGEF mediate a signaling pathway for the cell shape changes in Drosophila gastrulation. *Cell* **91**, 905-15.

Bateman, J. M. and McNeill, H. (2004). Temporal control of differentiation by the insulin receptor/tor pathway in Drosophila. *Cell* **119**, 87-96.

Baumgartner, R., Poernbacher, I., Buser, N., Hafen, E. and Stocker, H. (2010). The WW domain protein Kibra acts upstream of Hippo in Drosophila. *Dev Cell* **18**, 309-16.

Bennett, F. C. and Harvey, K. F. (2006). Fat cadherin modulates organ size in Drosophila via the Salvador/Warts/Hippo signaling pathway. *Curr Biol* **16**, 2101-10.

Bertet, C., Rauzi, M. and Lecuit, T. (2009). Repression of Wasp by JAK/STAT signalling inhibits medial actomyosin network assembly and apical cell constriction in intercalating epithelial cells. *Development* **136**, 4199-212.

Bertet, C., Sulak, L. and Lecuit, T. (2004). Myosin-dependent junction remodelling controls planar cell intercalation and axis elongation. *Nature* **429**, 667-71.

Bilder, D. (2004). Epithelial polarity and proliferation control: links from the Drosophila neoplastic tumor suppressors. *Genes Dev* **18**, 1909-25.

Blair, S. S. (1995). Compartments and appendage development in Drosophila. *Bioessays* **17**, 299-309.

Blankenship, J. T., Backovic, S. T., Sanny, J. S., Weitz, O. and Zallen, J. A. (2006). Multicellular rosette formation links planar cell polarity to tissue morphogenesis. *Dev Cell* **11**, 459-70.

Boedigheimer, M. J., Nguyen, K. P. and Bryant, P. J. (1997). Expanded functions in the apical cell domain to regulate the growth rate of imaginal discs. *Dev Genet* **20**, 103-10.

Bohni, R., Riesgo-Escovar, J., Oldham, S., Brogiolo, W., Stocker, H., Andruss, B. F., Beckingham, K. and Hafen, E. (1999). Autonomous control of cell and organ size by CHICO, a Drosophila homolog of vertebrate IRS1-4. *Cell* **97**, 865-75.

Brand, A. H., Manoukian, A. S. and Perrimon, N. (1994). Ectopic expression in Drosophila. *Methods Cell Biol* **44**, 635-54.

Brumby, A. M. and Richardson, H. E. (2003). scribble mutants cooperate with oncogenic Ras or Notch to cause neoplastic overgrowth in Drosophila. *EMBO J* **22**, 5769-79.

Brunn, G. J., Hudson, C. C., Sekulic, A., Williams, J. M., Hosoi, H., Houghton, P. J., Lawrence, J. C., Jr. and Abraham, R. T. (1997). Phosphorylation of the translational repressor PHAS-I by the mammalian target of rapamycin. *Science* **277**, 99-101.

Bryant, P. J. and Simpson, P. (1984). Intrinsic and extrinsic control of growth in developing organs. *Q Rev Biol* **59**, 387-415.

Burnett, P. E., Barrow, R. K., Cohen, N. A., Snyder, S. H. and Sabatini, D. M. (1998). RAFT1 phosphorylation of the translational regulators p70 S6 kinase and 4E-BP1. *Proc Natl Acad Sci U S A* **95**, 1432-7.

Calleja, M., Herranz, H., Estella, C., Casal, J., Lawrence, P., Simpson, P. and Morata, G. (2000). Generation of medial and lateral dorsal body domains by the pannier gene of Drosophila. *Development* **127**, 3971-80.

Castrillon, D. H. and Wasserman, S. A. (1994). Diaphanous is required for cytokinesis in Drosophila and shares domains of similarity with the products of the limb deformity gene. *Development* **120**, 3367-77.

Cavey, M., Rauzi, M., Lenne, P. F. and Lecuit, T. (2008). A two-tiered mechanism for stabilization and immobilization of E-cadherin. *Nature* **453**, 751-6.

Cavodeassi, F., Modolell, J. and Gomez-Skarmeta, J. L. (2001). The Iroquois family of genes: from body building to neural patterning. *Development* **128**, 2847-55.

Cavodeassi, F., Rodriguez, I. and Modolell, J. (2002). Dpp signalling is a key effector of the wing-body wall subdivision of the Drosophila mesothorax. *Development* **129**, 3815-23.

Chen, C., Jack, J. and Garofalo, R. S. (1996). The Drosophila insulin receptor is required for normal growth. *Endocrinology* **137**, 846-56.

Cho, E., Feng, Y., Rauskolb, C., Maitra, S., Fehon, R. and Irvine, K. D. (2006). Delineation of a Fat tumor suppressor pathway. *Nat Genet* **38**, 1142-50.

Cohen, M., Georgiou, M., Stevenson, N. L., Miodownik, M. and Baum, B. (2011). Dynamic filopodia transmit intermittent Delta-Notch signaling to drive pattern refinement during lateral inhibition. In *Dev Cell*, vol. 19 (ed., pp. 78-89.

Cole, L. K. and Ross, L. S. (2001). Apoptosis in the developing zebrafish embryo. *Dev Biol* **240**, 123-42.

Costa, M., Wilson, E. T. and Wieschaus, E. (1994). A putative cell signal encoded by the folded gastrulation gene coordinates cell shape changes during Drosophila gastrulation. *Cell* **76**, 1075-89.

Cross, D. A., Alessi, D. R., Cohen, P., Andjelkovich, M. and Hemmings, B. A. (1995). Inhibition of glycogen synthase kinase-3 by insulin mediated by protein kinase B. *Nature* **378**, 785-9.

Cubadda, Y., Heitzler, P., Ray, R. P., Bourouis, M., Ramain, P., Gelbart, W., Simpson, P. and Haenlin, M. (1997). u-shaped encodes a zinc finger protein that regulates the proneural genes achaete and scute during the formation of bristles in Drosophila. *Genes Dev* **11**, 3083-95.

Day, S. J. and Lawrence, P. A. (2000). Measuring dimensions: the regulation of size and shape. *Development* **127**, 2977-87.

de la Cova, C., Abril, M., Bellosta, P., Gallant, P. and Johnston, L. A. (2004). Drosophila myc regulates organ size by inducing cell competition. *Cell* **117**, 107-16.

De La Cruz, E. M. and Ostap, E. M. (2004). Relating biochemistry and function in the myosin superfamily. *Curr Opin Cell Biol* **16**, 61-7.

De Moed, G. H., Kruitwagen, C. L. J. J., De Jong, G. and Scharloo, W. (1999). Critical weight for the induction of pupariation in Drosophila melanogaster: genetic and environmental variation. *Journal of Evolutionary Biology* **12**, 852–858.

Dedhar, S. (2000). Cell-substrate interactions and signaling through ILK. *Curr Opin Cell Biol* **12**, 250-6.

Dietzl, G., Chen, D., Schnorrer, F., Su, K. C., Barinova, Y., Fellner, M., Gasser, B., Kinsey, K., Oppel, S., Scheiblauer, S. et al. (2007). A genome-wide transgenic RNAi library for conditional gene inactivation in Drosophila. *Nature* **448**, 151-6.

Dong, J., Feldmann, G., Huang, J., Wu, S., Zhang, N., Comerford, S. A., Gayyed, M. F., Anders, R. A., Maitra, A. and Pan, D. (2007). Elucidation of a universal size-control mechanism in Drosophila and mammals. *Cell* **130**, 1120-33.

Drees, F., Pokutta, S., Yamada, S., Nelson, W. J. and Weis, W. I. (2005). Alpha-catenin is a molecular switch that binds E-cadherin-beta-catenin and regulates actin-filament assembly. *Cell* **123**, 903-15.

Dufner, A. and Thomas, G. (1999). Ribosomal S6 kinase signaling and the control of translation. *Exp Cell Res* **253**, 100-9.

Edwards, K. A., Chang, X. J. and Kiehart, D. P. (1995). Essential light chain of Drosophila nonmuscle myosin II. *J Muscle Res Cell Motil* **16**, 491-8.

Egelhoff, T. T., Lee, R. J. and Spudich, J. A. (1993). Dictyostelium myosin heavy chain phosphorylation sites regulate myosin filament assembly and localization in vivo. *Cell* **75**, 363-71.

Emoto, Y. (2008). Cellular aggregation facilitates anoikis in MDCK cells. *J Physiol Sci* **58**, 371-80.

Evans, T., Rosenthal, E. T., Youngblom, J., Distel, D. and Hunt, T. (1983). Cyclin: a protein specified by maternal mRNA in sea urchin eggs that is destroyed at each cleavage division. *Cell* **33**, 389-96.

Farhadifar, R., Roper, J. C., Aigouy, B., Eaton, S. and Julicher, F. (2007). The influence of cell mechanics, cell-cell interactions, and proliferation on epithelial packing. *Curr Biol* **17**, 2095-104.

Farquhar, M. G. and Palade, G. E. (1963). Junctional complexes in various epithelia. *J Cell Biol* **17**, 375-412.

Fernandes, J. J., Celniker, S. E. and VijayRaghavan, K. (1996). Development of the indirect flight muscle attachment sites in Drosophila: role of the PS integrins and the stripe gene. *Dev Biol* **176**, 166-84.

Fernandez, B. G., Arias, A. M. and Jacinto, A. (2007). Dpp signalling orchestrates dorsal closure by regulating cell shape changes both in the amnioserosa and in the epidermis. *Mech Dev* **124**, 884-97.

Fernandez-Gonzalez, R., Simoes Sde, M., Roper, J. C., Eaton, S. and Zallen, J. A. (2009). Myosin II dynamics are regulated by tension in intercalating cells. *Dev Cell* **17**, 736-43.

Franke, J. D., Montague, R. A. and Kiehart, D. P. (2005). Nonmuscle myosin II generates forces that transmit tension and drive contraction in multiple tissues during dorsal closure. *Curr Biol* **15**, 2208-21.

Frisch, S. M., Vuori, K., Ruoslahti, E. and Chan-Hui, P. Y. (1996). Control of adhesion-dependent cell survival by focal adhesion kinase. *J Cell Biol* **134**, 793-9.

Fristrom, D. (1988). The cellular basis of epithelial morphogenesis. A review. *Tissue Cell* **20**, 645-90.

Froldi, F., Ziosi, M., Garoia, F., Pession, A., Grzeschik, N. A., Bellosta, P., Strand, D., Richardson, H. E. and Grifoni, D. (2010). The lethal giant larvae tumour suppressor mutation requires dMyc oncoprotein to promote clonal malignancy. *BMC Biol* **8**, 33.

Gao, X., Neufeld, T. P. and Pan, D. (2000). Drosophila PTEN regulates cell growth and proliferation through PI3K-dependent and -independent pathways. *Dev Biol* **221**, 404-18.

Gao, X. and Pan, D. (2001). TSC1 and TSC2 tumor suppressors antagonize insulin signaling in cell growth. *Genes Dev* **15**, 1383-92.

Garrett, W. S., Chen, L. M., Kroschewski, R., Ebersold, M., Turley, S., Trombetta, S., Galan, J. E. and Mellman, I. (2000). Developmental control of endocytosis in dendritic cells by Cdc42. *Cell* **102**, 325-34.

Genevet, A., Wehr, M. C., Brain, R., Thompson, B. J. and Tapon, N. (2010). Kibra is a regulator of the Salvador/Warts/Hippo signaling network. *Dev Cell* **18**, 300-8.

Georgiou, M., Marinari, E., Burden, J. and Baum, B. (2008). Cdc42, Par6, and aPKC regulate Arp2/3-mediated endocytosis to control local adherens junction stability. *Curr Biol* **18**, 1631-8.

Gerlitz, O., Nellen, D., Ottiger, M. and Basler, K. (2002). A screen for genes expressed in Drosophila imaginal discs. *Int J Dev Biol* **46**, 173-6.

Ghazi, A., Anant, S. and VijayRaghavan, K. (2000). Apterous mediates development of direct flight muscles autonomously and indirect flight muscles through epidermal cues. *Development* **127**, 5309-18.

Ghazi, A., Paul, L. and VijayRaghavan, K. (2003). Prepattern genes and signaling molecules regulate stripe expression to specify Drosophila flight muscle attachment sites. *Mech Dev* **120**, 519-28.

Giancotti, F. G. and Ruoslahti, E. (1999). Integrin signaling. *Science* **285**, 1028-32.

Gibson, M. C. and Perrimon, N. (2005). Extrusion and death of DPP/BMP-compromised epithelial cells in the developing Drosophila wing. *Science* **307**, 1785-9.

Gloushankova, N. A., Alieva, N. A., Krendel, M. F., Bonder, E. M., Feder, H. H., Vasiliev, J. M. and Gelfand, I. M. (1997). Cell-cell contact changes the dynamics of lamellar activity in nontransformed epitheliocytes but not in their ras-transformed descendants. *Proc Natl Acad Sci U S A* **94**, 879-83.

Gomez-Skarmeta, J. L., Diez del Corral, R., de la Calle-Mustienes, E., Ferre-Marco, D. and Modolell, J. (1996). Araucan and caupolican, two members of the novel iroquois complex, encode homeoproteins that control proneural and vein-forming genes. *Cell* **85**, 95-105.

Goulev, Y., Fauny, J. D., Gonzalez-Marti, B., Flagiello, D., Silber, J. and Zider, A. (2008). SCALLOPED interacts with YORKIE, the nuclear effector of the hippo tumor-suppressor pathway in Drosophila. *Curr Biol* **18**, 435-41.

Graner, F. and Glazier, J. A. (1992). Simulation of biological cell sorting using a two-dimensional extended Potts model. *Phys Rev Lett* **69**, 2013-2016.

Grewal, S. S. (2009). Insulin/TOR signaling in growth and homeostasis: a view from the fly world. *Int J Biochem Cell Biol* **41**, 1006-10.

Grosshans, J., Wenzl, C., Herz, H. M., Bartoszewski, S., Schnorrer, F., Vogt, N., Schwarz, H. and Muller, H. A. (2005). RhoGEF2 and the formin Dia control the formation of the furrow canal by directed actin assembly during Drosophila cellularisation. *Development* **132**, 1009-20.

Gu, Y., Forostyan, T., Sabbadini, R. and Rosenblatt, J. (2011). Epithelial cell extrusion requires the sphingosine-1-phosphate receptor 2 pathway. *J Cell Biol* **193**, 667-76.

Guck, J., Ananthakrishnan, R., Mahmood, H., Moon, T. J., Cunningham, C. C. and Kas, J. (2001). The optical stretcher: a novel laser tool to micromanipulate cells. *Biophys J* **81**, 767-84.

Gumbiner, B. M. (2005). Regulation of cadherin-mediated adhesion in morphogenesis. *Nat Rev Mol Cell Biol* **6**, 622-34.

Halder, G. and Johnson, R. L. (2011). Hippo signaling: growth control and beyond. *Development* **138**, 9-22.

Hamaratoglu, F., Willecke, M., Kango-Singh, M., Nolo, R., Hyun, E., Tao, C., Jafar-Nejad, H. and Halder, G. (2006). The tumour-suppressor genes NF2/Merlin and Expanded act through Hippo signalling to regulate cell proliferation and apoptosis. *Nat Cell Biol* **8**, 27-36.

Harris, T. J. and Peifer, M. (2004). Adherens junction-dependent and -independent steps in the establishment of epithelial cell polarity in Drosophila. *J Cell Biol* **167**, 135-47.

Hartenstein, V. and Posakony, J. W. (1990). A dual function of the Notch gene in Drosophila sensillum development. *Dev Biol* **142**, 13-30.

Harvey, K. F., Pfleger, C. M. and Hariharan, I. K. (2003). The Drosophila Mst ortholog, hippo, restricts growth and cell proliferation and promotes apoptosis. *Cell* **114**, 457-67.

Heitzler, P. and Simpson, P. (1991). The choice of cell fate in the epidermis of Drosophila. *Cell* **64**, 1083-92.

Hochmuth, R. M. (2000). Micropipette aspiration of living cells. *J Biomech* **33**, 15-22.

Homem, C. C. and Peifer, M. (2008). Diaphanous regulates myosin and adherens junctions to control cell contractility and protrusive behavior during morphogenesis. *Development* **135**, 1005-18.

Huang, J., Wu, S., Barrera, J., Matthews, K. and Pan, D. (2005). The Hippo signaling pathway coordinately regulates cell proliferation and apoptosis by inactivating Yorkie, the Drosophila Homolog of YAP. *Cell* **122**, 421-34.

Hufnagel, L., Teleman, A. A., Rouault, H., Cohen, S. M. and Shraiman, B. I. (2007). On the mechanism of wing size determination in fly development. *Proc Natl Acad Sci U S A* **104**, 3835-40.

Hutson, M. S., Tokutake, Y., Chang, M. S., Bloor, J. W., Venakides, S., Kiehart, D. P. and Edwards, G. S. (2003). Forces for morphogenesis investigated with laser microsurgery and quantitative modeling. *Science* **300**, 145-9.

Igaki, T., Kanda, H., Yamamoto-Goto, Y., Kanuka, H., Kuranaga, E., Aigaki, T. and Miura, M. (2002). Eiger, a TNF superfamily ligand that triggers the Drosophila JNK pathway. *EMBO J* **21**, 3009-18.

Igaki, T., Pastor-Pareja, J. C., Aonuma, H., Miura, M. and Xu, T. (2009). Intrinsic tumor suppression and epithelial maintenance by endocytic activation of Eiger/TNF signaling in Drosophila. *Dev Cell* **16**, 458-65.

Ingber, D. E. (2008). Tensegrity-based mechanosensing from macro to micro. *Prog Biophys Mol Biol* **97**, 163-79.

Ip, Y. T., Park, R. E., Kosman, D., Yazdanbakhsh, K. and Levine, M. (1992). dorsal-twist interactions establish snail expression in the presumptive mesoderm of the Drosophila embryo. *Genes Dev* **6**, 1518-30.

Irvine, K. D. and Wieschaus, E. (1994). Cell intercalation during Drosophila germband extension and its regulation by pair-rule segmentation genes. *Development* **120**, 827-41.

Ishimaru, S., Ueda, R., Hinohara, Y., Ohtani, M. and Hanafusa, H. (2004). PVR plays a critical role via JNK activation in thorax closure during Drosophila metamorphosis. *EMBO J* **23**, 3984-94.

Jacinto, A., Wood, W., Balayo, T., Turmaine, M., Martinez-Arias, A. and Martin, P. (2000). Dynamic actin-based epithelial adhesion and cell matching during Drosophila dorsal closure. *Curr Biol* **10**, 1420-6.

Jacinto, A., Wood, W., Woolner, S., Hiley, C., Turner, L., Wilson, C., Martinez-Arias, A. and Martin, P. (2002). Dynamic analysis of actin cable function during Drosophila dorsal closure. *Curr Biol* **12**, 1245-50.

Jia, J., Zhang, W., Wang, B., Trinko, R. and Jiang, J. (2003). The Drosophila Ste20 family kinase dMST functions as a tumor suppressor by restricting cell proliferation and promoting apoptosis. *Genes Dev* **17**, 2514-9.

Johnston, L. A. and Gallant, P. (2002). Control of growth and organ size in Drosophila. *Bioessays* **24**, 54-64.

Juliano, R. L. and Varner, J. A. (1993). Adhesion molecules in cancer: the role of integrins. *Curr Opin Cell Biol* **5**, 812-8.

Justice, R. W., Zilian, O., Woods, D. F., Noll, M. and Bryant, P. J. (1995). The Drosophila tumor suppressor gene warts encodes a homolog of human myotonic dystrophy kinase and is required for the control of cell shape and proliferation. *Genes Dev* **9**, 534-46.

Kafer, J., Hayashi, T., Maree, A. F., Carthew, R. W. and Graner, F. (2007). Cell adhesion and cortex contractility determine cell patterning in the Drosophila retina. *Proc Natl Acad Sci U S A* **104**, 18549-54.

Kaltschmidt, J. A., Lawrence, N., Morel, V., Balayo, T., Fernandez, B. G., Pelissier, A., Jacinto, A. and Martinez Arias, A. (2002). Planar polarity and actin dynamics in the epidermis of Drosophila. *Nat Cell Biol* **4**, 937-44.

Kango-Singh, M., Nolo, R., Tao, C., Verstreken, P., Hiesinger, P. R., Bellen, H. J. and Halder, G. (2002). Shar-pei mediates cell proliferation arrest during imaginal disc growth in Drosophila. *Development* **129**, 5719-30.

Karess, R. E., Chang, X. J., Edwards, K. A., Kulkarni, S., Aguilera, I. and Kiehart, D. P. (1991). The regulatory light chain of nonmuscle myosin is encoded by spaghetti-squash, a gene required for cytokinesis in Drosophila. *Cell* **65**, 1177-89.

Kiehart, D. P., Galbraith, C. G., Edwards, K. A., Rickoll, W. L. and Montague, R. A. (2000). Multiple forces contribute to cell sheet morphogenesis for dorsal closure in Drosophila. *J Cell Biol* **149**, 471-90.

Kiehart, D. P., Lutz, M. S., Chan, D., Ketchum, A. S., Laymon, R. A., Nguyen, B. and Goldstein, L. S. (1989). Identification of the gene for fly non-muscle myosin heavy chain: Drosophila myosin heavy chains are encoded by a gene family. *EMBO J* **8**, 913-22.

Kobielak, A. and Fuchs, E. (2004). Alpha-catenin: at the junction of intercellular adhesion and actin dynamics. *Nat Rev Mol Cell Biol* **5**, 614-25.

Kolahgar, G., Bardet, P. L., Langton, P. F., Alexandre, C. and Vincent, J. P. (2011). Apical deficiency triggers JNK-dependent apoptosis in the embryonic epidermis of Drosophila. *Development* **138**, 3021-31.

Kolsch, V., Seher, T., Fernandez-Ballester, G. J., Serrano, L. and Leptin, M. (2007). Control of Drosophila gastrulation by apical localization of adherens junctions and RhoGEF2. *Science* **315**, 384-6.

Kooh, P. J., Fehon, R. G. and Muskavitch, M. A. (1993). Implications of dynamic patterns of Delta and Notch expression for cellular interactions during Drosophila development. *Development* **117**, 493-507.

Kosman, D., Ip, Y. T., Levine, M. and Arora, K. (1991). Establishment of the mesoderm-neuroectoderm boundary in the Drosophila embryo. *Science* **254**, 118-22.

Kovar, D. R., Harris, E. S., Mahaffy, R., Higgs, H. N. and Pollard, T. D. (2006). Control of the assembly of ATP- and ADP-actin by formins and profilin. *Cell* **124**, 423-35.

Krendel, M. and Mooseker, M. S. (2005). Myosins: tails (and heads) of functional diversity. *Physiology (Bethesda)* **20**, 239-51.

Lai, Z. C., Wei, X., Shimizu, T., Ramos, E., Rohrbaugh, M., Nikolaidis, N., Ho, L. L. and Li, Y. (2005). Control of cell proliferation and apoptosis by mob as tumor suppressor, mats. *Cell* **120**, 675-85.

Landsberg, K. P., Farhadifar, R., Ranft, J., Umetsu, D., Widmann, T. J., Bittig, T., Said, A., Julicher, F. and Dahmann, C. (2009). Increased cell bond tension governs cell sorting at the Drosophila anteroposterior compartment boundary. *Curr Biol* **19**, 1950-5.

le Duc, Q., Shi, Q., Blonk, I., Sonnenberg, A., Wang, N., Leckband, D. and de Rooij, J. (2010). Vinculin potentiates E-cadherin mechanosensing and is recruited to actin-anchored sites within adherens junctions in a myosin II-dependent manner. *J Cell Biol* **189**, 1107-15.

Lecuit, T. (2010). alpha-catenin mechanosensing for adherens junctions. *Nat Cell Biol* **12**, 522-4.

Lecuit, T. and Lenne, P. F. (2007). Cell surface mechanics and the control of cell shape, tissue patterns and morphogenesis. *Nat Rev Mol Cell Biol* **8**, 633-44.

Lee, J. C., VijayRaghavan, K., Celniker, S. E. and Tanouye, M. A. (1995). Identification of a Drosophila muscle development gene with structural homology to mammalian early growth response transcription factors. *Proc Natl Acad Sci U S A* **92**, 10344-8.

Leevers, S. J., Weinkove, D., MacDougall, L. K., Hafen, E. and Waterfield, M. D. (1996). The Drosophila phosphoinositide 3-kinase Dp110 promotes cell growth. *EMBO J* **15**, 6584-94.

Leong, G. R., Goulding, K. R., Amin, N., Richardson, H. E. and Brumby, A. M. (2009). Scribble mutants promote aPKC and JNK-dependent epithelial neoplasia independently of Crumbs. *BMC Biol* **7**, 62.

Leptin, M. (1991). twist and snail as positive and negative regulators during Drosophila mesoderm development. *Genes Dev* **5**, 1568-76.

Leptin, M. and Grunewald, B. (1990). Cell shape changes during gastrulation in Drosophila. *Development* **110**, 73-84.

Leung, T., Chen, X. Q., Tan, I., Manser, E. and Lim, L. (1998). Myotonic dystrophy kinase-related Cdc42-binding kinase acts as a Cdc42 effector in promoting cytoskeletal reorganization. *Mol Cell Biol* **18**, 130-40.

Levayer, R., Pelissier-Monier, A. and Lecuit, T. (2011). Spatial regulation of Dia and Myosin-II by RhoGEF2 controls initiation of E-cadherin endocytosis during epithelial morphogenesis. *Nat Cell Biol* **13**, 734.

Li, W. and Baker, N. E. (2007). Engulfment is required for cell competition. *Cell* **129**, 1215-25.

Liu, R., Woolner, S., Johndrow, J. E., Metzger, D., Flores, A. and Parkhurst, S. M. (2008). Sisyphus, the Drosophila myosin XV homolog, traffics within filopodia transporting key sensory and adhesion cargos. *Development* **135**, 53-63.

Machesky, L. M., Mullins, R. D., Higgs, H. N., Kaiser, D. A., Blanchoin, L., May, R. C., Hall, M. E. and Pollard, T. D. (1999). Scar, a WASp-related protein, activates nucleation of actin filaments by the Arp2/3 complex. *Proc Natl Acad Sci U S A* **96**, 3739-44.

Mahajan, R. K. and Pardee, J. D. (1996). Assembly mechanism of Dictyostelium myosin II: regulation by K+, Mg2+, and actin filaments. *Biochemistry* **35**, 15504-14.

Manjon, C., Sanchez-Herrero, E. and Suzanne, M. (2007). Sharp boundaries of Dpp signalling trigger local cell death required for Drosophila leg morphogenesis. *Nat Cell Biol* **9**, 57-63.

Martin, A. C., Kaschube, M. and Wieschaus, E. F. (2009a). Pulsed contractions of an actin-myosin network drive apical constriction. *Nature* **457**, 495-9.

Martin, F. A., Herrera, S. C. and Morata, G. (2009b). Cell competition, growth and size control in the Drosophila wing imaginal disc. *Development* **136**, 3747-56.

Martin-Blanco, E., Pastor-Pareja, J. C. and Garcia-Bellido, A. (2000). JNK and decapentaplegic signaling control adhesiveness and cytoskeleton dynamics during thorax closure in Drosophila. *Proc Natl Acad Sci U S A* **97**, 7888-93.

Matsumura, F. (2005). Regulation of myosin II during cytokinesis in higher eukaryotes. *Trends Cell Biol* **15**, 371-7.

McNeill, H., Craig, G. M. and Bateman, J. M. (2008). Regulation of neurogenesis and epidermal growth factor receptor signaling by the insulin receptor/target of rapamycin pathway in Drosophila. *Genetics* **179**, 843-53.

Menendez, J., Perez-Garijo, A., Calleja, M. and Morata, G. (2010). A tumor-suppressing mechanism in Drosophila involving cell competition and the Hippo pathway. *Proc Natl Acad Sci U S A* **107**, 14651-6.

Mesquita, D., Dekanty, A. and Milan, M. (2010). A dp53-dependent mechanism involved in coordinating tissue growth in Drosophila. *PLoS Biol* **8**, e1000566.

Millard, T. H. and Martin, P. (2008). Dynamic analysis of filopodial interactions during the zippering phase of Drosophila dorsal closure. *Development* **135**, 621-6.

Miron, M., Verdu, J., Lachance, P. E., Birnbaum, M. J., Lasko, P. F. and Sonenberg, N. (2001). The translational inhibitor 4E-BP is an effector of PI(3)K/Akt signalling and cell growth in Drosophila. *Nat Cell Biol* **3**, 596-601.

Montagne, J., Stewart, M. J., Stocker, H., Hafen, E., Kozma, S. C. and Thomas, G. (1999). Drosophila S6 kinase: a regulator of cell size. *Science* **285**, 2126-9.

Montero, J. A., Carvalho, L., Wilsch-Brauninger, M., Kilian, B., Mustafa, C. and Heisenberg, C. P. (2005). Shield formation at the onset of zebrafish gastrulation. *Development* **132**, 1187-98.

Morata, G. and Ripoll, P. (1975). Minutes: mutants of drosophila autonomously affecting cell division rate. *Dev Biol* **42**, 211-21.

Moreno, E. and Basler, K. (2004). dMyc transforms cells into super-competitors. *Cell* **117**, 117-29.

Moreno, E., Basler, K. and Morata, G. (2002). Cells compete for decapentaplegic survival factor to prevent apoptosis in Drosophila wing development. *Nature* **416**, 755-9.

Morin, X., Daneman, R., Zavortink, M. and Chia, W. (2001). A protein trap strategy to detect GFP-tagged proteins expressed from their endogenous loci in Drosophila. *Proc Natl Acad Sci U S A* **98**, 15050-5.

Muliyil, S., Krishnakumar, P. and Narasimha, M. (2011). Spatial, temporal and molecular hierarchies in the link between death, delamination and dorsal closure. *Development* **138**, 3043-54.

Mullins, R. D., Heuser, J. A. and Pollard, T. D. (1998). The interaction of Arp2/3 complex with actin: nucleation, high affinity pointed end capping, and formation of branching networks of filaments. *Proc Natl Acad Sci U S A* **95**, 6181-6.

Myers, M. P., Stolarov, J. P., Eng, C., Li, J., Wang, S. I., Wigler, M. H., Parsons, R. and Tonks, N. K. (1997). P-TEN, the tumor suppressor from human chromosome 10q23, is a dual-specificity phosphatase. *Proc Natl Acad Sci U S A* **94**, 9052-7.

Nakagawa, M., Fukata, M., Yamaga, M., Itoh, N. and Kaibuchi, K. (2001). Recruitment and activation of Rac1 by the formation of E-cadherin-mediated cell-cell adhesion sites. *J Cell Sci* **114**, 1829-38.

Neto-Silva, R. M., Wells, B. S. and Johnston, L. A. (2009). Mechanisms of growth and homeostasis in the Drosophila wing. *Annu Rev Cell Dev Biol* **25**, 197-220.

Neufeld, T. P., de la Cruz, A. F., Johnston, L. A. and Edgar, B. A. (1998). Coordination of growth and cell division in the Drosophila wing. *Cell* **93**, 1183-93.

Niimura, M., Isoo, N., Takasugi, N., Tsuruoka, M., Ui-Tei, K., Saigo, K., Morohashi, Y., Tomita, T. and Iwatsubo, T. (2005). Aph-1 contributes to the stabilization and trafficking of the gamma-secretase complex through mechanisms involving intermolecular and intramolecular interactions. *J Biol Chem* **280**, 12967-75.

Nolo, R., Morrison, C. M., Tao, C., Zhang, X. and Halder, G. (2006). The bantam microRNA is a target of the hippo tumor-suppressor pathway. *Curr Biol* **16**, 1895-904.

Noren, N. K., Niessen, C. M., Gumbiner, B. M. and Burridge, K. (2001). Cadherin engagement regulates Rho family GTPases. *J Biol Chem* **276**, 33305-8.

Nurse, P. (1990). Universal control mechanism regulating onset of M-phase. *Nature* **344**, 503-8.

Oda, H. and Tsukita, S. (2001). Real-time imaging of cell-cell adherens junctions reveals that Drosophila mesoderm invagination begins with two phases of apical constriction of cells. *J Cell Sci* **114**, 493-501.

Oda, H., Tsukita, S. and Takeichi, M. (1998). Dynamic behavior of the cadherin-based cell-cell adhesion system during Drosophila gastrulation. *Dev Biol* **203**, 435-50.

Oda, H., Uemura, T., Shiomi, K., Nagafuchi, A., Tsukita, S. and Takeichi, M. (1993). Identification of a Drosophila homologue of alpha-catenin and its association with the armadillo protein. *J Cell Biol* **121**, 1133-40.

Oh, H. and Irvine, K. D. (2008). In vivo regulation of Yorkie phosphorylation and localization. *Development* **135**, 1081-8.

Oh, H. and Irvine, K. D. (2009). In vivo analysis of Yorkie phosphorylation sites. *Oncogene* **28**, 1916-27.

Oh, H., Reddy, B. V. and Irvine, K. D. (2009). Phosphorylation-independent repression of Yorkie in Fat-Hippo signaling. *Dev Biol* **335**, 188-97.

Pagliarini, R. A., Quinones, A. T. and Xu, T. (2003). Analyzing the function of tumor suppressor genes using a Drosophila model. *Methods Mol Biol* **223**, 349-82.

Pagliarini, R. A. and Xu, T. (2003). A genetic screen in Drosophila for metastatic behavior. *Science* **302**, 1227-31.

Paluch, E. and Heisenberg, C. P. (2009). Biology and physics of cell shape changes in development. *Curr Biol* **19**, R790-9.

Paluch, E., Sykes, C., Prost, J. and Bornens, M. (2006). Dynamic modes of the cortical actomyosin gel during cell locomotion and division. *Trends Cell Biol* **16**, 5-10.

Pantalacci, S., Tapon, N. and Leopold, P. (2003). The Salvador partner Hippo promotes apoptosis and cell-cycle exit in Drosophila. *Nat Cell Biol* **5**, 921-7.

Parks, A. L. and Muskavitch, M. A. (1993). Delta function is required for bristle organ determination and morphogenesis in Drosophila. *Dev Biol* **157**, 484-96.

Peifer, M. (1993). The product of the Drosophila segment polarity gene armadillo is part of a multi-protein complex resembling the vertebrate adherens junction. *J Cell Sci* **105 (Pt 4)**, 993-1000.

Pellock, B. J., Buff, E., White, K. and Hariharan, I. K. (2007). The Drosophila tumor suppressors Expanded and Merlin differentially regulate cell cycle exit, apoptosis, and Wingless signaling. *Dev Biol* **304**, 102-15.

Peng, H. W., Slattery, M. and Mann, R. S. (2009). Transcription factor choice in the Hippo signaling pathway: homothorax and yorkie regulation of the microRNA bantam in the progenitor domain of the Drosophila eye imaginal disc. *Genes Dev* **23**, 2307-19.

Perrimon, N., Lanjuin, A., Arnold, C. and Noll, E. (1996). Zygotic lethal mutations with maternal effect phenotypes in Drosophila melanogaster. II. Loci on the second and third chromosomes identified by P-element-induced mutations. *Genetics* **144**, 1681-92.

Polakis, P. (2000). Wnt signaling and cancer. *Genes Dev* **14**, 1837-51.

Pollard, T. D. and Beltzner, C. C. (2002). Structure and function of the Arp2/3 complex. *Curr Opin Struct Biol* **12**, 768-74.

Pollard, T. D., Blanchoin, L. and Mullins, R. D. (2000). Molecular mechanisms controlling actin filament dynamics in nonmuscle cells. *Annu Rev Biophys Biomol Struct* **29**, 545-76.

Pollard, T. D. and Borisy, G. G. (2003). Cellular motility driven by assembly and disassembly of actin filaments. *Cell* **112**, 453-65.

Potter, C. J., Huang, H. and Xu, T. (2001). Drosophila Tsc1 functions with Tsc2 to antagonize insulin signaling in regulating cell growth, cell proliferation, and organ size. *Cell* **105**, 357-68.

Pullen, N., Dennis, P. B., Andjelkovic, M., Dufner, A., Kozma, S. C., Hemmings, B. A. and Thomas, G. (1998). Phosphorylation and activation of p70s6k by PDK1. *Science* **279**, 707-10.

Raftery, L. A. and Sutherland, D. J. (1999). TGF-beta family signal transduction in Drosophila development: from Mad to Smads. *Dev Biol* **210**, 251-68.

Ramain, P., Heitzler, P., Haenlin, M. and Simpson, P. (1993). pannier, a negative regulator of achaete and scute in Drosophila, encodes a zinc finger protein with homology to the vertebrate transcription factor GATA-1. *Development* **119**, 1277-91.

Rauzi, M. and Lecuit, T. (2009). Closing in on mechanisms of tissue morphogenesis. *Cell* **137**, 1183-5.

Rauzi, M., Lenne, P. F. and Lecuit, T. (2010). Planar polarized actomyosin contractile flows control epithelial junction remodelling. *Nature* **468**, 1110-4.

Rauzi, M., Verant, P., Lecuit, T. and Lenne, P. F. (2008). Nature and anisotropy of cortical forces orienting Drosophila tissue morphogenesis. *Nat Cell Biol* **10**, 1401-10.

Ren, F., Zhang, L. and Jiang, J. (2010). Hippo signaling regulates Yorkie nuclear localization and activity through 14-3-3 dependent and independent mechanisms. *Dev Biol* **337**, 303-12.

Reynolds, A. B., Daniel, J., McCrea, P. D., Wheelock, M. J., Wu, J. and Zhang, Z. (1994). Identification of a new catenin: the tyrosine kinase substrate p120cas associates with E-cadherin complexes. *Mol Cell Biol* **14**, 8333-42.

Rhiner, C., Lopez-Gay, J. M., Soldini, D., Casas-Tinto, S., Martin, F. A., Lombardia, L. and Moreno, E. (2010). Flower forms an extracellular code that reveals the fitness of a cell to its neighbors in Drosophila. *Dev Cell* **18**, 985-98.

Ribeiro, P. S., Josue, F., Wepf, A., Wehr, M. C., Rinner, O., Kelly, G., Tapon, N. and Gstaiger, M. (2010). Combined functional genomic and proteomic approaches identify a PP2A complex as a negative regulator of Hippo signaling. *Mol Cell* **39**, 521-34.

Riesgo-Escovar, J. R. and Hafen, E. (1997). Common and distinct roles of DFos and DJun during Drosophila development. *Science* **278**, 669-72.

Rimm, D. L., Koslov, E. R., Kebriaei, P., Cianci, C. D. and Morrow, J. S. (1995). Alpha 1(E)-catenin is an actin-binding and -bundling protein mediating the attachment of F-actin to the membrane adhesion complex. *Proc Natl Acad Sci U S A* **92**, 8813-7.

Rohatgi, R., Ho, H. Y. and Kirschner, M. W. (2000). Mechanism of N-WASP activation by CDC42 and phosphatidylinositol 4, 5-bisphosphate. *J Cell Biol* **150**, 1299-310.

Rohatgi, R., Ma, L., Miki, H., Lopez, M., Kirchhausen, T., Takenawa, T. and Kirschner, M. W. (1999). The interaction between N-WASP and the Arp2/3 complex links Cdc42-dependent signals to actin assembly. *Cell* **97**, 221-31.

Rosenblatt, J., Raff, M. C. and Cramer, L. P. (2001). An epithelial cell destined for apoptosis signals its neighbors to extrude it by an actin- and myosin-dependent mechanism. *Curr Biol* **11**, 1847-57.

Sato, M. and Saigo, K. (2000). Involvement of pannier and u-shaped in regulation of decapentaplegic-dependent wingless expression in developing Drosophila notum. *Mech Dev* **93**, 127-38.

Schafer, D. A. (2002). Coupling actin dynamics and membrane dynamics during endocytosis. *Curr Opin Cell Biol* **14**, 76-81.

Seher, T. C., Narasimha, M., Vogelsang, E. and Leptin, M. (2007). Analysis and reconstitution of the genetic cascade controlling early mesoderm morphogenesis in the Drosophila embryo. *Mech Dev* **124**, 167-79.

Sellers, J. R. (2000). Myosins: a diverse superfamily. *Biochim Biophys Acta* **1496**, 3-22.

Senoo-Matsuda, N. and Johnston, L. A. (2007). Soluble factors mediate competitive and cooperative interactions between cells expressing different levels of Drosophila Myc. *Proc Natl Acad Sci U S A* **104**, 18543-8.

Shen, J. and Dahmann, C. (2005). Extrusion of cells with inappropriate Dpp signaling from Drosophila wing disc epithelia. *Science* **307**, 1789-90.

Silva, E., Tsatskis, Y., Gardano, L., Tapon, N. and McNeill, H. (2006). The tumor-suppressor gene fat controls tissue growth upstream of expanded in the hippo signaling pathway. *Curr Biol* **16**, 2081-9.

Simpson, P. (1976). Analysis of the compartments of the wing of Drosophila melanogaster mosaic for a temperature-sensitive mutation that reduces mitotic rate. *Dev Biol* **54**, 100-15.

Simpson, P. (2007). The stars and stripes of animal bodies: evolution of regulatory elements mediating pigment and bristle patterns in Drosophila. *Trends Genet* **23**, 350-8.

Simpson, P., Woehl, R. and Usui, K. (1999). The development and evolution of bristle patterns in Diptera. *Development* **126**, 1349-64.

Slattum, G., McGee, K. M. and Rosenblatt, J. (2009). P115 RhoGEF and microtubules decide the direction apoptotic cells extrude from an epithelium. *J Cell Biol* **186**, 693-702.

Sokac, A. M., Co, C., Taunton, J. and Bement, W. (2003). Cdc42-dependent actin polymerization during compensatory endocytosis in Xenopus eggs. *Nat Cell Biol* **5**, 727-32.

Solon, J., Kaya-Copur, A., Colombelli, J. and Brunner, D. (2009). Pulsed forces timed by a ratchet-like mechanism drive directed tissue movement during dorsal closure. *Cell* **137**, 1331-42.

Stephens, L., Anderson, K., Stokoe, D., Erdjument-Bromage, H., Painter, G. F., Holmes, A. B., Gaffney, P. R., Reese, C. B., McCormick, F., Tempst, P. et al. (1998). Protein kinase B kinases that mediate phosphatidylinositol 3,4,5-trisphosphate-dependent activation of protein kinase B. *Science* **279**, 710-4.

Stocker, H. and Hafen, E. (2000). Genetic control of cell size. *Curr Opin Genet Dev* **10**, 529-35.

Stronach, B. E. and Perrimon, N. (2001). Investigation of leading edge formation at the interface of amnioserosa and dorsal ectoderm in the Drosophila embryo. *Development* **128**, 2905-13.

Sweeton, D., Parks, S., Costa, M. and Wieschaus, E. (1991). Gastrulation in Drosophila: the formation of the ventral furrow and posterior midgut invaginations. *Development* **112**, 775-89.

Tamori, Y., Bialucha, C. U., Tian, A. G., Kajita, M., Huang, Y. C., Norman, M., Harrison, N., Poulton, J., Ivanovitch, K., Disch, L. et al. (2010). Involvement of Lgl and Mahjong/VprBP in cell competition. *PLoS Biol* **8**, e1000422.

Tapon, N., Harvey, K. F., Bell, D. W., Wahrer, D. C., Schiripo, T. A., Haber, D. A. and Hariharan, I. K. (2002). salvador Promotes both cell cycle exit and apoptosis in Drosophila and is mutated in human cancer cell lines. *Cell* **110**, 467-78.

Tapon, N., Ito, N., Dickson, B. J., Treisman, J. E. and Hariharan, I. K. (2001). The Drosophila tuberous sclerosis complex gene homologs restrict cell growth and cell proliferation. *Cell* **105**, 345-55.

Thompson, B. J. and Cohen, S. M. (2006). The Hippo pathway regulates the bantam microRNA to control cell proliferation and apoptosis in Drosophila. *Cell* **126**, 767-74.

Thompson, D. (1917). On Growth and Form. *revised edition, Dover,New York.*

Toyama, Y., Peralta, X. G., Wells, A. R., Kiehart, D. P. and Edwards, G. S. (2008). Apoptotic force and tissue dynamics during Drosophila embryogenesis. *Science* **321**, 1683-6.

Twitty, V. C. and Schwind, J. L. (1931). The growth of eyes and limbs transplanted heteroplastically between two species of Amblystoma. *Journal of Experimental Zoology* **59**, 61–86.

Tyler, D. M. and Baker, N. E. (2007). Expanded and fat regulate growth and differentiation in the Drosophila eye through multiple signaling pathways. *Dev Biol* **305**, 187-201.

Tyler, D. M., Li, W., Zhuo, N., Pellock, B. and Baker, N. E. (2007). Genes affecting cell competition in Drosophila. *Genetics* **175**, 643-57.

Tzolovsky, G., Millo, H., Pathirana, S., Wood, T. and Bownes, M. (2002). Identification and phylogenetic analysis of Drosophila melanogaster myosins. *Mol Biol Evol* **19**, 1041-52.

Udan, R. S., Kango-Singh, M., Nolo, R., Tao, C. and Halder, G. (2003). Hippo promotes proliferation arrest and apoptosis in the Salvador/Warts pathway. *Nat Cell Biol* **5**, 914-20.

Usui, K. and Kimura, K. (1993). Sequential emergence of the evenly spaced microchaetes on the notum of Drosophila. *Dev. Genes Evol.* **203**, 151–158.

Vachon, P. H. (2011). Integrin signaling, cell survival, and anoikis: distinctions, differences, and differentiation. *J Signal Transduct* **2011**, 738137.

Vasioukhin, V., Bauer, C., Degenstein, L., Wise, B. and Fuchs, E. (2001). Hyperproliferation and defects in epithelial polarity upon conditional ablation of alpha-catenin in skin. *Cell* **104**, 605-17.

Vereshchagina, N., Bennett, D., Szoor, B., Kirchner, J., Gross, S., Vissi, E., White-Cooper, H. and Alphey, L. (2004). The essential role of PP1beta in Drosophila is to regulate nonmuscle myosin. *Mol Biol Cell* **15**, 4395-405.

Weinkove, D., Neufeld, T. P., Twardzik, T., Waterfield, M. D. and Leevers, S. J. (1999). Regulation of imaginal disc cell size, cell number and organ size by Drosophila class I(A) phosphoinositide 3-kinase and its adaptor. *Curr Biol* **9**, 1019-29.

Willecke, M., Hamaratoglu, F., Kango-Singh, M., Udan, R., Chen, C. L., Tao, C., Zhang, X. and Halder, G. (2006). The fat cadherin acts through the hippo tumor-suppressor pathway to regulate tissue size. *Curr Biol* **16**, 2090-100.

Winter, C. G., Wang, B., Ballew, A., Royou, A., Karess, R., Axelrod, J. D. and Luo, L. (2001). Drosophila Rho-associated kinase (Drok) links Frizzled-mediated planar cell polarity signaling to the actin cytoskeleton. *Cell* **105**, 81-91.

Woods, D. F. and Bryant, P. J. (1991). The discs-large tumor suppressor gene of Drosophila encodes a guanylate kinase homolog localized at septate junctions. *Cell* **66**, 451-64.

Wu, H. W., Kuhn, T. and Moy, V. T. (1998). Mechanical properties of L929 cells measured by atomic force microscopy: effects of anticytoskeletal drugs and membrane crosslinking. *Scanning* **20**, 389-97.

Wu, S., Huang, J., Dong, J. and Pan, D. (2003). hippo encodes a Ste-20 family protein kinase that restricts cell proliferation and promotes apoptosis in conjunction with salvador and warts. *Cell* **114**, 445-56.

Wu, S., Liu, Y., Zheng, Y., Dong, J. and Pan, D. (2008). The TEAD/TEF family protein Scalloped mediates transcriptional output of the Hippo growth-regulatory pathway. *Dev Cell* **14**, 388-98.

Wullschleger, S., Loewith, R. and Hall, M. N. (2006). TOR signaling in growth and metabolism. *Cell* **124**, 471-84.

Xu, T. and Rubin, G. M. (1993). Analysis of genetic mosaics in developing and adult Drosophila tissues. *Development* **117**, 1223-37.

Xu, T., Wang, W., Zhang, S., Stewart, R. A. and Yu, W. (1995). Identifying tumor suppressors in genetic mosaics: the Drosophila lats gene encodes a putative protein kinase. *Development* **121**, 1053-63.

Yamada, S., Pokutta, S., Drees, F., Weis, W. I. and Nelson, W. J. (2005). Deconstructing the cadherin-catenin-actin complex. *Cell* **123**, 889-901.

Yarar, D., To, W., Abo, A. and Welch, M. D. (1999). The Wiskott-Aldrich syndrome protein directs actin-based motility by stimulating actin nucleation with the Arp2/3 complex. *Curr Biol* **9**, 555-8.

Yonemura, S., Wada, Y., Watanabe, T., Nagafuchi, A. and Shibata, M. (2010). alpha-Catenin as a tension transducer that induces adherens junction development. *Nat Cell Biol* **12**, 533-42.

Young, P. E., Pesacreta, T. C. and Kiehart, D. P. (1991). Dynamic changes in the distribution of cytoplasmic myosin during Drosophila embryogenesis. *Development* **111**, 1-14.

Yu, J., Zheng, Y., Dong, J., Klusza, S., Deng, W. M. and Pan, D. (2010). Kibra functions as a tumor suppressor protein that regulates Hippo signaling in conjunction with Merlin and Expanded. *Dev Cell* **18**, 288-99.

Yumura, S., Yoshida, M., Betapudi, V., Licate, L. S., Iwadate, Y., Nagasaki, A., Uyeda, T. Q. and Egelhoff, T. T. (2005). Multiple myosin II heavy chain kinases: roles in filament assembly control and proper cytokinesis in Dictyostelium. *Mol Biol Cell* **16**, 4256-66.

Zallen, J. A. and Wieschaus, E. (2004). Patterned gene expression directs bipolar planar polarity in Drosophila. *Dev Cell* **6**, 343-55.

Zeitlinger, J. and Bohmann, D. (1999). Thorax closure in Drosophila: involvement of Fos and the JNK pathway. *Development* **126**, 3947-56.

Zhang, L., Ren, F., Zhang, Q., Chen, Y., Wang, B. and Jiang, J. (2008). The TEAD/TEF family of transcription factor Scalloped mediates Hippo signaling in organ size control. *Dev Cell* **14**, 377-87.

Zhao, B., Lei, Q. Y. and Guan, K. L. (2008). The Hippo-YAP pathway: new connections between regulation of organ size and cancer. *Curr Opin Cell Biol* **20**, 638-46.

Zhao, B., Wei, X., Li, W., Udan, R. S., Yang, Q., Kim, J., Xie, J., Ikenoue, T., Yu, J., Li, L. et al. (2007). Inactivation of YAP oncoprotein by the Hippo pathway is involved in cell contact inhibition and tissue growth control. *Genes Dev* **21**, 2747-61.

Ziosi, M., Baena-Lopez, L. A., Grifoni, D., Froldi, F., Pession, A., Garoia, F., Trotta, V., Bellosta, P. and Cavicchi, S. (2010). dMyc functions downstream of Yorkie to promote the supercompetitive behavior of hippo pathway mutant cells. *PLoS Genet* **6**.

Zusman, S. B. and Wieschaus, E. F. (1985). Requirements for zygotic gene activity during gastrulation in Drosophila melanogaster. *Dev Biol* **111**, 359-71.

9. APPENDIX

9.1 Abbreviations

4E-BP1 – 4E binding protein 1

A/P – anterior/posterior

AC – actin cable

AJs – Adherens Junctions

AP – after pupariation

Arp2/3 – Actin related proteins 2 and 3

AS – Amnioserosa

ATP – Adenosine triphosphate

DC – dorsal closure

Dia – Diaphanous

DIAP1 – *Drosophila* inhibitor of apoptosis 1

Dlg – Discs large

Dpp – Decapentaplegic

E-cad – E-cadherin

EM – Electron microscopy

Ex – Expanded

Fwe- Flower

GEF – Guanine nucleotide exchange factor

GFP – Green fluorescent protein

GSK-3 – Glycogen synthase kinase 3

GTP – Guanosine triphosphate

Hpo – Hippo

LE – leading edge

Lgl – lethal giant larvae

Mats – Mob-as-tumor suppressor

MHC – Myosin heavy chain

MLC – Myosin light chain

MLCK – Myosin light chain kinase

MRLC – Myosin regulatory light chain

Myo-II – Myosin-II

PDK1 – Pyruvate dehydrogenase kinase

PI3K – Phosphatydilinositol 3-kinase

PIP2 –Inositol 4,5-biphosphate

PIP3 –Inositol 3,4,5-triphosphate

PKB – Protein kinase B

PP2A – Protein phosphatase 2A

PTEN – Phosphatase and tensin homolog

RNAi – RNA interference

Rok – Rho kinase

S6K – S6 kinase

Scrib – Scribble

Sd – Scalloped

Sqh – Spaghetti squash

STRIPAK – Striatin-interacting phosphatase and kinase

Tkv – Thickvein

TOR – Target of rapamycin

TSC1/2 – Tuberous sclerosis complex 1/2

Wg – Wingless

Wts – Warts

Yki – Yorkie

ZA – Zonula adherens

Zip – Zipper

9.2 List of Figures

9.3 List of Videos

All movies are on the attached CD.

Video 1

Developing notum visualized with E-cadherin::GFP. The movie covers the period 14-26h AP, during which cells delaminate. Total time is 740 min, with frames at 10 min intervals.

Video2

Developing notum visualized with E-cadherin::GFP, expressing p110 PI3K driven by the *pnr* promoter. Time interval between frames is 10 min and the video length is 650 min.

Video 3

Developing notum visualized with E-cadherin::GFP, expressing Tsc1 and Tsc2 driven by the *pnr* promoter. Time interval between acquired frames is 10 min and the video length is 670 min.

Video 4

Developing notum visualized with E-cadherin::GFP, expressing RNAi for r5s driven by the *pnr* promoter. Time interval between frames is 10 min and the video length is 770 min.

Video 5

Developing notum visualized with E-cadherin::GFP, expressing RNAi for Cdc25 driven by the *pnr* promoter. Cells do not divide but delaminate during this time interval. Time interval between acquired frames is 5 min and the video length is 135 min.

Video 6

Developing notum visualized with E-cadherin::GFP, expressing DIAP1 driven by the *pnr* promoter. Time interval between frames is 10 min and the video length is 730 min.